Structure and activity of protein-nanoparticle conjugates: towards a strategy for optimizing the interface

by

Marie-Eve Aubin-Tam

B.Eng., École Polytechnique de Montréal (2002)
Diplôme d'Ingénieur, École Polytechnique de Paris (2003)

Submitted to the Department of Biological Engineering
in partial fulfillment of the requirements for the degree of

Doctor of Philosophy

at the

MASSACHUSETTS INSTITUTE OF TECHNOLOGY

May 2008

Author .....
Department of Biological Engineering
May 30, 2008

Certified by .....
Kimberly Hamad-Schifferli
Assistant Professor of Mechanical Engineering and of Biological Engineering
Thesis Supervisor

Accepted by .....
Alan J. Grodzinsky
Chair, Department of Biological Engineering Department Graduate Program Committee

Certified by.....

Kimberly Hamad-Schifferli
Thesis Supervisor and Thesis Committee Member, Assistant Professor of Mechanical Engineering and of Biological Engineering

Certified by.....

Matthew J. Lang
Thesis Committee Member, Assistant Professor of Mechanical Engineering and of Biological Engineering

Certified by.....

Scott R. Manalis
Thesis Committee Chair, Professor of Mechanical Engineering and of Biological Engineering

Structure and activity of protein-nanoparticle conjugates: towards a strategy for optimizing the interface

by

Marie-Eve Aubin-Tam

Submitted to the Department of Biological Engineering
on May 30, 2008, in partial fulfillment of the
requirements for the degree of
Doctor of Philosophy

Abstract

Nanoparticle-protein conjugates have a variety of applications in imaging, sensing, assembly and control. The nanoparticle-protein interface is made of numerous complex interactions between protein side-chains and the nanoparticle surface, which are likely to affect protein structure and compromise activity. Ribonuclease S and cytochrome *c* are covalently linked to nanoparticles *via* attachment to a specific surface cysteine, with the goal of optimizing protein structure and activity, and understanding conditions that minimize non-specific adsorption. Protein behavior is explored as a function of the nanoparticle surface chemistry and material, the density of proteins on the nanoparticle surface, and the position of the labeled site.

Ribonuclease S is attached to Au nanoparticles by utilizing its two-piece structure. Enzymatic activity is determined using RNA substrate with a FRET pair. Conjugation lowers the ribonucleatic activity, which is rationalized by the presence of negative charges and steric hindrance which impede RNA in reaching the active site.

Cytochrome *c* is linked to Au and $CoFe_2O_4$ nanoparticles. The protein is denatured when the nanoparticle ligands are charged, but remains folded when neutral. The presence of salt in the buffer improves folding. This indicates that electrostatic interactions of charged amino acids with the charged ligands are prone to lead to protein denaturation. The attachment site can be controlled by mutations of surface residues to cysteines. Protein unfolding is more severe for nanoparticle attached in the vicinity of charged amino acids. Molecular dynamics simulations of the conjugate reveal that electrostatic interactions with the nanoparticle ligand lead to local unfolding of α-helices of cyt *c*. Furthermore, the nanoparticle induces more structural disturbance when it is attached on the N- and C-terminal α-helices foldon, which is the most stable motif of cyt *c* and the most essential for folding.

Thesis Supervisor: Kimberly Hamad-Schifferli
Title: Assistant Professor of Mechanical Engineering and of Biological Engineering

Acknowledgments

Many people have contributed to my experience as PhD student and have made the past six years of my life so wonderful.

First of all, this work would not have been possible without the support of my advisor Professor Kimberly Hamad-Schifferli. She shared with me precious advice and expertise. I am very grateful for her openness and her ability to discuss and welcome ideas.

Then, I am grateful to my thesis committee Professor Scott Manalis and Professor Matthew Lang for their helpful comments and feedback on my work. I am especially thankful to Prof. Manalis for the experience that I gained in his lab and for his guidance at the beginning of my PhD studies.

It has been a pleasure to collaborate with Professor Wonmuk Hwang. I learned a lot from him and thank him for his guidance with the MD simulations.

I learned also a lot from my labmates Kate, Suhno, Andy, Hui, Victor, Josh and Shariar. I owe them many thanks. I mentored several undergraduate students during my graduate studies that contributed to this thesis. I want to thank especially Diana, Viviana and Sisi, for the good time that we had working together and their help with different projects.

Several laboratories were gracious enough to let me use their facilities. I would like to thank especially the laboratories of Professors Yang Shao-Horn, Thomas Schwartz, Krystyn Van Vliet, Douglas Lauffenburger and Robert Sauer. I also want to thank Debbie Pheasant from the CSBI Biophysical facilities where I spent many hours using the CD spectrophotometer.

I am deeply thankful to my family. My parents have always been a major source of motivation and inspiration. From very early on, they encouraged me to have ambition and a vision. I thank them, as well as my sisters, for their support, love and prayers.

I gained more than a PhD in Boston. I made friends that are very dear to my heart. I give special thanks to Nami, Mary and Sungyon. I also met a friend that was to become my husband and then the father of our little girl Raphaelle. Daniel,

without any doubt, you are the person who contributed the most to my thesis. I thank you for your continuous encouragement and love.

Above all, my final thanks are going to my Father in heaven, for His infinite love and care, and for His help in every aspect of my life, including the work that is described herein. "The LORD is my rock and my fortress and my deliverer, my God, my rock, in whom I take refuge; my shield and the horn of my salvation, my stronghold." Psalm 18:2

Contents

List of Figures

List of Tables

Chapter 1

Introduction

Nanoparticles (NPs) have gained interest in the last decades due to their unique properties compared to bulk material. When the size of materials is reduced to the nanoscale, changes in optical, magnetic, electrical and chemical properties are observed and the ratio of surface atoms increases significantly [1]. Novel possibilities of applications using NPs are now developed and envisioned across many fields such as medecine, material science and the energy. In particular, the attachment of NPs to proteins has found applications in imaging [2, 3, 4, 5], in catalysis [6], in sensing [7, 8], in delivery [9], in the design of new tools for assembly [10, 11, 12], in the control of protein activity with an external field [13, 14], and in understanding local structure in protein folding [15].

In spite of this, the details of the interface between NPs and proteins remain to be fully characterized. As of today, most research effort has focused on finding new and original applications for NP-protein assemblies, but is lacking rigorous treatment of the complexes themselves. Generally, little or no verification is performed to identify the site of attachment of the NP on the protein, non-specific interactions are often ignored and the protein is frequently assumed to be fully active and well folded when immobilized on nanostructures. These assumptions are often invalid, as this thesis intends to demonstrate. Proteins can form numerous chemical interactions with NPs, which are likely to affect the protein structure and compromise its activity. In order to create bio-inorganic hybrid devices that properly function biologically, the

interface must be optimized in such manner to preserve the biological function of the biomolecule.

For number of applications, it is advantageous to have an attachment that is both *covalent* and *site specific*. A *covalent* bonding of the NP to the protein increases the linkage stability over a wider range of physical characteristic of the milieu like the ionic strength and pH. The ability to choose the site of attachment on a *specific residue* allows control over the protein orientation on the surface, which is required for a large fraction of NP-protein applications. For example, the protein active site may need to be blocked by the NP to inactivate the enzyme, while other applications may demand to maintain the active site free to interact with other molecules. Control over the attachment site is also desirable in order to minimize the interference of the NP with the protein structure and function. Site-specific labeling of large and even very complex proteins with small dyes or spin labels has been utilized for some time now, and has led to many advances in dynamics of biological processes, in structural studies and in imaging [16]. Site directed mutagenesis allows placement of the dye on specific amino acids on the protein. Labeled proteins have been crystallized and the effect on the structure has been studied [17, 18]. It is desirable to gain the same versatility with NPs as for small dyes. Although tremendous progress has been made, analogous capabilities for NP labeling are challenging. NPs are considerably larger than dyes, and possess a lot of surface area which increase non-specific interactions of amino acid side chains of the protein with the NP ligand or surface. As a result, the ability to control the site of NP attachment has been achieved on a limited set of proteins.

For those reasons, it is extremely significant to do an extensive structural study of proteins that are covalently attached to NPs at specific sites. This thesis consists of the first structural characterization of such complexes. The strategy employed for the NP labeling consists of linking the NP to a single cysteine on the surface of the protein, which forms a strong covalent Au-thiol bond with the NP core or a thiol-thiol bond with a thiolated NP ligand.

The main objectives of this thesis is to control the attachment site of proteins to

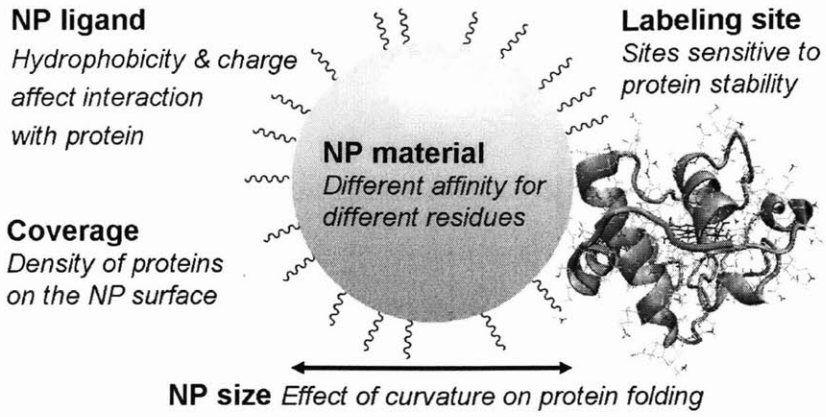

Figure 1-1: Parameters that affect the protein structure and activity.

NPs, and to characterize the protein structure and activity as a function of conjugates properties. Parameters that affect the protein include the NP material, the NP surface chemistry, the NP size, the protein coverage on the NP, the nature of the NP attachment and the attachment site on the protein (Figure 1-1). Experimental studies as well as molecular dynamics simulations are performed to explain the protein behavior on the NPs surfaces and, more generally, to build a set of rules for the design of more efficient conjugation.

The first part of this thesis (Chapter 2) consists of an overview of strategies commonly used to synthesize and characterize NP-protein conjugates. The different existing labeling methods are described, and their advantages and limitations are identified. Then, Chapter 3 describes the site-specific labeling of the protein ribonuclease S with 3nm Au NPs. The NP attachment is facilitated by the two-piece structure of this protein. The ribonucleatic activity of the conjugate is also measured. The following chapters (Chapters 4-5) treat of a more direct approach for site-specific covalent labeling. The protein cytochrome *c* is labeled at specific sites with Au NPs and with $CoFe_2O_4$ magnetic NPs having varying surface chemistries. The effects of the NP ligand charge and of the position of labeling site are studied. Molecular dynamics simulations bring a better understanding on the effects of the NP by considering the protein with atomistic detail. Lastly, Chapter 6 summarizes the thesis and points toward future work that should follow this research.

Chapter 2

Nanoparticle-protein conjugates purification and characterization

A large variety of methods exists for the preparation of NP-protein conjugates. This section intends to do an overview of NP-protein functionalization schemes and of the methods to characterize the structure and activity of the NP-protein bioconjugates.

2.1 Synthesis of nanoparticles for bioapplications

Centuries ago, Au NPs already started to be used, mainly for their reputed medicinal properties and for staining artwork such as glass windows. Soon afterwards, they became the subject of investigation of many early scientists such as Selmi, Faraday, Graham, Tyndall, Rayleigh, Ostwald, Mie and Bredig [19]. In recent years, significant progress have been made in the synthesis and characterization of NPs [20] made of Au or other materials.

Typically, metallic NPs are formed in the presence of ligand molecules that binds to the metal and forms the surface capping groups of the NP. The ligand molecules are essential to obtain stable NPs with a narrow size distribution and to prevent their aggregation. These surface stabilizing ligands confer to the NP its solubility. For water soluble NPs, they usually consists of either short charged molecules that can self-assemble into a monolayer, or of longer polymeric molecules [21, 22, 23]. For NPs

soluble in nonpolar solvents, an hydrophobic self-assembled monolayer is typically used [24, 25].

For biological applications, the NP must be water soluble, stable at physiological pH and nontoxic. Nanotoxicology is still a developing discipline [26] and many studies remain to be done to insure the safety of nanomaterials for medical applications. Reports have pointed out that the cytotoxicity of NPs highly depends on their capping group [27] and on their size [28]. Au NPs were also found to be significantly less toxic than their precursors [29].

2.2 Nanoparticle functionalization with proteins

Biofunctionalization of NPs with proteins can be challenging as a NP is much more complex than a simple hard sphere and can interact in number of ways with proteins. Instead, it has multiple surface coating ligands that have endgroups and sidechains that can interact with the protein. NP surfaces represent a significant portion of the particle and the ratio of surface atoms exceeds 50% for NP size below 2nm. NP surfaces are not uniform but have multiple crystal lattices, vertices, and edges, each of which can have different chemical affinities for adsorption [30]. Furthermore, surface coating ligands on the NP are labile. They can adopt multiple conformations and can migrate to different sites on the NP surface. This rearrangement of ligands have been exploited to optimize the interaction with a protein of interest [31, 32]. Consequently, bioconjugation strategies must consider the NP as a chemical system as nearly as complex as proteins.

Strategies to link a protein to the NP have taken four main approaches (Figure 2-1): 1) electrostatic adsorption, 2) conjugation to the ligand on the NP surface, 3) conjugation to a small cofactor molecule that the protein can recognize and bind, and 4) direct conjugation to the NP surface.

These four strategies are employed in this thesis. 1) In Chapters 4 and 5, horse cytochrome *c* is electrostatically adsorbed on Au and $CoFe_2O_3$ NPs. 2) In Chapter 5, yeast cytochrome *c* is covalently linked to a thiol of the NP ligand. 3) In Chapter

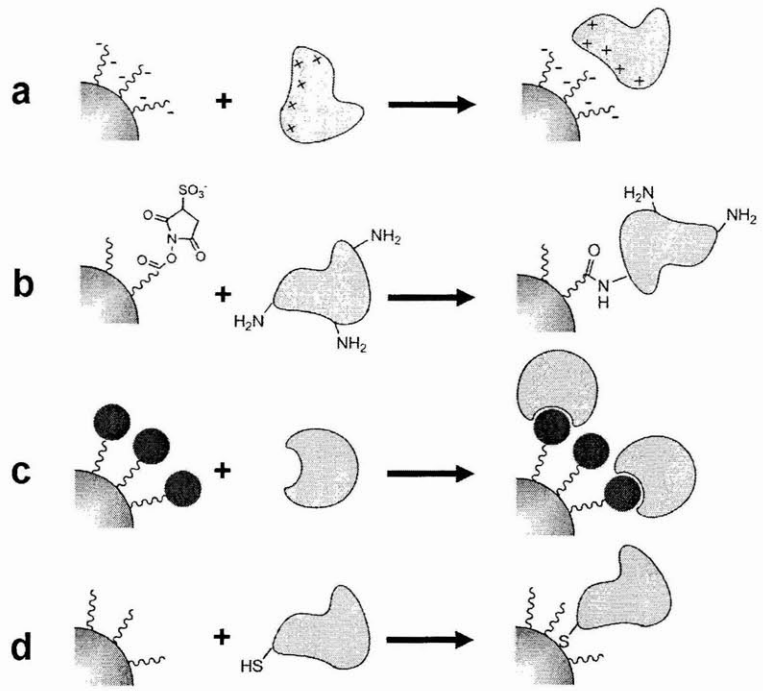

Figure 2-1: NP-protein labeling strategies: a) electrostatic/hydrophobic attachment of protein, b) covalent attachment to NP ligand, c) attachment of protein cofactor on NP, and d) direct linkage of amino acid on NP core.

3, S-protein is attached to its cofactor (S-peptide) previously immobilized on the NP.

4) In Chapter 4, yeast cytochrome *c* is covalently linked to the surface of Au NPs.

2.2.1 Electrostatic adsorption

The most widely used linkage approach consists of electrostatic adsorption. This is the simplest as it requires no chemical reaction, and has been used for a while already as an electron dense marker in histology [33].

Appropriate conditions for the NP ligands and protein side chains to become electrostatically attracted to each other must be determined. The interaction may be modulated by the pH or charge screening via controlling the ionic strength of the medium. Because it is inherently a non-specific interaction, the protein may interact with the NP in any of a number of orientations or have the NP positioned at any number of labeling sites. However, strategic modification of NP surface chemistry has enabled regio-specific interactions with the protein [34].

2.2.2 Linking to nanoparticle ligand

Another general method for NP-protein conjugation is covalently linking of a protein to the NP ligand.

Many have exploited the binding of Ni-nitrilotriacetate (Ni-NTA) or Co-NTA groups on the NP to His tags on protein [35, 36, 37]. Because the His tag can be cloned into a protein sequence, it enables site-specific labeling. Typically the His tag is put at the termini of the proteins and is relatively simple to be cloned in. This results in a strong bond, with a dissociation constant of approximately $K_d = 10^{-13}$M at pH 8 [38].

Another popular labeling chemistry utilizes the covalent binding of primary amines with sulfo-NHS esters or R-COOH groups *via* reaction with EDC [39, 40]. Au NPs labeled with NHS esters can react to form covalent bonds with the primary amine of lysine on a protein. In addition, Au NPs coated with maleimide groups can react with the thiol of cysteine on a protein.

An additional route consists of linking a free surface cysteine residue with a ligand having a solvent exposed free thiol. In this thesis, the ligand dimercaptosuccinic acid (DMSA) is used to form a disulfide bridge with a surface cysteine residue of cytochrome *c* [41] (Chapter 5).

If the NP has multiple ligands that can react with the protein, this can result in a distribution in the number of proteins on the NP. The stoichiometry can be influenced by varying the ratio of the reaction. A population of NP-protein conjugates with various protein:NP ratios is usually produced. This approach has been greatly advanced by extreme control over the surface chemistry of the NPs. For example, pioneering work by Hainfeld *et al* have been able to isolate Au NPs with exactly one reactive group [4], which would enable limiting the coverage of proteins on the NP surface. Although this chemistry was originally intended for imaging by electron microscopy (EM), it has enabled capabilities well beyond EM imaging such as electron transfer [42].

2.2.3 Linking using specific affinity of protein for cofactor

Alternatively, NP-protein conjugation can be achieved by using specific affinity of a protein for a small molecule. The classic example is the biotin-streptavidin binding. In effect, labeling NPs with biotin ligands allows linkage to streptavidin, which due to its multivalent nature can be bound to other biotin labeled species. The biotin-streptavidin interaction is strong enough to be nearly covalent, with a dissociation constant on the order of $K_d = 10^{-14}$M [43]. Enzymes can also be used to link a biotin to a specific peptide sequence, thus catalyzing the NP attachment [44]. Although this strategy limits the position of NP at only few positions, it offers high specificity for in vivo labeling. Because there are a wide variety of linkers that can be functionalized with biotin, it is a versatile way to achieve a specific linkage. Consequently, it has been utilized extensively for both biological conjugation as well as inorganic-biological conjugation.

Recent advances in aptamer chemistry have been exploited to use them as binders to proteins [45, 46]. Because DNA chemistry is much simpler to modify artificially than proteins, this is a versatile linker for NP-protein conjugation.

NPs capped with protein cofactors are used to attach NPs on specific receptors at the cell surface. For example, serotonin capped CdSe NPs bind to serotonin transporters [47], and mannose capped gold NPs bind to mannose receptor on *E. Coli* type 1 pili [48].

2.2.4 Direct reaction with nanoparticle core surface atoms

A direct reaction of a chemical group on the protein without the use of a linker [49, 50, 51] is usually desired if the particle is used as a biosensor where FRET or electron transfer is used. These processes are sensitive to distance changes on the Angstrom scale, and long floppy linkers can adopt multiple conformations, resulting in a variable protein-NP distance that can be problematic in sensing. In addition, long linkers can result in conjugates that are larger than the NP or protein, which can decrease circulation times in the blood or cause problems in cellular uptake. Direct

linkage to the protein in these cases would be much more desirable.

For Au NPs, this can be achieved by the Au-thiol chemistry where a protein with a cysteine covalently bonds to an Au NP. The conjugation requires only incubation of the two species together as the Au-S bond is strongly favored, even over a S-S bond. This results in a short, direct link from the protein side chain to the NP surface. However, this can be problematic as NP labeling can potentially break up dithiols of protein, which can compromise stability of protein and lead to denaturation. In the case of proteins that have free cysteines close to the protein surface that are not tied up as dithiols, this is a highly convenient way to conjugate a protein to an Au NP. Similarly, for sulfur containing NPs such as ZnS/CdSe, cysteine can directly from a disulfide bridge with surface S atom [52].

Direct linkages can also be achieved by His tags, which can attach directly to Zn, Ni, Cu, Co, Fe, Mn atoms. NPs made of materials such as Ni, CdSe/ZnS and CdS/ZnS [53, 54, 13] were labeled in that fashion, obviating the need for addition of a metal ion chelating agent like NTA.

An important concern in direct labeling of the NP core is steric crowding on the NP surface. It may be difficult for the targeted protein residue to reach the NP surface if the NP ligand is too densely packed on the surface or too long. For example, polyethylene glycol is a popular ligand for NPs as it prevents non-specific adsorption of protein side chains with the NP core [55, 23, 50]. However, its long chain may hinder access to the conjugation site. Also, if the strength of interaction of ligand with NP surface is similar or higher than the bond linking proteins to NPs, it may not be able to displace the ligand from NP surface and attach the protein. In this case, a large excess of protein in the reaction is necessary.

2.3 Site specific labeling

For numerous applications, it is important for the NP-protein conjugate function to label the protein at a particular site. For example, NPs are linked to proteins to sense when the protein binds to its substrate, typically by FRET. For this purpose,

it is crucial that the NP be placed in a particular site of the protein so that it is regio-specific or even site-specific. Also, for NPs used as EM imaging tags to localize a specific structure within a large protein [51, 56, 57], it is advantageous to attach the NP in close vicinity of the residues or motifs of interest. Even if one can control the stoichiometry of the resulting product (NP:protein ratio), and assuming that the protein is fully folded upon labeling, most labeling chemistries do not have the ability to single out a single amino acid. Instead, there is a probability that the NP can be placed at any number of the available sites (Figure 2-2), such as labeling the primary amines or carboxylic acids. This results in the protein assuming random orientations on the NP surface. Moreover, if one of these sites is in a non-ideal position, such as within the binding site, those proteins will not be able to bind to its substrate. If the experimental probe is an ensemble measurement, then one would not be able to distinguish this a decrease in activity due to all proteins having a lower activity due to the presence of the NP, or due to only a proportion of them being totally inactive. This distribution of labeling sites is also a problem if one wants to use the NP to obtain quantitative information about protein function, such as via FRET pairs in which the distance of the NP to a chromophore matters. This is further complicated by the fact that the protein has only 20 amino acids, so for larger proteins the possibility of having a unique amino acid that can link to a NP is difficult. For instance, if labeling is achieved via chemistry conjugating to the primary amine of lysine, and a protein has multiple lysines, a distribution of labeling sites would result, some of which may be detrimental for protein function.

Nevertheless, labeling of NPs to a specific amino acid on a protein has been achieved by a variety of methods. Table 2.1 lists examples of where proteins are linked directly to a NP core, and Table 2.2 those which link to a ligand on the NP surface.

As an example, lipase was genetically engineered so that it contains only one solvent accessible lysine. This lysine was then modified by carbodiimide chemistry to result in an acetylene group. This acetylene group could then be coupled to Au NPs functionalized with azide ligands via click chemistry, which is the 1,2,3-triazole

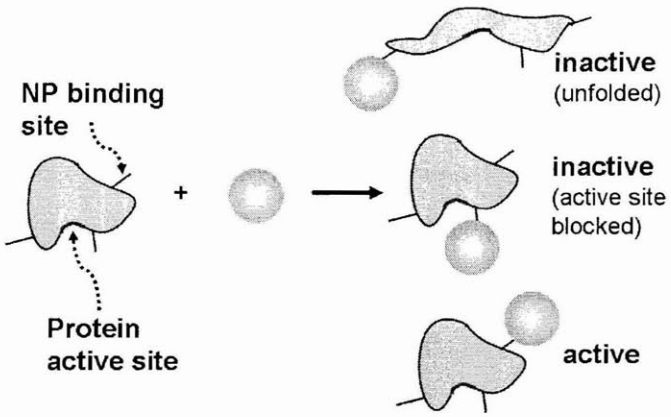

Figure 2-2: Protein with several NP binding sites. NP attachment can inactivate the protein via denaturation or blocking of the active site.

Labeled residue - NP material	*Examples of labeled protein*	*Molecular weigth*	*Ref.*
Cys - Au	Cytochrome *c*	12.6 kDa	[50], Chapter 4
	Ribonuclease S	13.7 kDa	[58], Chapter 3
	70 s ribosome	2.5 MDa	[51]
	Single chain Fv antibody	25 kDa	[49]
	Chaperonin	60 kDa	[52]
Cys - CdSe/ZnS	Chaperonin	60 kDa	[52]
	Human serum albumin	67 kDa	[15]
	α-chymotrypsin	21.6 kDa	[59]
His Tag - CdSe/ZnS	Maltose binding protein	40.6 kDa	[60]
His Tag - Ni	Green fluorescent protein	27 kDa	[53]

Table 2.1: Strategies to label a specific residue that involve direct linkage to NP core.

Labeled residue - NP ligand	*Examples of labeled protein*	*Molecular weigth*	*Ref.*
Cys - dimercaptosuccinic acid	Cytochrome *c*	12.6 kDa	[41], Chapter 5
His Tag - Ni-NTA	Adenovirus serotype 12 knob	60.6 kDa	[36]
	20S proteasome	750 kDa	[37]
	Streptopain	42 kDa	[61]
	Green fluorescent protein	27 kDa	[62]
His Tag - Co-NTA	Horseradish peroxidase	44 kDa	[35]
Lys - azide	Lipase	30 kDa	[63]

Table 2.2: Strategies to label a specific residue that involve linkage to NP ligand.

formation between azides and terminal acetylenes that is catalyzed by copper(I) [63].

Other recent strategies include functionalizing the protein with a highly specific ligation reaction, which introduces a reactive group that links with a NP. This strategy has been used to label the GTPase Rab6a with an Au NP [64]. Rab6A was modified on its N-terminal with a PEG linker with a free thiol. As Rab6A lacks cysteines, only this exposed thiol will react with the NP. Once labeled, the Rab6A still binds to its substrate (BodipyFL-GTP) like the wild type version, which can be detected by fluorescence quenching.

2.4 Purification of conjugates

Once the NP-protein conjugation is achieved, it must be purified from both the free protein and free NP species. This has been achieved by a variety of approaches, such as spin columns [65], ion exchange [49], HPLC [37, 50] and gel filtration [40, 49]. In addition, multiple washes and centrifugation have been successful in isolating the NP-protein conjugate [63].

If the NP is magnetic, magnetic separation can be used to purify the NP-protein conjugate away from free protein [62]. This strategy has been developed for commercial use, and large beads containing multiple magnetic species can be used to purify proteins. However, from a labeling perspective, introduction of a magnet precipitates all the magnetic NPs, including those which are unlabeled. While this is adequate for applications in which a particular protein needs to be pulled out of solution away from other proteins, it may not be feasible for synthesizing and purifying a NP-protein conjugate, because you would obtain a sample that would have a mixture of both NPs linked to protein and free NPs. Nevertheless, adjustment of reaction stoichiometry may ameliorate this problem.

Gel electrophoresis has been used for many years to separate biomolecules of different lengths and even conformations. It was demonstrated in 2001 by Alivisatos *et al* that it can be used to purify NP-DNA conjugates of desired stoichiometry [66], and soon after for NPs linked to proteins [67]. Electrophoresis can be used both as a

means to isolate the conjugate from other species, or as a means to assay the purity of a sample. Electrophoresis utilizes the fact that the conjugate has a mobility that differs from both the free protein and free NP. This change in mobility is influenced by both a change in the size or charge. Both acrylamide [49, 67] and agarose gel electrophoresis [68, 58, 50] can be used. In the work presented in this thesis, agarose gel electrophoresis was found to be a better option for purification. As agarose gels are horizontal, they allow sample to run in both directions, so both positive and negative species can be viewed simultaneously, which is useful for conjugating proteins to oppositely charged NPs. In addition, the band containing the conjugate can also be cut from the gel and the conjugate can be extracted from the agarose by spin centrifugation columns, allowing purification of the conjugate from both free NP and free protein. Sample wells in agarose gels tend to be larger than acrylamide gels so higher quantities of protein and NP can be loaded into the gel.

2.5 Biophysical characterization of nanoparticle-protein conjugates

Once the NP-protein conjugate is synthesized and isolated from other species, the conjugate must be biophysically characterized. This requires measuring both the structure and function of the protein when labeled with the NP.

2.5.1 Structural characterization

The protein structure is related to its function. It is therefore important to probe the protein structure for assaying whether the protein in the conjugate form is functional. Unfolding might occur upon conjugation to a NP, as interaction of the protein's side chains with the NP surface or ligands is likely to occur, resulting in non-specific adsorption and perturbation of the native structure.

There are numerous techniques that have been applied to study structure of proteins by themselves. Unfortunately, only a few have been applied to study the struc-

ture of proteins when conjugated to NPs. However, this can be also viewed as an opportunity to expand the set of techniques to characterize these systems. Challenges include requirements in sample quantity, as yields for purified NP-protein conjugates can be low.

The techniques described below have been able to evaluate the effect of NP size on the structure of non-covalently attached proteins such as lysozyme [69] and cytochrome *c* [70]. Structural studies have been able to determine the orientation of cytochrome *c* on Au or Ag NPs [71, 72], and how it is affected by the NP ligand functional groups [34]. This thesis uses some of those techniques to study the effect of NP surface chemistry on the structure of cytochrome *c* on Au NPs [50] and $CoFe_2O_3$ NPs [41].

Measuring the protein structure is not only important for creating biologically functioning NP-protein conjugates. With such information, one can take this further and study how to engineer the NP ligand so that proteins or peptides can adopt a particular conformation when adsorbed on the NP surface. If more methods to study protein structure when conjugated to NPs were to be explored, it could expand the functional utility of NP-protein conjugates.

Circular dichroism spectroscopy

Circular dichroism (CD) spectroscopy has been traditionally used to measure the secondary structure of a protein. It has also served as a useful tool for probing secondary structure of the protein when it is linked to a NP. The basis of CD spectroscopy is the difference of absorption of right handed and left handed circularly polarized light through a sample. This difference spectrum is related to chirality of the protein. In the UV region, it reflects the secondary structure of the protein. Protein motifs such as α-helices, β-sheets, and random coils have certain CD signatures in the UV range. Furthermore, one can deconvolute a spectrum to determine the relative amounts of each motif. Spectra can be compared to a database of known protein structures, which are usually determined by x-ray crystallography and NMR.

The benefits of CD are that it is a standard technique and has been used to

characterize many proteins, so signatures of numerous proteins are well known. Furthermore, it can be performed in solution which is the standard form of NP-protein conjugates. Therefore, it is a direct probe of the protein structure on the NP. It has been the most widely used technique to assay protein structure in conjugates, and has been used successfully for several NP-protein systems: lysozyme and peptides on silica [69, 73]; α-chymotrypsin on CdS [59] and on Au [74]; albumin on CdTe [67]; and cytochrome c on Au [50, 31].

However, CD spectroscopy of NP-protein conjugates is complicated by the fact that NP contribution to optical absorption at short wavelengths can be significant enough to swamp the signal. This makes difference measurements very noisy unless averaging over long times is done. Corrections for absorption flattening were found to be necessary for large nanoparticles which have stronger absorption [69]. In addition, it is an ensemble measurement so it cannot distinguish between 50% of all the proteins being fully denatured from all of the proteins being half denatured.

Plasmon resonance

When an external electric field is applied to a metallic NP, its electrons move collectively in what is called plasmon resonance. The resonance frequency of the surface plasmon is a function of the NP material, size, shape, aggregation state and surface chemistry. As proteins adsorb on the surface of metallic NPs, the local refractive index around the NP changes, leading to a red-shift of the plasmon resonance peak. The structure of the NP labeled protein was also found to alter the position plasmon peak. This led to the development of colorimetric sensors to monitor protein denaturation on NP surfaces. Examples of such sensors were reported for cytochrome c [2] and amyloid β protein [75] on Au NPs.

Electron microscopy

Direct EM imaging of the protein when conjugated to the NP can also been used to assay structure. Small Au NPs have served as imaging agents. By reconstructing several images one can obtain a three-dimensional map of the protein. Large proteins

have been successfully imaged by this method down to 6-8 Å resolution [37]. This requires imaging of many complexes and sophisticated image deconvolution techniques. Labeling of proteins with Au NPs have been used in cryo-EM to image many proteins, such as MAP2 and tau on microtubules [76], F-actin [77], the ribosome [78, 79], the scrapie prion protein [80], and conformational changes in kinesin [81] and myosin [82], among many others.

Atomic Force Microscopy

Atomic force microscopy (AFM) could be used to probe the structure of the protein in the complex. In essence, the structure of protein is inferred from a height measurement [83]. Phase imaging also allows mapping areas of adhesion and friction. Imaging of proteins on surfaces has improved due to new fabrication techniques for AFM tips and imaging methodologies. AFM can now resolve secondary structure in proteins such as individual α-helices [84, 85]. If the tip is chemically functionalized, it can be used to chemically image a sample. AFM offers large benefits as the sample requirements are small and it consists of a single molecule imaging technique so it does not represent an ensemble average. However, because it requires the sample to be on a substrate, protein interactions with the surface may denature the protein, and obscure the effects of the NP.

SAXS

Small angle x-ray scattering (SAXS) have been used to measure the periodicity of the NPs and thus infer the inter-particle spacing, which can be correlated to the protein size [74]. If the protein denatures, the interparticle spacing decreases and thus changes the SAXS spectra. The sample form is solid for SAXS, so it can be employed in samples that are not soluble.

Other techniques

Femtosecond time-resolved spectroscopy studies of the photosynthetic bacterial light harvesting complex on TiO_2 NPs was used to yield information on the structural

deformation of the protein on the NP [86]. H/D exchange can also be used to assess the structure of conjugates by examining the exposed protons on the protein [34]. Optical spectroscopy can be used to probe the protein in special cases where the protein has a chromophore or an optically absorbing cofactor, such as a heme for proteins like cytochrome *c* and hemoglobin. In this case, optical absorption can yield information on the redox state of protein, which can be used to infer the secondary structure of the protein. For example, for cytochrome *c*, it is known that as the protein is more unfolded, it is more readily oxidized, and this is reflected by a shift in the Soret band and changes in Q-band intensity. Therefore, optical absorption can yield information on the degree of folding in the protein. However, the NP contribution to the optical spectra can swamp out the heme spectra, as extinction coefficients near heme absorption features can be an order of magnitude higher. Subtraction of the NP contribution, when possible, can aid in identifying heme features.

2.5.2 Probing activity of protein

NP induced protein structural disturbance is prone to affect its activity, as structure and function are closely linked in proteins. The assay for activity depends on the protein. It is typically measured via reaction with the enzyme substrate, or via electrochemistry for redox active enzyme.

Reaction with a substrate

For an enzyme to be active, its substrate must reach the active site, the protein must act on it, and finally release the product. All of these steps are going to be dramatically influenced by the presence of a relatively large particle with numerous molecules on its surface. Also, as the NP-protein net charge usually differs from that of the protein, the altered electrostatic interaction can affect the substrate binding or the product release. The enzyme activity could be significantly reduced if, for example, both the substrate and NP are negatively (or positively) charged, or if the product remains electrostatically linked to the NP-protein complex.

The activity of several NP-enzyme conjugates has been studied. Sastry and coworkers found that 3.5nm Au NPs conjugated with fungal protease (F-prot) [87] or with pepsin [88] have a proteolytic activity comparable to the one of the free enzyme when incubated with hemoglobin. F-prot immobilized on NPs produces only slightly less digest fragments then the free enzyme. Huang and coworkers studied the proteolytic activity of trypsin attached on 13nm Au NPs and found a lower enzymatic activity and a different specificity for cleavage [89]. While a decrease in activity of enzymes on NPs was also observed by several groups [90, 91, 59, 92], we should note that others report unchanged or enhanced activity [93, 94, 95].

Electrochemistry

The activity of redox proteins such as heme proteins, copper-containing proteins, and iron-sulfur proteins are typically measured via electrochemical measurements [96, 97]. Many experiments of plain unlabeled protein on electrode surfaces have gained information on the protein conformation and orientation on the surface [98, 99]. Analogous electrochemical studies for protein on NP surfaces are desirable.

The electrode/NP/protein interface is generally self-assembled using one of the following strategies. 1) NPs are linked to the electrode and then immerse in a solution of redox enzymes [42, 100, 101]. Or, 2) the NP-protein conjugates are prepared in solution, purified, and then immobilized on the electrode [42, 102, 103]. Willner and coworkers [42] obtained same density of NP-proteins attached on the electrode via route 1 and 2.

The use of NPs in bioelectrochemistry has gained interest in the past decade [104]. In particular, NPs are found capable of wiring redox proteins to electrodes. They can act as an antenna that provides a conducting path to facilitate electron transfer between the protein redox center and the electrode [42, 105, 101]. From the rate of electron transfer, one can estimate the distance between the NP and the protein redox center, and thus determine the protein orientation [98]. The rate of electron transfer is typically measured by cyclic voltammetry. A Laviron analysis of the peak-to-peak potential separation at various scan rates yields electron transfer

rate constants [106].

The protein structural integrity can also be probed by electrochemistry. The redox potential depends on the environment of the redox center, which almost certainly changes when the protein unfolds. Denaturation of the protein could also make it electroinactive. The model protein horse cytochrome *c* is found to be active when attached on various nanostructures [107, 101], with a redox potential very close to the one reported for well-folded horse cytochrome *c* [108].

Antibody activity

NP labeling of antibodies is a widely used technique for sensing, FRET, and general imaging. While the structure of antibodies is not known completely, the activity assay is relatively straightforward. One needs only to test if the conjugate binds to its target, such as in testing that CdS labeled anti-CD4 monoclonal antibody still binds to target cells. This is assayed by fluorescence spectroscopy or FACS [109].

There are other assays of activity such as those involved in more complex biological processes. For example, peptide-gold conjugates bound to neurons were found to still exhibit neuronal activity [110].

Chapter 3

Site-specific labeling of ribonuclease S via two-step assembly

Ribonuclease S (RNase S) is a two-piece protein that consist of the two proteolytic fragments of RNase A when digested with subtilisin (RNase S, Figure 3-1 from PDB # 1CJQ [111]). The shorter piece of this complex is a 20 residue peptide called the S-peptide, and the larger fragment (104 residues) is called the S-protein. S-protein spontaneously assembles with S-peptide to form an active enzyme that cleaves RNA pyrimidines by acid-base catalysis. The S-peptide or S-protein alone exhibits no enzymatic activity.

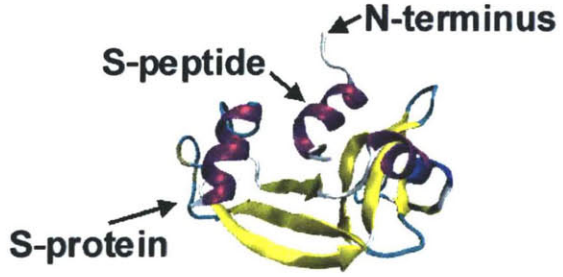

Figure 3-1: Ribonuclease S. α-helices are represented in purple and β-sheets in yellow. The NP is attached on a cysteine mutated on the N-terminus.

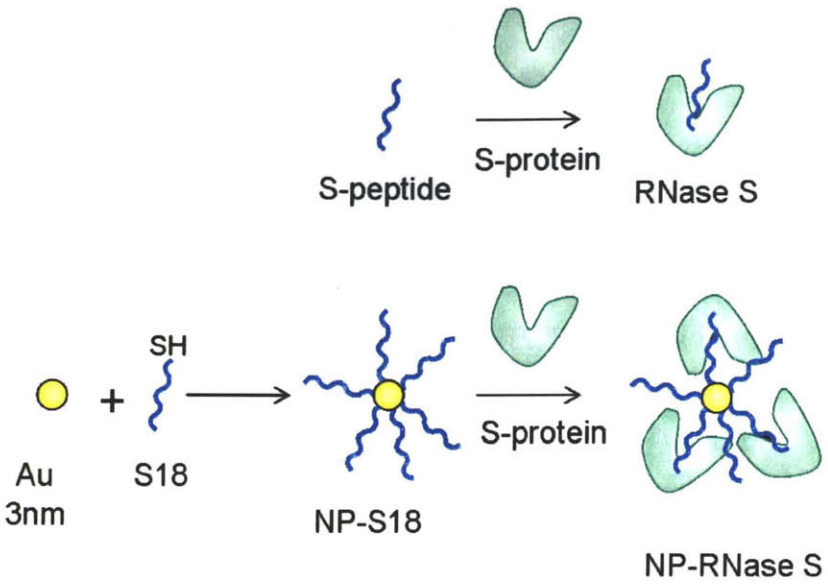

Figure 3-2: Strategy for labeling RNase S via a two step reaction. Au NPs are first linked to the S18 peptide (blue) that possesses a unique cysteine. The NP-S18 conjugate is then incubated with S-protein (green) to yield a fully formed complex.

The dissociation constant (k_d) of this complex can be as low as 3.1×10^{-11}M under optimum pH, salt concentration and temperature [112]. It permits the use of S-peptides as affinity tags for protein purification [113]. Modification of S-peptide has been done extensively, both by mutagenesis and with chromophores and artificial groups for applications of control by light or chemical moieties.

Here, a cysteine residue is added to the N-terminus of S-peptide in order to self-assemble a monolayer of S-peptides on the NP. Afterwards, this NP-S-peptide conjugate is incubated with S-protein in order to reconstitute the full RNase S enzyme (Figure 3-2). This chapter demonstrates first site-specific attachment of RNase S to Au NPs. Then follows a quantitative analysis of ribonucleatic activity measurements[1].

[1]Reproduced in part with permission from M.-E. Aubin, D.G. Morales, K. Hamad-Schifferli, "Labeling Ribonuclease S with a 3nm Au nanoparticle by two-step assembly," *Nano Letters*, 2005, 5, 519-522. Copyright 2005 American Chemical Society.

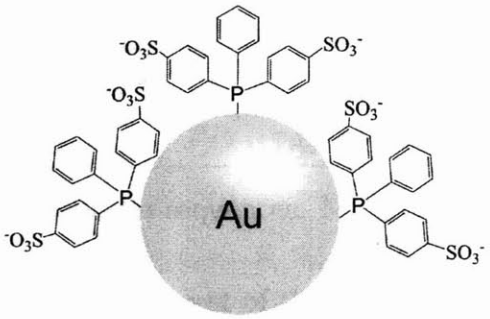

Figure 3-3: BPS ligands on the surface of Au NP. The NP is not pictured to scale.

3.1 Synthesis of Au nanoparticles

Water soluble Au NPs were synthesized based on a variation of a reported method [114]. In summary, a 60mL solution of 6.8mM sodium citrate with tannic acid and sodium carbonate is heated to 60°C. NPs size can be tuned by the amount of tannic acid and sodium carbonate. Then, a 300mL solution of 294μM $HAuCl_4$ at 60°C is rapidly added and mixed during 10 minutes. NPs are functionalized with the ligand bis(p-sulphonatophenyl) phenylphosphine dihydrate (BPS, Figure 3-3) by incubation overnight with 0.1g of BPS. Then, NPs are purified with agarose gel electrophoresis and extracted from the gel with 0.2 μm centrifugal filters (Nanosep, PALL). A thin band is cut in order to narrow the NP size distribution. NPs of 3.0 $\pm$ 0.4nm and 16.3 $\pm$ 2.9nm were synthesized as determined by transmission electron microscopy (TEM).

3.2 Conjugation of nanoparticles with ribonuclease S

NP labeling of ribonuclease S is done in two steps as shown in Figure 3-2. Mutagenic studies have shown that S-peptide can be truncated to its 15 first residues or have residues added to the N-terminus without perturbing enzymatic function. Therefore, this permits extension of the S-peptide with a cysteine which provides a unique thiol on the S-peptide (S18) for linking to a Au NP. Two glycine spacers are also added

Name	*Sequence*
S18	**CGG** KETAAAKFER QHMDS
S19	KETA**W**AI**F**V**R** QHMDSSTSA
wild-type S-peptide	KETAAAKFER QHMDSSTSAA

Table 3.1: S-peptides sequences. Mutations are in bold.

between the linking cysteine and the rest of the peptide, as shown in Table 3.1. S18 was synthesized commercially (Sigma-Genosys, purity 77%). The low yield of the synthesis is determined to be primarily due to dithiol linkages, evidenced by a dimer in the mass spectrometry data. 3nm NPs are linked to S18 by incubation in 1× PBS for 1 hour at 25°C with a NP concentration at 10 μM. The NP:S18 conjugates are then incubated with S-protein for 1 hour at 25°C. Conjugation is confirmed by agarose gel electrophoresis and plasmon resonance shifts. Purification of NP:proteins is performed by agarose gel electrophoresis.

3.2.1 Gel electrophoresis

The electrophoretic mobility of NPs in a gel is modified when proteins attach on their surfaces, due to the changes in size and charge. This enables the use of agarose gels to demonstrate conjugation of RNase S to Au NPs. Competitions assay are also performed in order to confirm the site of attachment.

Non-specific attachment of proteins on NPs

Nonspecific interactions between proteins or DNA and Au surfaces are well known. The synthesized NPs are incubated with various proteins to show this effect (Figure 3-4). If Au NPs are incubated with proteins that do not possess a surface thiol for linking, nonspecific adsorption is observed. Gel electrophoresis of 5μL 3nm Au NPs incubated overnight with 1:10 RNase A (lane 2 in Figure 3-4), 1:10 horse heart cytochrome *c* (lane 3), and 1:10 bovine serum albumin (lane 4) shows significant shifts of all bands towards lower mobility relative to unlabeled Au NPs (lane 1) due to nonspecific adsorption with the NP, demonstrating the prevalence of this effect. In addition, S-protein incubated with NPs alone also shifts mobility (Figure 3-6,

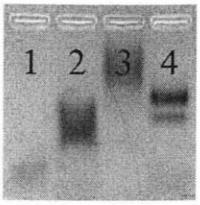

Figure 3-4: 3% agarose gel electrophoresis of proteins non-specifically attached on Au NPs. Au NP (1) incubated with RNase S (2), cytochome *c* (3), and albumin (4).

lanes 5 and 9). These proteins have no exposed surface thiols except for bovine serum albumin, but an abundance of lysines, which are known to stick to NP surfaces through the amine or by electrostatic interaction with the negatively charged BPS molecules.

Site-specific attachment of RNase S

Figure 3-5 shows a gel of 3nm NPs linked to RNase S by the two-step method described in Figure 3-2. Lane 1 shows plain NPs. Lanes 2 and 3 are NP-S18 conjugates of 1:5 and 1:25 NP:S18 ratio respectively. Lanes 4-6 are 1:25 NP-S18 samples further incubated with S-protein (NP:S18:S-protein ratios of 1:25:1, 1:25:5, 1:25:10). Addition of S-protein to the 1:25 shifts the mobility considerably.

Furthermore, as the NP:S18 ratio is increased, incubation of S-protein results in a smaller shift relative to the position of the NP-S18 without S-protein. This is observed in the gel of Figure 3-6, that shows systematic increases of S18 followed by incubation with S-protein. Lanes 1-4 of the gel are increasing NP:S18 alone, lanes 5-8 are increasing NP:S18 with 1× S-protein (1:S18:1 NP:S18:S-protein), and Lanes 9-12 are increasing NP:S18 with 10× S-protein (1:S18:10). Lanes 5 and 9 show that NPs incubated with S-proteins were retarded in the gel, showing non specific adsorption of S-protein on the NP. S-protein is positively charged, so S-protein is linking to the NP by electrostatic interactions to the BPS molecules. Presumably, higher coverages of S18 on the NP would prevent these nonspecific interactions, as S18 peptides replace BPS molecules and less of the NP surface would be exposed. The 1:0:10 sample is more retarded in the gel than the 1:50:10 sample, indicating that S-protein attaches more easily on naked Au surface than on a very dense monolayer of S18. This could

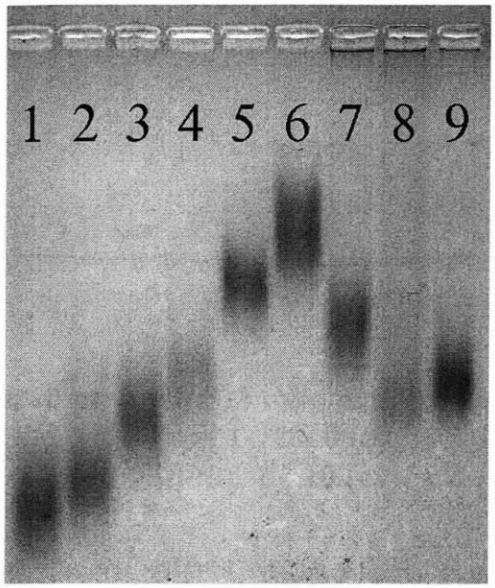

Figure 3-5: 4% agarose gel electrophoresis of 3nm NP(1), incubated 1h with S18 in a NP:S18 ratio of 1:5 (2) and 1:25 (3), followed by 1h incubation with S-protein in a NP:S18:S-protein ratio of 1:25:1 (4), 1:25:5 (5) and 1:25:10 (6). The 1:25:10 sample was subsequently incubated overnight with S19 in a concentration 50× [NP] (7). The S19 was incubated overnight with the 1:5 sample (8) and the 1:25 sample (9), in a concentration of 50× [NP]

be due to steric hindrance of S-protein binding to S18 on the NP surface at higher S18 coverages. It is known that the S-peptide has a random coil configuration but adopts an α-helical structure upon binding to S-protein. Presumably at these higher S18 coverages there is not enough space for the S18 to adopt the proper conformation, or for S-protein to get close enough to the S18 to properly bind.

To explore how the NP:S18 ratio affects nonspecific adsorption, 1:5 and 1:25 samples are incubated overnight with 50× S19 (a variant of S-peptide without cysteine, Table 3.1). The 1:5 sample incubated with S19 (Figure 3-5, lane 8) is shifted to higher mobility relative to its original position in lane 2, indicating an interaction between the two species. However, the 1:25 incubated with S19 (lane 9) does not show an appreciable shift from its original position (lane 3), which could be due to the 1:25 NP:S18 having a fully saturated surface, lacking room for S19 to nonspecifically adsorb.

Therefore, an optimal ratio of NP:S18 is found at around 1:25. At this ratio, both

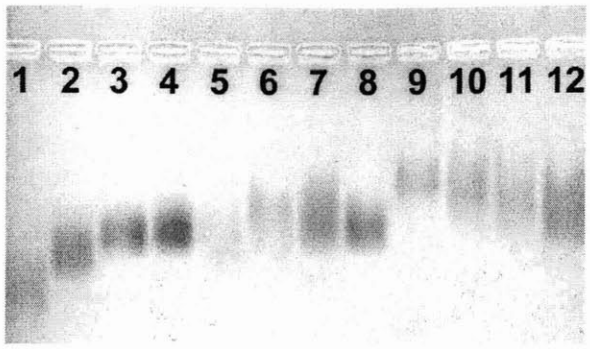

Figure 3-6: Exploring the effect of NP:S18 ratio with 3% agarose gel electrophoresis. NP:S18:S-protein in ratios of 1:0:0 (lane 1), 1:5:0 (2), 1:25:0 (3), 1:50:0 (4), 1:0:1 (5), 1:5:1 (6), 1:25:1 (7), 1:50:1 (8), 1:0:10 (9), 1:5:10 (10), 1:25:10 (11), 1:50:10 (12).

non-specific adsorption and steric effects which hinder the attachment of S-protein can be minimized.

To show that binding between the S-protein and S18 on the NP is specific, a competition binding assay is performed. S19 is a mutated S-peptide that binds 110× more tightly to S-protein than the wild-type [115] and which has no cysteine (sequence in Table 3.1). S19 was chemically synthesized at a purity of 95% (Sigma-Genosys). S19 is incubated with the 1:25:10 sample overnight at 50× the NP concentration, and its gel mobility was compared to samples before exposure to S19. The 1:25:10:50 (NP:S18:S-protein:S19) band (Figure 3-5, lane 7) runs faster than the 1:25:10 sample, indicating that S19 has extracted S-protein from the S18 on the NP surface.

Finally, in order to insure that the S18 attached to the NP by the covalent thiol-Au bond, a competition with a short thiol is performed (Figure 3-7). This strategy has been used to displace nonspecific adsorption of DNA on NPs [116, 117]. In the NP-S19 samples, S19 is non-covalently adsorbed on the NP and can presummably be removed from the surface if a thiol can cover the surface. S18 attachment would be significantly less affected by the presence of such a thiol. Both S18 and S19 have a neutral net charge at the pH of the gel buffer, so adsorption is not due to electrostatic interactions. The 1:25 NP:S19 sample (Figure 3-7, lane 4) is incubated with the thiol mercaptoproprionic acid ($HS(CH_2)_2CO_2H$, MPA) in a 1mM concentration for 4 hours (lane 5). This results in a shifting of the band in the direction of the position of plain NP (lane 1), indicating displacement of the S19 nonspecifically bound to the NP.

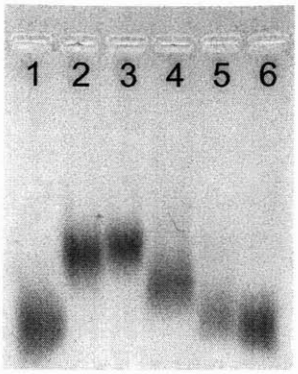

Figure 3-7: MPA displacement of nonspecific adsorption on NP surfaces. 4% agarose gel of Au NPs (1), 1:25 NP:S18 (2), 1:25 NP:S18 with MPA (3), 1:25 NP:S19 (4), 1:25 NP:S19 with MPA (5), Au NPs with MPA (6).

However, incubation of 1:25 NP:S18 (lane 2) with MPA under identical conditions (lane 3) results in a negligible mobility change, suggesting that S18 is covalently attached to the NP and does not get displaced. NPs incubated with MPA shows no noticeable change in mobility (lane 6).

Varying the NP size

For NPs of different size, the *optimum* ratio of NP:S18 for S-protein attachment would differ. As a first step, gel electrophoresis is used to quantify how many S-peptide are able to attach on the NP surface.

Figure 3-8 shows 16.3nm Au NPs (lane 1) incubated with increasing amount of S18. Lane 2 has 1:50 (NP:S18) and there is a factor 2 increase of S18 concentration between successive lanes. With larger particles, the shift in mobility is smaller, and it becomes more complicated to evaluate the S18 concentration at which the NP surface becomes saturated. This shows that gel electrophoresis is more efficient to purify conjugates made of smaller NPs. The NP seems to reach saturation of its surface at around lane 6, which corresponds to a NP:S18 incubation ratio of 1:800. A surface area of 0.214nm^2 has been determined for alkanethiols on a flat Au surface by electron diffraction studies [118]. If there were a same S18 density on 16.3nm NPs, there would be up to 3900 S18 moelcules that can attach on the NP. Evidently, the S18 density is lower on the NP surface.

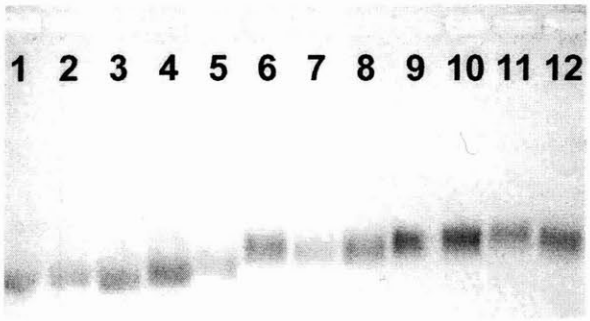

Figure 3-8: Gel electrophoresis of 16.3nm Au NP-S18 conjugates.

3.2.2 Plasmon resonance

Surface plasmon resonance also confirms protein attachment. Optical absorption spectroscopy was performed on a Varian Cary 100 in a 1cm quartz cuvette, with 0.1nm steps in 1×PBS at room temperature. The NP-bioconjugates are extracted from the agarose gels by slicing out the band and separating by spin centrifugation through a filter column. UV-vis shows plasmon peak around 510nm, as expected for spherical Au NPs of that size.

A red shift in the Au NP surface plasmon resonance is observed for the 1:5, 1:10, and 1:25 (NP:S18) samples upon increasing amounts of S-protein added (Figures 3-9 and 3-10), an effect consistent with increasing amounts of protein on the NP surface. It should be noted that when comparing the 1:5, 1:10, and 1:25 plasmon resonance positions, higher amounts of S18 result in a blue shift. Comparable blue shifts are observed if the BPS ligands are displaced with the thiolated molecule MPA as shown in Figure 3-11. Therefore, the blue shifts observed with increasing amount of S18 are most likely due to a displacement of the BPS ligand by the thiol on S18.

Addition of S19 to the 1:25:10 sample is able to blue-shift the plasmon resonance (Figure 3-10), which is consistent with S-proteins being removed from the NP surface. This confirms again that S-protein attach on the NP by interaction with S18 and not simply by electrostatic attractions or other non-specific interactions.

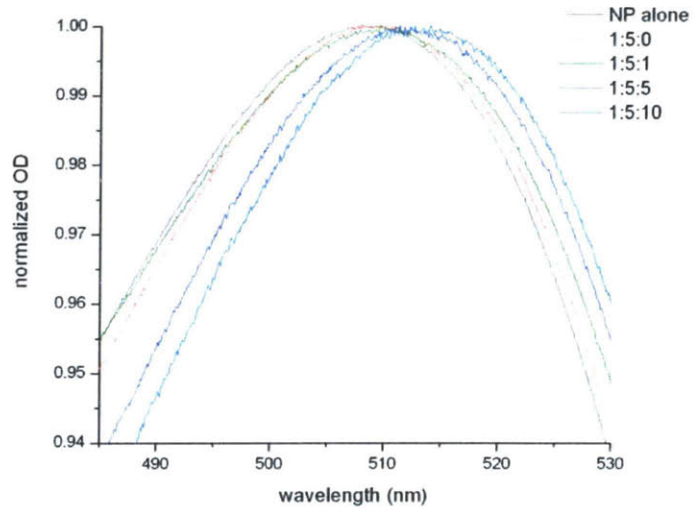

Figure 3-9: Optical absorption spectra of NP-RNase S conjugates around the plasmon resonance. NP:S18:Sprot ratios of the samples are in the legend.

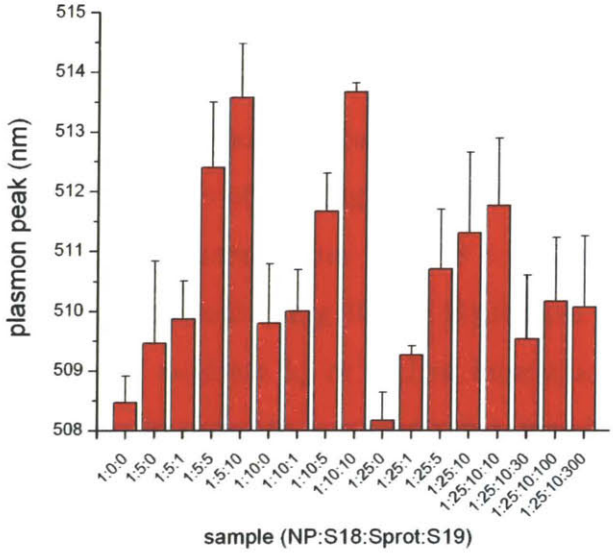

Figure 3-10: Surface plasmon resonance shifts for Au NPs with subsequent addition of S18, S-protein and S19 (NP:S18:S-protein:S19). The peak maxima of the surface plasmon resonance is determined by optical absorption spectroscopy for the different NP bioconjugates.

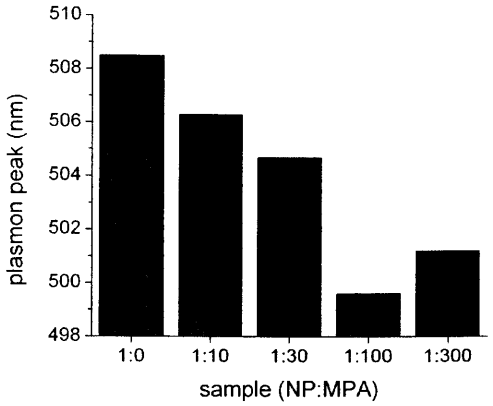

Figure 3-11: Surface plasmon resonance shifts for Au NPs with addition of mercaptopropionic acid (NP:MPA).

3.2.3 Isothermal titration calorimetry

To assay the thermodynamic properties of NP-protein conjugates, calorimetry can be performed. Differential scanning calorimetry can obtain the heat capacity (C_P) and enthalpy change (ΔH) of unfolding, as well as the melting temperature (T_m). This information can be used to understand the stability of proteins linked to NPs. In addition, isothermal titration calorimetry (ITC) can determine the thermodynamic parameters of interactions between NPs and proteins. ITC was used by Rotello *et al* [119] to quantify the thermodynamics parameters of binding of NPs to proteins. They found that the ΔH and ΔS of binding depend on the NP surface chemistry.

In a preliminary ITC experiment, 8nm NP-S18 complex (NP:S18 ratio of 1:60) were injected into a 1.4mL cell containing 100nM S-proteins. The shape of the titration curve did not allow to estimate k_d or ΔH of interaction between the NP-S18 complexes and S-proteins. In order to accurately measure k_d, the concentration of S-protein in the cell has to be of approximately $100\times k_d$ [120], which is well above the amount available for this study.

3.3 Enzymatic activity measurement

Activity of the NP-labeled RNase S is investigated. The bioconjugate is extracted from the gel in lanes 4 and 6 by spin centrifugation of gel slices and tested for activity by exposure to a substrate of a DNA oligo with a central RNA nucleotide, rU, the cleavage point for the enzyme: 5'-(6-FAM)-$(dA)_3$rU$(dA)_4$-(6-TAMRA)-3'. This FAM/TAMRA FRET pair enables fluorescence spectroscopy to probe strand cleavage. As the enzyme cleaves the strand at rU, FAM is no longer quenched by TAMRA, so FAM fluorescence increases. FAM emission of samples in 1× PBS is measured at room temperature on a Spex Fluoromax 3 fluorometer in a 3×3 path length quartz cuvette with sample volumes of 200μL. FAM fluorescence is performed by exciting at a wavelength of 490nm, and detecting emission at a wavelength of 515nm with excitation and emission slits at 1nm and 1nm.

Fluorescence increases with time for Au-RNase S (1:25:10) at 50nM with 15nM substrate, demonstrating activity of the RNase S (Figure 3-12). Kinetic analysis of the activity curves is performed using the equations

$$I = I_f - (I_f - I_0)exp\left[\frac{-k_{cat}}{K_M}[E]_{total}t\right] \tag{3.1}$$

for long times and

$$I = I_0 + (I_f - I_0)\left[\frac{-k_{cat}}{K_M}[E]_{total}t\right] \tag{3.2}$$

for the linear region at short times (inset, Figure 3-12). The derivation of those equations is shown in the Appendix A.

I_0 and I_f are the initial and final fluorescence intensities, respectively, and $[E]$ is the enzyme concentration. This yields a value for k_{cat}/K_M, the turnover rate per protein. However, protein concentration here cannot be accurately determined. Typically this is achieved by optical absorption, but the protein absorption at 280nm is superimposed on top of the NP spectrum. This is further complicated by the fact

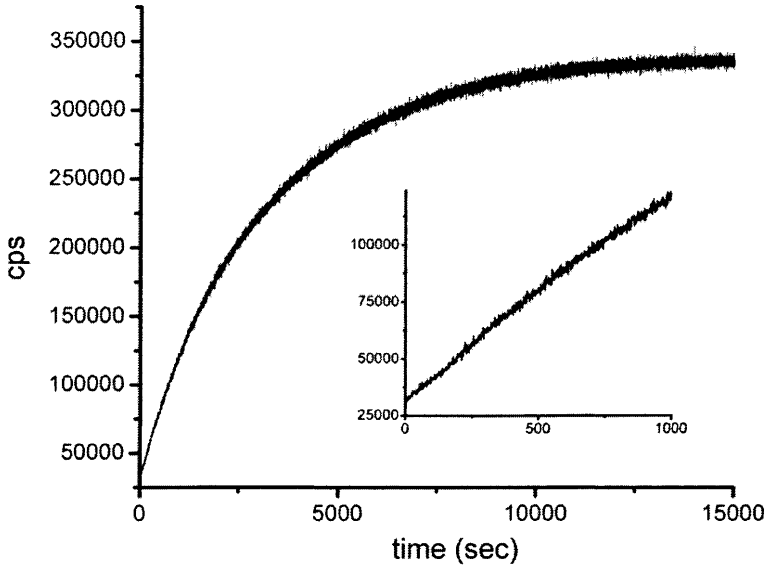

Figure 3-12: Enzymatic activity of NP:RNase S for the 1:25:10 (NP:S18:S-protein) sample. Fluorescence intensity vs. time for a 1:25:10 incubated with the substrate 5'-(6-FAM)-$(dA)_3$rU$(dA)_4$-(6-TAMRA)-3'. Inset: linear region at short times (0-1000 s).

that the protein molar extinction coefficient is at least two orders of magnitude lower than the NP, not accounting for the absorption of the NP ligand BPS. On the other hand, NP concentration can be determined using 2.5×10^6 $M^{-1}cm^{-1}$ at the plasmon peak absorption, in the range of 508-515nm, where the protein does not absorb. The NP extinction coefficient is obtained by calibration with known NP concentrations and correspondence with literature results. Therefore, a value for k_{cat}/K_M as the turnover rate per NP is reported. The k_{cat}/K_M is 1.39 $\pm$ 0.04 $mM^{-1}s^{-1}$ for the 1:25:1 sample and 7.8 $\pm$ 1.2 $mM^{-1}s^{-1}$ for 1:25:10, a 5.5$\times$ increase. k_{cat}/K_M of RNase S formed with S19 and S-protein under identical conditions is 580 $\pm$ 80 $mM^{-1}s^{-1}$, showing that labeling lowers enzyme efficiency by two orders of magnitude.

The lower turnover rate could be caused by several factors. First, the NP-RNase S conjugate has a net negative charge (as opposed to RNase S), so it is not electrostatically favorable for the negatively charged RNA molecules to bind to the complex. Also, the NP can bring steric hindrance near the active site of RNase S, which is

at the interface between the S-peptide and the S-protein. Finally, as absorption of proteins on solid surfaces is known to be a cause of protein unfolding [121, 122, 123], RNase S structure could be disturbed upon NP attachment.

Correspondence with the results from gel mobility allows estimation of the ratio of S-protein per NP. k_{cat}/K_M of the 1:25:10 sample that has been incubated with 50× S19 is 2,500 ± 600 $mM^{-1}s^{-1}$. This is largely a measurement of the activity of the S19-S-protein complex since the S19-S-protein activity is signicantly higher than the one from the S-proteins remaining on the NP-S18. This value implies that S19 can remove approximately 4-5 S-protein per NP. Based on the gel migration results in Figure 3-5, incubation of S19 with the 1:25:10 sample under identical conditions still leaves some S-protein bound to the NP-S18 complex. Assuming that 1:25:5 sample has as an upper bound of 5 S-proteins per NP, and noting that the relative position of the 1:25:10 + 50× S19 lies in between the 1:25:1 and 1:25:5 bands, it can be approximated that competitive binding with S19 leaves all but about 2-4 S-proteins per NP. Therefore, the 1:25 sample has the capacity to bind approximately 8 S-proteins per NP. Again, the observed increase in activity of only 5.5× between the 1:25:1 sample and the 1:25:10 instead of a 8× increase could possibly be explained by steric hindrance on the NP surface.

3.4 Summary

In summary, a strategy for labeling a protein by using its cofactor attached on the NP is described. Changes in electrophoretic mobility and shifts in plasmon resonance confirmed conjugation. Nonspecific adsorption arguments justify the first step of this approach, consisting of assembling a monolayer of mutated S-peptide (S18) on Au NPs. As steric effects are found to hinder the correct assembly of RNaseS on NPs, an optimum S18 coverage is determined. The protein remains active after labeling with the NP. The turnover rate is lower as a result of protein structural disturbance, crowding between the S18 on the NP surface, and/or electrostatic repulsion between RNA molecules and the conjugates which could impede the RNA in reaching the

active site. Further work include investigating structure of the protein, quantifying the NP:RNase S stoichiometry and characterizing the k_d of interactions between NP-S18/S-proteins.

Chapter 4

Site-specific labeling of cytochrome *c* with Au nanoparticles

Cytochrome *c* (cyt *c*) is a well-characterized model protein that is commonly used for NP-protein conjugates [34, 124, 125]. Its structure [126] and folding have been extensively studied, both experimentally [127, 128] and computationally [129, 130]. Furthermore, cyt *c* on charged surfaces has served as a model for studying how it interacts with charged transmembrane proteins. Because of its small size (approximately 100 amino acids), high stability and availability, this well-characterized model protein is an ideal candidate for conjugation studies. The structure and orientation of cyt *c* at the interface with NPs have been studied by others for electrostatically attached cyt *c* on Au NPs conjugates [34, 74]. However, in these experiments, cyt *c* was not site-specifically labeled, but was free to interact to the NP with multiple residues.

Here, the structure of cyt *c* is studied as it is linked covalently to 1.5nm Au NPs *via* a specific cysteine residue. The ligand chemistry and the site of attachment are both found to significantly affect the protein folding. Ligands of various charge (negative, positive and neutral) are used and the protein structure in each of the conjugates is probed by circular dichroism (CD) spectroscopy. The neutral ligand is found to be the best at keeping the protein folded. The conformational stability of cyt *c* site-specifically labeled at five different sites is analyzed. In addition to

CD spectroscopy, molecular dynamics (MD) simulations are performed in order to elucidate the atomistic details of the experimental observations.

It is found that electrostatic interactions play a role in destabilizing the protein structure. In addition, cyt *c* is found to be less stable when the NP conjugation site belongs to a domain critical for structural maintenance. These results show that the labeling position for a NP, a previously ignored factor, can be crucial in the biological function of a NP-protein conjugate.

4.1 Synthesis of 1.5nm Au nanoparticles

1.5nm diameter Au NPs were synthesized in toluene with triphenylphosphine (TPP) ligands following reported procedures [25]. Three different ligands were used to passivate the NP to permit water solubility and to change the charge on the NP surface (Figure 4-1): positively charged aminoethanethiol (AET), negatively charged bis(p-sulfonatopehnyl)phenylphosphine (BPS) and neutral hexaethyleneglycol thiol (PEG-SH). All three water soluble samples were obtained by ligand exchange into water from a single as-synthesized TPP-NP sample. A solution of ligand in water (50mM AET, 5mM PEG-SH or 200mM BPS) was vigorously mixed with the TPP-NP solution in toluene until the NPs exchange into the water phase. The exchange occured in the order of minutes for AET and PEG-SH, but took two days for the BPS because of lower affinity of phosphine for Au compared to thiol. Excess PEG-SH ligand was removed by dialysis. Excess BPS was removed by gel electrophoresis for studies on the effect of ligand, and by size-exclusion HPLC with TSK-gel G4000PW column for studies on the effect of labeling site.

TEM showed that the NPs had a diameter of 1.5 $\pm$ 0.2 nm (Figure 4-2). NP absorption spectra showed no plasmon peak, confirming that the NP size is below 2nm.

Inductively Coupled Plasma Optical Emission Spectrometry (ICP-OES) confirmed that the BPS coverage is comparable to the one reported for TPP on Au NPs of the same size, i.e. 21 ligands per NP [25]. BPS and NP molar ratios were measured

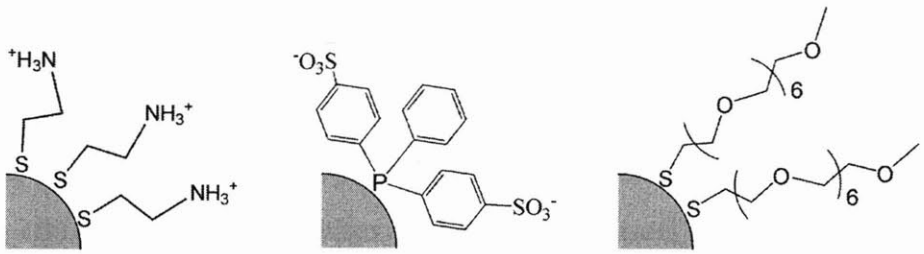

Figure 4-1: Chemical structure of the ligands at the surface of the AET NPs (left), BPS NPs (center) and PEG NPs (right).

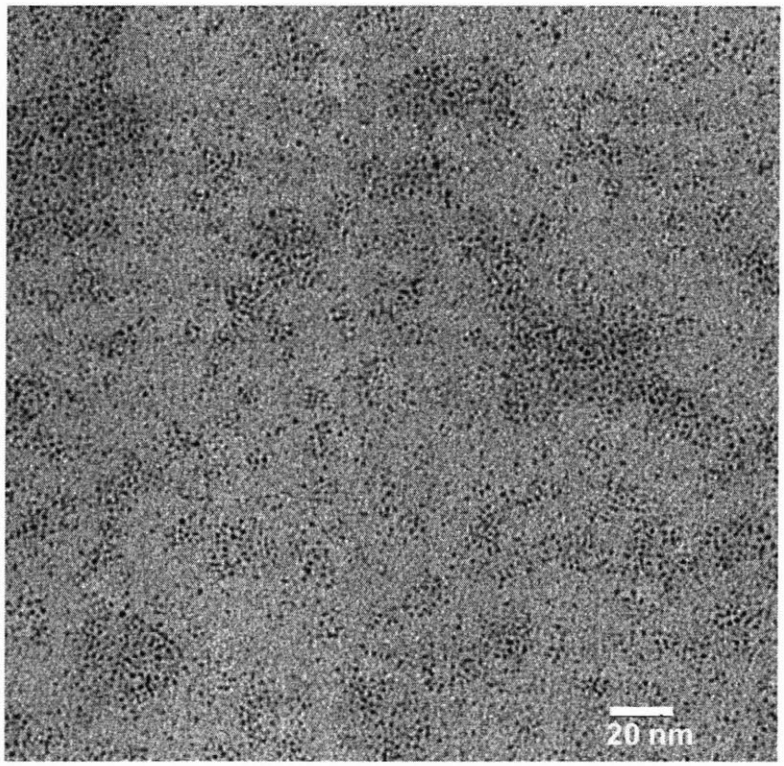

Figure 4-2: TEM picture of BPS NPs.

-5	*1*	*11*	*21*
TEFKA	GSAKKGATLF	KTRCLQCHTV	EKGGPHKVGP
31	*41*	*51*	*61*
ANIKKNVLWD	ENNMSEYLTN	NLHGIFGRHS	GQAEGYSYTD
71	*81*	*91*	*101*
PKKYIPGTKM	AFGGLKKEKD	RNDLITYLKK	ACE

Table 4.1: Amino acid sequence of yeast cyt *c*.

assuming 100 atoms per NP. Sulfur molar concentration was 2.2 times lower than gold molar concentration.

4.2 Conjugation of nanoparticles with cyt *c*

Cyt *c* from yeast *Saccharomyces cerevisiae* is conjugated to the NPs at cysteine C102 (Sequence in Table 4.1)[1]. Yeast cyt *c* has three cysteine residues (C14, C17 and C102). C14 and C17 are bound to the heme, thus only C102 is available for conjugation.

Purification of conjugates shows that linking to yeast cyt *c* is site specific. Purification of NP-yeast cyt *c* (NP-YCC) conjugates is achieved by reverse-phase HPLC or agarose gel electrophoresis. In each case, NPs are incubated with horse cyt *c* as a control for non-specific adsorption. Horse cyt *c*, while lacking C102, has a very similar structure, charge and sequence. Extinction coefficients of 106.1 $mM^{-1}cm^{-1}$ at 410nm for cyt *c* and 110 $mM^{-1}cm^{-1}$ at 420nm for NPs are used for concentration determination.

4.2.1 Site-specific attachment to AET nanoparticles

Reverse-phase HPLC is used to show attachment of yeast cyt *c* to AET NPs (Figure 4-3). After incubation of AET NPs with yeast and horse cyt *c* in a 10:1 NP:cyt *c* molar ratio, the samples are eluted in a wide pore C5 column (Supelco). From 1.0 min to 5.0 min, the elution gradient goes from 100% water to 60% water 40% acetonitrile.

[1]Reproduced in part with permission from M.-E. Aubin-Tam and K. Hamad-Schifferli, "Gold nanoparticle-cytochrome *c* complexes: the effect of nanoparticle ligand charge on protein structure," *Langmuir*, 2005, 21 (26) 12080 - 12084. Copyright 2005 American Chemical Society.

From 5.0 min to 35.0 min, the gradient goes from 60% to 55% of water. All solvents have 0.1% TFA in order to sharpen peaks and improve resolution.

AET-NP runs at 3 min 26 sec, yeast cyt *c* at 8 min 56 sec, and the NP-YCC complex at 8 min 34 sec without any unlabeled yeast cyt *c* at 8 min 56 sec. The absorption spectrum of NP:YCC taken at 8 min 34 sec shows a Soret band at 395nm indicative of the presence of yeast cyt *c* on top of a broad curve similar to that observed for AET-NP (Figure 4-4). The absorption spectrum taken at 8 min 56 sec is also a signature of the conjugate indicating that all yeast cyt *c* are labeled. To evaluate non-specific adsorption, AET-NP:HCC conjugates were compared. The elution curve of AET-NP:HCC lacks peaks aside from free AET-NP and free HCC at 9 min 06 sec (Figure 4-3). The absorption spectrum at 9 min 06 sec lacks NP features (Figure 4-4), indicating that no complex is made. This is most likely due to strong electrostatic repulsion between the AET-NP and the HCC. Therefore, under these conditions non-specific adsorption between AET-NP and cyt *c* is avoided and AET-NP:YCC is most likely site-specifically labeled. AET-NP:YCC complexes were collected, lyophilized and redissolved in 40mM phosphate buffer (pH 6.5) for UV-vis and CD spectroscopy. The absorption spectrum of the purified resuspended conjugate (Figure 4-4, thick line) shows a red-shift of the Soret peak from 395nm to 408nm due to acidity change.

4.2.2 Site-specific attachment to BPS nanoparticles

Agarose gel electrophoresis was used to show site-specific attachment of yeast cyt *c* to BPS NPs. Figure 4-5 shows a 3% gel for separation of BPS-NP incubated with yeast or horse cyt *c* in a ratio of 1:2 (NP:cyt *c*). The running buffer was 0.5 × TBE and the field strength was 10V/cm. YCC (lane 3) and HCC (lane 5) run toward the positive direction (upward from the well) while BPS-NPs run in the negative direction (lane 1). The BPS-NP:YCC (lane 2) and BPS-NP:HCC (lane 4) complexes are retarded relative to BPS-NPs (selected areas in image). NP-cyt c conjugates have reduced gel mobility compared to free NPs because of their larger size and lower net charge. BPS-NP-CC complexes were cut from selected areas, filtered in centrifugal tubes, and

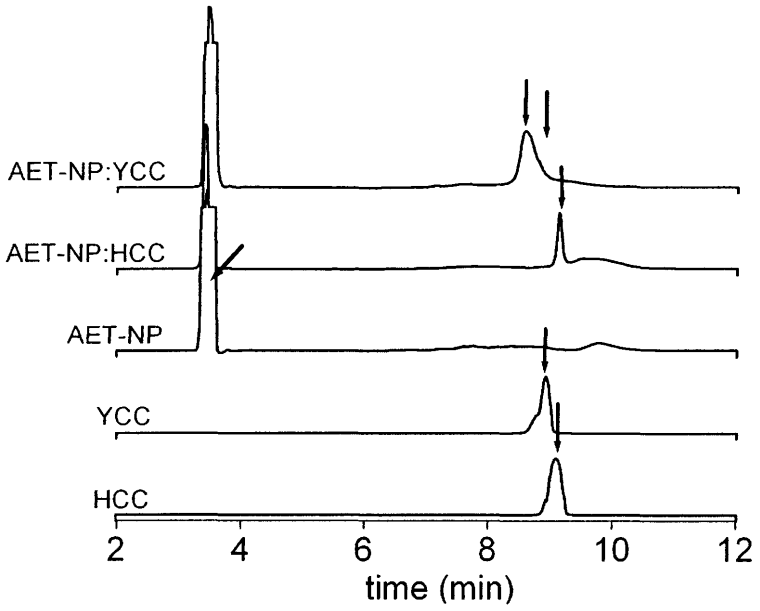

Figure 4-3: Reverse-phase HPLC purification of NP-cyt *c* complexes. Chromatograms of HCC, YCC, AET-NP, AET-NP:HCC and AET-NP:YCC at Soret band wavelength (395nm). A break was introduced in the y-axis for better visualization of cyt *c* peaks.

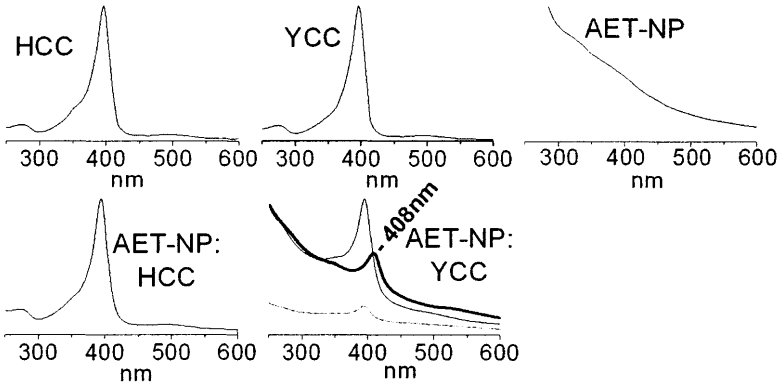

Figure 4-4: Absorption spectra at elution time indicated by arrows in Figure 4-3. AET-NP:YCC absorption spectra also shows the absorption at 8 min 56 sec, the eluting time of YCC chromatogram peak (dashed gray line), and the absorption of purified AET-NP:YCC resuspended in 40mM phosphate buffer (thick black line).

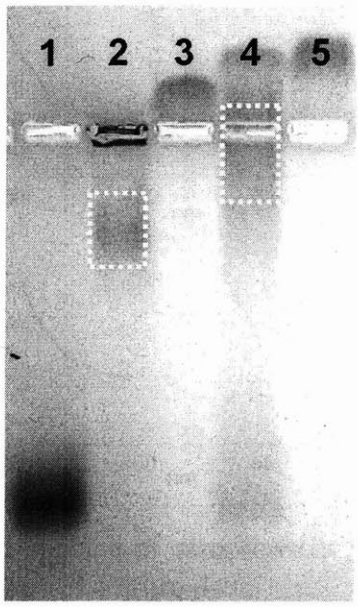

Figure 4-5: Gel electrophoresis of BPS-NP (lane 1), BPS-NP incubated with YCC (lane 2), YCC (lane 3), BPS-NP incubated with HCC (lane 4), and HCC (lane 5).

analyzed by UV-vis spectroscopy (Figure 4-6). Both YCC and HCC complexes show a Soret band and a broad absorption band due to the NP. The attachment of the positively charged horse cyt *c* on the negatively charged NP surface is governed by Coulombic interactions [131, 132, 133]. The absorption spectra indicate that there is a NP:cyt *c* ratio of 1:1 in the purified complexes.

To check if the NP is site-specifically and covalently labeled and not non-specifically adsorbed onto the protein, the conjugation of yeast cyt *c* and horse cyt *c* to NPs is compared in presence of 1M NaCl (Figure 4-7). Conditions under which yeast cyt *c* form conjugates to the NPs with higher yields than horse cyt *c* are determined. The NP:cyt *c* incubation ratio was 1.5:1 which ensures that there is at most one protein per NP.

Lane 1 of the gel in Figure 4-7 contains free NPs which run towards the anode. Lanes 2 and 3 have respectively yeast and horse cyt *c* incubated with the NPs in 0.5× TBE. As observed in Figure 4-5, both yeast and horse cyt *c* are attaching to the NPs, as evidenced by the appearance of a lower mobility band in both lanes. The gel with lanes 1'-3' is blue stained for proteins (with SimplyBlue SafeStain, Invitrogen). It confirms the presence of proteins in the lower mobility bands and shows that all cyt

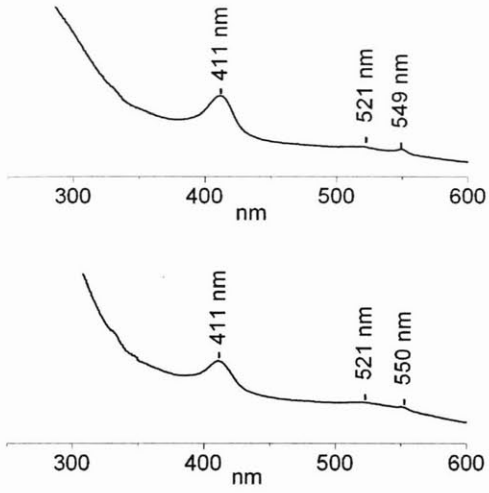

Figure 4-6: UV-vis absorption spectra of sample extracted from the selected area in lane 2 (bottom) and lane 4 (top) of Figure 4-5.

c are NP-labeled as no band runs toward the cathode.

Lanes 4-6 of Figure 4-7 are the same samples but in presence of 1M NaCl. The efficiency of horse cyt *c* labeling is reduced, likely due to salt screening, but the labeling efficiency of yeast cyt *c* is unaffected. This is illustrated by a protein band upon blue staining that runs towards the cathode. Absorption spectra of the bands A and B in lane 6' confirm the presence of unlabeled horse cyt *c* running towards the cathode (Figure 4-8), as evidenced by an absorption feature at 410nm that is assignable to the Soret peak and the absence of the broad band absorption of NPs. Also, there is an increased intensity of the naked NP band at higher mobility in lane 6, compared to lane 5 that has the NPs incubated yeast cyt *c*. This shows that in 1M NaCl, attachment to the NP occurs with a higher yield for yeast cyt *c* than for horse cyt *c*, which indicates that the conjugation is covalent for yeast cyt *c* and is most likely targeted to the surface Cys residue that forms a thiol-Au bond with the NP.

4.2.3 Site-specific attachment to PEG nanoparticles

Figure 4-9 shows gel electrophoresis of PEG-NP incubated with cyt *c* in a 1:10 ratio. The PEG-NPs run upwards from the well and are net positively charged (lane 1), as

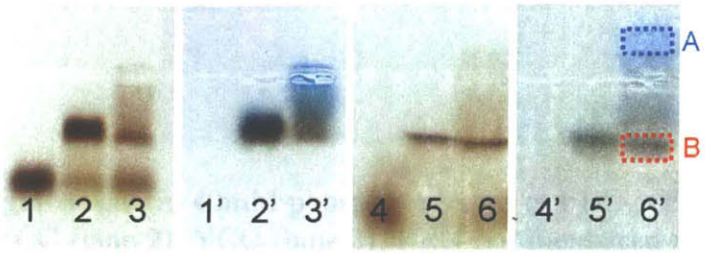

Figure 4-7: Effect of salt on the yield of NP labeled yeast and horse cyt *c*. Agarose gel electrophoresis of NP alone (lane 1), NP incubated with yeast cyt *c* (lane 2) or horse cyt *c* (lane 3) in 0.5× TBE buffer. Lane 3-6 are *idem* with 1M NaCl. Lanes 1'-6' are after blue staining for proteins.

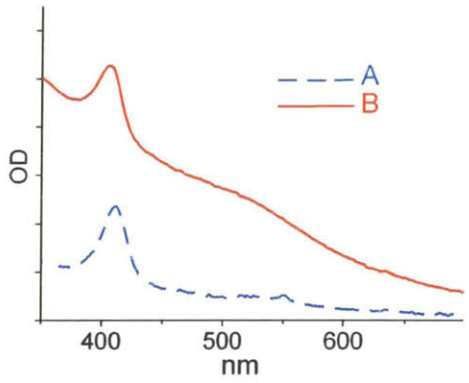

Figure 4-8: Absorption spectra of samples extracted from gel areas A and B shown in Figure 4-7. Absorption of NP-cyt *c* conjugates (solid line) is the sum of a Soret peak at 410 nm due to cyt *c* and a broad absorption band due to NPs.

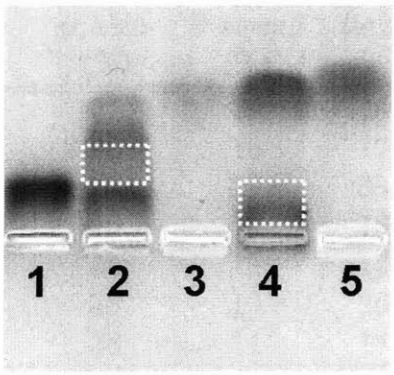

Figure 4-9: 2% agarose gels in 40mM phosphate buffer of PEG-NP (lane 1), PEG-NP incubated with YCC (lane 2), YCC (lane 3), PEG-NP incubated with HCC (lane 4), and HCC (lane 5).

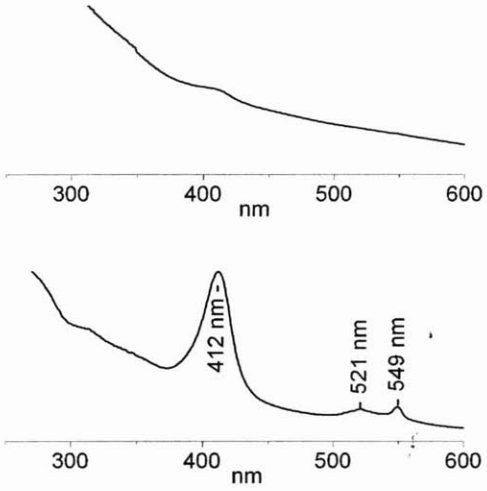

Figure 4-10: UV-vis absorption spectra of sample extracted from the selected area in lane 2 (bottom) and lane 4 (top) of Figure 4-9.

observed before [23].

Because both PEG-SH and the original ligand the NP was synthesized in (TPP) are neutral, we conclude that the net charge is probably due to Au surface atoms. This results in a situation in which the NP surface is charged but the ends of the ligands are neutral. YCC (lane 3) and HCC (lane 5) run further towards the negative electrode than the PEG-NP. The absorption spectra of the area selected in lane 2 (PEG-NP:YCC) shows a Soret band and a broad NP absorption, indicating that a complex is formed with a NP:YCC ratio of approximately 1:3 (Figure 4-10). HCC incubated with the PEG-NP does not show a band in between the free HCC and

	α *helix* (%)	β *strand* (%)	*turns* (%)	*unordered* (%)
YCC	35	11	18	35
YCC dimers	30	16	17	36
AET-NP-YCC	7	21	34	20
BPS-NP-YCC	19	16	16	49
PEG-NP-YCC	35	13	17	36
HCC	38	10	20	33
BPS-NP-HCC	38	14	18	31

Table 4.2: Secondary structure of cyt *c* and NP-cyt *c* conjugates.

free NP band (Figure 4-9, lane 4). The NP band is slightly retarded, indicating that some protein may nonspecifically adsorb on the NP surface. However, UV-vis of the NP band (selected area in lane 4) shows that the concentration of PEG-NP-HCC is negligible (Figure 4-10).

4.3 Structure of nanoparticle-cyt *c* conjugates

The effects of NP conjugation on the structure of cyt *c* are studied *in vitro* with circular dichroism (CD) spectroscopy, and *in silico* by molecular dynamics (MD) simulations. The position of the labeling site is changed by inserting cysteine mutations elsewhere in yeast cyt *c*. Both the NP ligand charge and the position of the labeled residue are found to have major impact on the structure of the protein. CD measurements are carried out at 25°C on an Aviv Model 202 using a 1mm path length quartz cuvette. Spectral deconvolution is resolved using CDSSTR secondary structure algorithm [134].

4.3.1 Effect of nanoparticle ligand charge on cyt *c* structure

CD spectroscopy provides a measure of the structure of the purified NP-cyt *c* conjugates with the three different ligands (Figure 4-11 and Table 4.2)[2].

[2]Reproduced in part with permission from M.-E. Aubin-Tam and K. Hamad-Schifferli, "Gold nanoparticle-cytochrome *c* complexes: the effect of nanoparticle ligand charge on protein structure," *Langmuir*, 2005, 21 (26) 12080 - 12084. Copyright 2005 American Chemical Society.

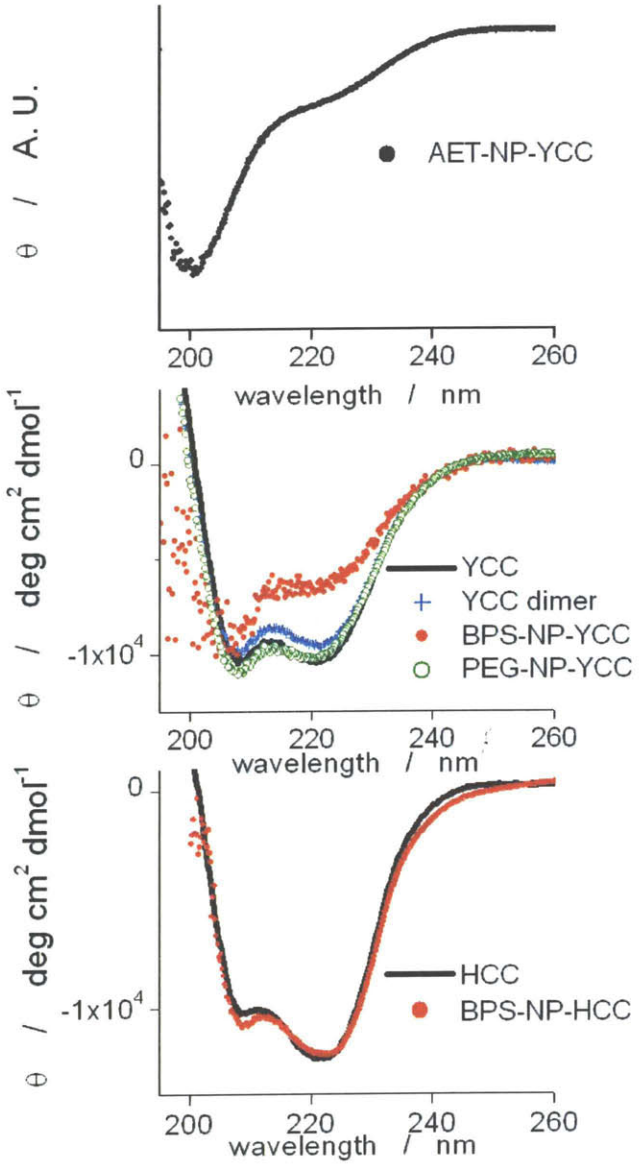

Figure 4-11: Circular dichroism spectra of cyt c on NPs with ligands of different charges.

Because C102 of YCC is buried in a hydrophobic pocket, exposing it for conjugation could perturb the structure of the protein, especially the α-helix it resides in. Therefore, CD spectra of NP-YCC are compared with YCC-YCC dimers. The dimers are obtained by incubating YCC with 20× copper sulfate in 200mM ammonium acetate during 5 hours at room temperature [135]. Figure 4-11 shows CD spectra of YCC and YCC-YCC in 40mM phosphate buffer of pH 6.5. Far UV CD spectrum of the dimer is predominantly α-helical and similar to monomeric YCC, with ellipticity minima at 222nm and 208nm. Spectral deconvolution shows a slight decrease in α-helicity upon dimerization from 35% to 30% (Table 4.2). Structural changes upon YCC dimerization have been also observed in the Soret region previously.

When attached to AET NPs, the CD spectrum of YCC changes dramatically by loosing the minima at 222nm and 208nm and exhibiting a minimum at 201 nm. This spectrum is characteristic of a random coil. Spectral deconvolution reveals that YCC α-helicity decreases to 7% (Table 4.2). Denaturation is most likely due to electrostatic repulsion between the NH_3^+ endgroups of AET and the numerous positive residues of the YCC. The CD signal is reported in arbitrary units (A.U.) as it was not possible to use the absorption at 410nm to calculate protein concentration accurately. We observe that the protein concentration is greater than heme concentration, most likely because of apocyt c present in the solution. Excess AET in the solution could remove the heme because of the high thiol concentration. This could also contribute to YCC denaturation, as well as the low pH of the HPLC purification conditions.

When YCC is attached to BPS-NP, α-helicity decreases to 19% (Table 4.2). HCC is known to non-specifically adsorb onto negatively charged NPs while retaining its structure [74], which is also observed here (Figure 4-11, bottom panel). Spectral deconvolution shows 38% α-helicity for both BPS-NP-HCC and unlabeled HCC. It is hypothesized that because HCC is not constrained to link to the BPS-NP at a specific site, it can adsorb in such a way that the protein structure is retained. Evidently, when forced to link by C102, the protein puts charged residues in proximity of the negatively charged BPS and thus distorts. Denaturation is less than for AET-NP:YCC, though it is still significant.

Finally, PEG-NP linked to YCC exhibits almost no denaturation (35% α-helix), with a structure closer to monomeric YCC (Figure 4-11, open green circles). Interestingly, NP with a neutral ligand causes less structural distortion than dimerization with another positively charged YCC. Evidently, the neutral PEG ligand cannot interact electrostatically with charged groups on the YCC. Although PEG-NPs are positively charged, their very low gel mobility indicates a lower charge density than BPS-NPs. Furthermore, as the positive charges are on the NP surface, they are further from the protein surface than in the case of AET-NP:YCC complexes. Therefore, the effects of the NP charge are lessened.

For all the spectra, CD deconvolution found β-strand contents in the samples. However, cyt c has only four residues that are part of β bridges. CD deconvolution of α-helical proteins spectra was found before to overestimate the β-sheet content [136, 137]. This was presumed to be a consequence of the smaller CD signals of β-sheets compared to α-helices above 195nm. However, the estimate of α-helix is found to be reliable [136].

4.3.2 Effect of nanoparticle labeling position on cyt *c* structure

Site-directed mutagenesis has inserted Cys mutations on different motifs of yeast cyt c [138, 139]. Details of protein expression and purification are in Appendix B. 1.5nm Au NP coated with BPS ligands are covalently linked to wild type yeast cyt c (having C102) and four other mutants (H39C, D50C, E66C and K99C) (Figure 4-12). BPS is chosen, because it partially unfolds cyt c when attached at C102 as shown in section 4.3.1. The Cys mutations are distributed throughout the surface of the protein on different motifs (39 = Loop B, 50 = Loop C, 66 = 60s helix, 99 and 102 = C-terminal helix). C102 is replaced with a serine in the four cyt c mutants. In addition, as *S. Cerevisiae* cyt c expressed in *E. coli* lacks the trimethylation at Lys72 that is found in the native protein, the K72A mutation was necessary for preventing the heme from binding to Lys72 [140]. Pletneva *et al* [139] have found

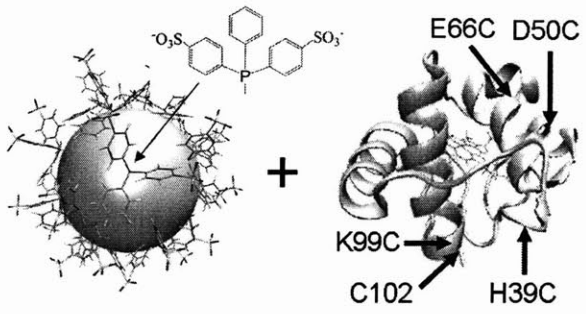

Figure 4-12: Labeling yeast cyt *c* (right) with 1.5nm Au NP with BPS capping groups (left). The positions of labeled Cys in all the mutants and in wild type are marked by arrows.

that the mutations (H39C/K72A/C102S, D50C/K72A/C102S, E66C/K72A/C102S and K72A/K99C/C102S) do not significantly perturb the folding of the protein into its native structure. K99C was tested in addition to C102 since C102 is buried in a hydrophobic pocket, while K99 is exposed to the solvent. Exposing C102 for conjugation can perturb the structure of the protein, as observed for the yeast cyt *c* dimers.

CD spectroscopy confirms that all unlabeled mutants are fully folded (Figure 4-13a) as reported before [139]. Figure 4-13bc shows the CD spectra of unlabeled wild type (WT) yeast cyt *c* (line) and of each of the mutants and WT conjugated to the NPs in 10 mM NaPi pH 7.3 with and without 0.1 M NaCl. The NP contribution to the CD signal is subtracted and the CD spectra of NP-cyt *c* conjugates are normalized to θ_{206}=-9.5$\times 10^3$ deg cm^2 dmol^{-1}. When cyt *c* is melted, an isodichroic point is found at θ_{206}. Glycerol-induced denaturation leads to the same isodichroic point [141]. As the cyt *c* concentration in the NP:cyt c solutions could not be computed with high precision from the absorption spectra because of NP absorbance in the Soret region, the CD spectra of NP-cyt *c* conjugates are normalized to this isodichroic value.

NP conjugation results in structural disturbance for all the proteins, as evidenced by an increase in the molar ellipticity at 222 nm, θ_{222}, as well as a decrease in α-helical content (Table 4.3). We find that the choice of labeling site for the NP can have a profound influence on the protein structure, which lead to different degrees

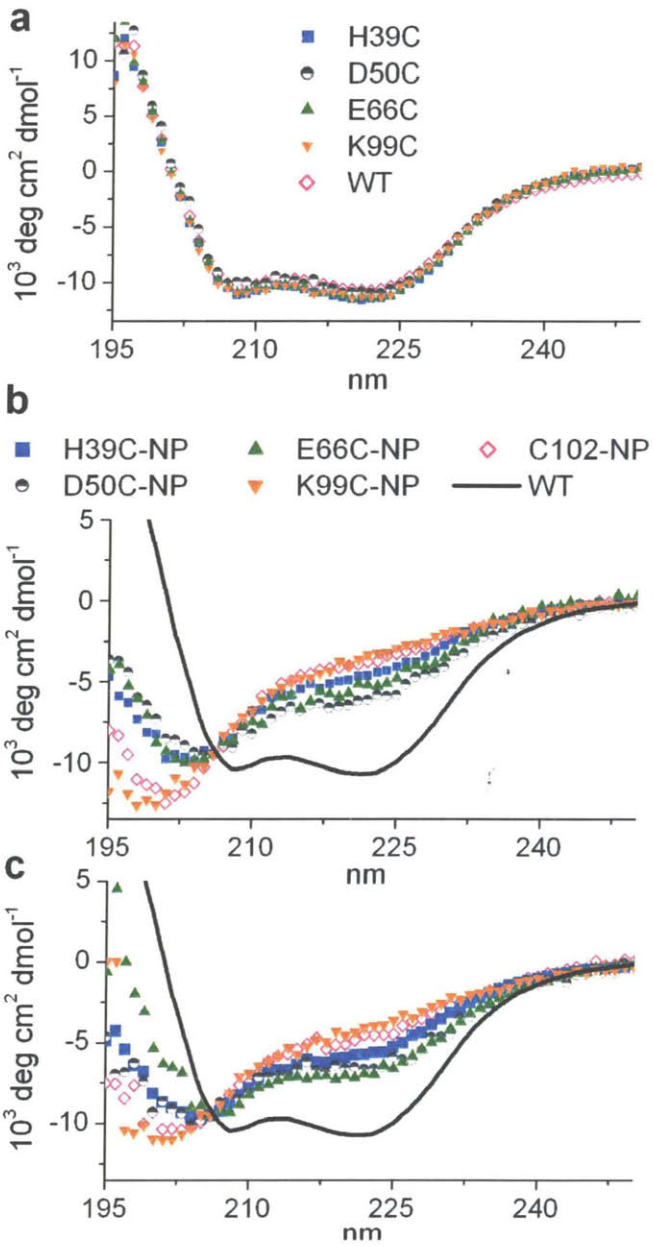

Figure 4-13: Circular dichroism spectra of: a) WT and mutants, b) NP-labeled WT and mutants with no salt, and c) with 0.1M NaCl.

Conjugate	*without salt* (%)	*with 0.1M NaCl* (%)	$\Delta\alpha$-*helicity* (%)
H39C-NP	7.3	15.6	8.3
D50C-NP	16.2	17.5	1.3
E66C-NP	7.7	20.7	13.0
K99C-NP	4.8	6.1	1.3
C102-NP	5.6	6.9	1.3

Table 4.3: α-helical content of NP-labeled cyt c and change in α-helicity in presence of 0.1M NaCl.

of denaturation. The % α-helicity for each of the conjugates is different, ranging from 4.8% to 16.2% (Table 4.3), demonstrating that denaturation is strongly affected by where on the protein the NP is covalently linked. The α-helicity of BPS-NP-YCC(C102) reported in section 4.3.1 is higher because of different NP:YCC labeling conditions (different buffer and NP:cyt c incubation ratio). In addition, here YCC were incubated with 1mM DTT prior to labeling in order to break YCC dimers and expose the Cys for conjugation. The protein is more disturbed when the NP is attached to the C-terminal helix (K99C-NP and C102-NP). In the absence of salt, the D50C-NP conjugate retains its α-helicity the most. With 0.1M NaCl, folding improved in all cases to a different degree. The amount of structural recovery for each of the conjugates is different, with $\Delta\alpha$ ranging from 1.3% to 13.0% (Table 4.3). The improvement was only minimal for D50C, K99C, C102, while H39C and E66C benefited the most.

4.4 Molecular dynamics simulations of nanoparticle-cyt c conjugates

Molecular dynamics (MD) simulations yield insight on the molecular interactions involved and help explaining the results of CD spectroscopy. Experimental methods to probe individual NP-protein interactions (e.g. IR, Raman, and NMR) are limited, as they require high amount of sample and the NPs often contribute to spectral dampening and broadening. Therefore, MD simulations are a natural complement to

ensemble spectroscopic techniques like CD spectroscopy in order to yield insight on the molecular interactions involved in NP induced structural disturbance. Peptides and proteins were simulated before on flat surfaces [142, 143]. For example, YCC was tethered to an alkanethiol self-assembled monolayer (SAM) by covalent disulfide bonding between the thiol of C102 and a thiolated alkanethiol. Simulations of hydrophobic and hydrophilic SAMs showed that the hydrophilic SAM interacts more with the protein [143].

Simulations of proteins on NP surfaces are more challenging. Several complex interactions occur between the NP core, the NP ligands, and the protein side-chains. The nature of the interactions between metal surfaces and amino acids are not completely understood. Furthermore, simulating all the NP atoms with its ligands results in computationally expensive simulations, especially for large NPs. Molecular dynamics simulations of NPs with ligands have been done mostly for small (diameter of less than 2nm) Au NP with simple alkanethiol ligands [144, 145, 146]. Simulations of SAMs of alkanethiols on NPs and flat surfaces showed that the structure of the SAM depends strongly on the alkanethiol chain length, the surface curvature and the temperature [145]. In particular, the SAM is more tilted on NPs compared to flat surfaces. Additionally, the ligand density is found to vary on the NP surface. The thiolate chains located near the edges of the NP faces are more extended and accessible to the outside [146]. Interestingly, this is also where ligand exchange is believed to take place [30].

Here, MD simulations are performed in order to elucidate atomistic details of the structure and stability of NP-cyt *c* conjugates (methods for MD are in Appendix C) [147]. The NP is modeled as a 1.5 nm diameter dummy atom with 21 BPS ligands distributed on its surface. It is assumed that the protein displaces one BPS ligand from the NP surface when it forms a thiol bond with Au, resulting in 20 BPS ligands in the NP-protein conjugates.

MD simulations are run for 8ns at 300K. As unfolding of proteins on NP surfaces can take up to hours [91], the temperature is raised to 450K to accelerate unfolding [148]. A temperature of 450K is chosen as unlabeled yeast cyt *c* remains folded at

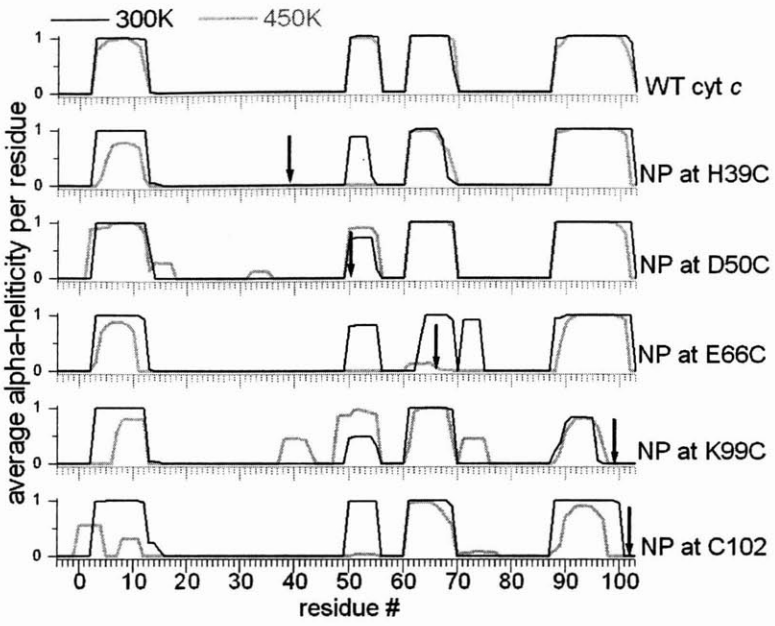

Figure 4-14: Comparison of α-helicity. Secondary structure is averaged over the last 500ps of simulations at 300K and at 450K. Arrows indicate the labeling sites of the NPs.

that temperature over the course of the simulations. Figure 4-15 shows snapshots of the protein conformation at the end of the simulations at 300K and at 450K, with the NP removed for clarity. The program VMD was used to generate this figure [149]. The secondary structures of cyt c are perturbed differently depending on the NP attachment site.

To compare the simulations directly with experimental results, the average α-helicity of each residue is calculated (Figure 4-14) using STRIDE [150]. NP labeling of residue 66 perturbs the 60's helix, while labeling residues 99 and 102 perturbs the N-helix and the C-helix, showing that generally the NP disturbs the α-helix on which it is attached, and often other portions of the protein.

Electrostatic effects

Figure 4-17 shows that side-chains of positively charged residues interact with BPS ligands. Those electrostatic interactions are believed to partipate to protein unfolding. After building the protein-NP conjugate and performing initial minimization, the distances of charged residues from the NP surface are calculated (Figure 4-16). During

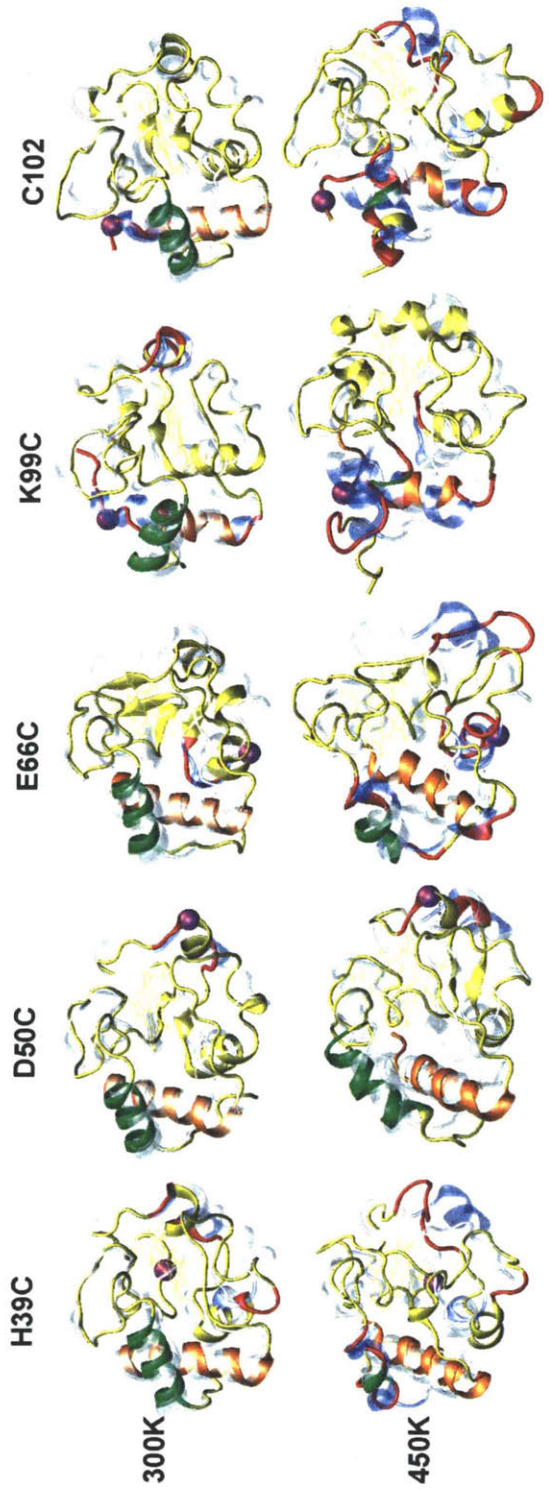

Figure 4-15: Snapshots of protein structure at the end of MD simulations at 300K and 450K. The N-helix is represented in green, the C-helix in orange, and unfolded α-helices in red. Folded cyt c is superimposed in white. The purple sphere indicates NP attachment site.

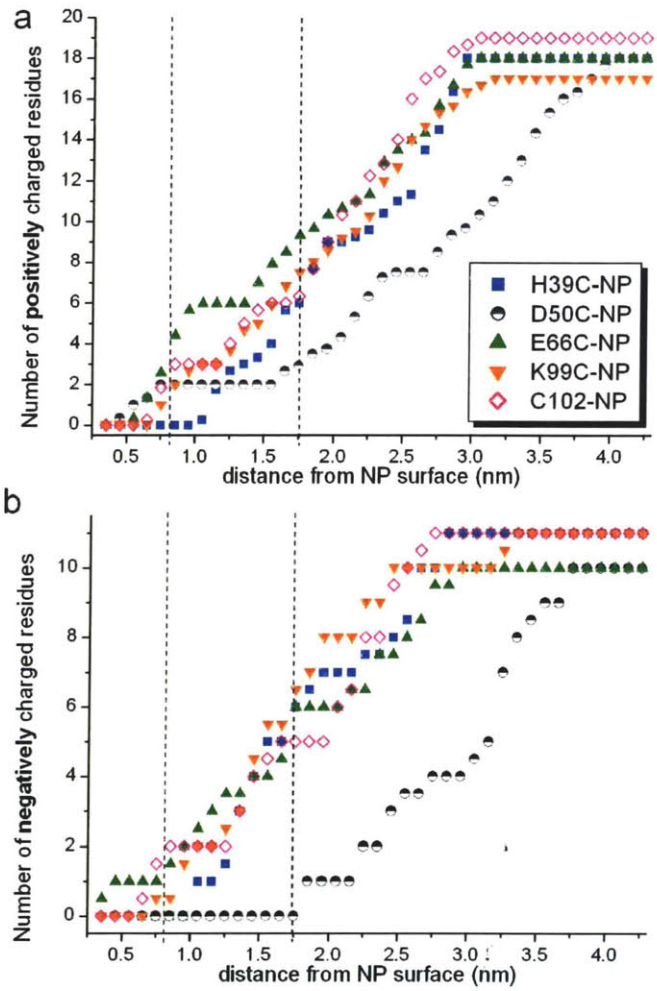

Figure 4-16: Distribution of (a) positively and (b) negatively charged residues around the NP before the MD when the protein structure is intact. Dashed lines: Average distance of BPS O atoms from NP surface (8 Å) and one Debye length (9.6 Å) away from BPS O atoms at 0.1M NaCl.

the MD simulations at 300K, the negatively charged oxygen atoms of BPS molecules are found to be on average at 0.8 nm from the NP surface. The Debye length at that salt concentration is 0.96 nm. A large proportion of charged residues are screened at 0.1M NaCl, as they are located further than 1.76nm from the NP surface, i.e. further than 0.96nm from BPS oxygen atoms. NP-D50C conjugate has significantly fewer charges in the vicinity of the BPS molecules. Interestingly, this conjugate is also the most folded both experimentally and in simulations, as evidenced by least disturbance of the α-helices (Figures 4-14 and 4-15).

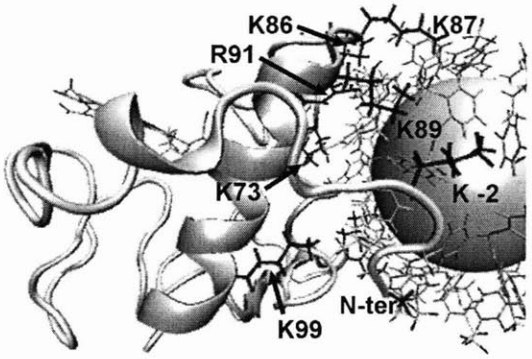

Figure 4-17: Interaction of positively charged side-chains with BPS molecules. The snapshot is from MD simulations of E66C-NP at 450K.

The present analysis confirms the local electrostatic effects observed in NP labeling of the wild type yeast cyt c observed when changing the charge of the NP ligand. It also indicates that based on electrostatic arguments alone, labeling sites with the least number of charged residues in the vicinity would result in the least amount of structural perturbation.

Labeling structures essential for folding

The different amounts of denaturation and recovery upon charge screening cannot be explained solely by electrostatics. In both experiments and MD, NP labeling of K99C and C102 results in strong denaturation of the protein which is barely improved by addition of salt ($\Delta\alpha = +1.3\%$). This contrasts with the labeled E66C mutant, which also has the surface Cys on an α-helical motif and has a similar number of charged residues as K99C, but retains significantly more of its structure in the presence of salt (7.7% versus 20.7% α-helicity). To understand this better, a description beyond simple local electrostatic interactions is necessary. MD simulations and previous studies on cyt c unfolding pathway helped describe this. When the NP is placed on positions 99 or 102, both of which are in the C-terminal α-helix, the N- and C-terminal helices are substantially distorted (Figures 4-14 and 4-15). This indicates that mere presence of the NP is a large enough perturbation to prevent these helices from folding properly. Folding studies of cyt c have shown that these positions are on a crucial

motif for folding, the C-terminal helix [151]. Through hydrogen exchange experiments on the folding of cyt *c*, it has been observed that the N- and C-terminal helices, known as the N-C foldon, fold first [127] and bind together by hydrophobic residues at their interface. Gly6, Phe10, Leu94 and Tyr97 are known to participate to the contact between the N- and C-terminal helices. Those are the only four conserved residues among known cyt *c* sequences that are not heme-binding residues [152], underscoring the importance of the N-C interface. Once the N-C foldon is locked in place, it guides the folding of the rest of the protein. Simulations also support this sequential stepwise folding pathway [129, 130]. The N-C helix foldon is crucial for the stability of the whole protein and mutations in either the N- or the C-terminal helices significantly affect folding [153]. In addition, this is the most stable part of the protein, and acts as a safety pin for the entire structure, while other motifs can denature easily without affecting the N-C helix foldon such as the 60's helix.

The hydrophobic cluster as the N-C interface is disrupted upon attachment of the NP on the N-C foldon (Figure 4-18). Therefore, the NP prohibits not only formation of the C-terminal helix but also the N-C helix contact, which affects the stability of the entire protein.

The H39C-NP and E66C-NP conjugates also showed substantial unfolding. MD simulations of these conjugates show that the N-terminal amino group and Lys-2 are close enough to the NP surface to form salt bridges with BPS molecules, which eventually lead to the disruption of the N-helix, as observed in Figure 4-17.

In contrast, NP labeling at position 50 does not affect the folding of the rest of the protein as dramatically, which is consistent with CD results. MD simulations show that the structure of the N-C helices is still maintained in these labeled mutants (Figures 4-15). Thus the disorder induced does not affect the N-C helix foldon and is more localized when the NP is attached on those sites.

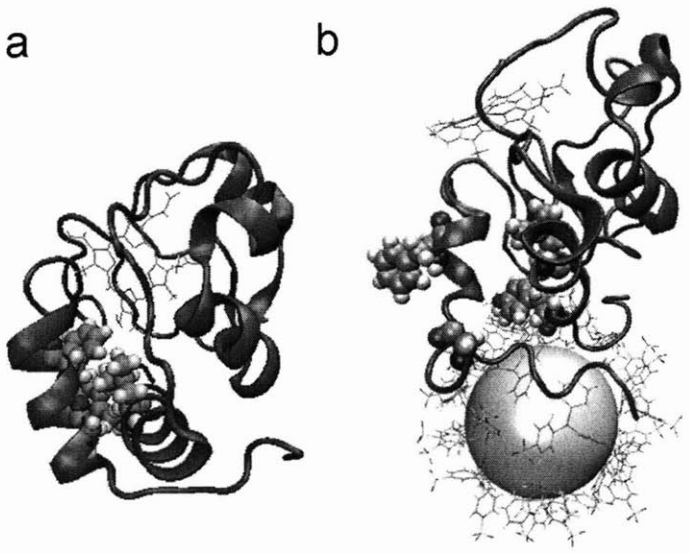

Figure 4-18: YCC structure with Van der Waals representation of Gly6, Phe10, Leu94 and Tyr97. a) YCC before NP labeling. b) Snapshot of MD trajectory at 450K of K99C-NP.

4.5 Probing the activity of nanoparticle-cyt *c*

Cyt *c* is an electron transfer protein. Its redox activity can be probed by electrochemical techniques. It is known that unfolded cyt *c* is more easily oxidized and has a lower heme redox potential compared to well-folded cyt *c* [154, 155].

Cyclic voltammetry (CV) can be used to measure the cyt *c* heme redox potential. Typically, a voltage is applied between a working electrode and a reference electrode in solution. The current flow between the working and counter electrodes is plotted versus the applied voltage. For this study, a working electrode made of a glass slide coated with indium tin oxide (ITO) with a resistance of 8-12 ohms is used. The ITO slides are washed in 20% (V/V) ethanolamine in Millipore water in ultrasonic bath at 80^{o}C during 30 minutes and rinsed with Millipore water. The ITO slides are then functionalized with 3-mercaptopropyl trimethoxysilane (MPTMS) by immersing the slides overnight in 5% (V/V) of MPTMS in methanol under argon atmosphere. Then, the slides are rinsed with ethanol and covered with a 100 μL drop of approximately 0.1mM BPS-NPs, BPS-NP-HCC or BPS-NP-YCC solution. CV curves are obtained at room temperature in a solution of 10mM KPi 0.1M NaCl at pH 7.3, with a platinum

wire counter electrode and a Ag/AgCl reference electrode.

Figure 4-19 shows the results of CV for NP-HCC conjugates immobilized on ITO. Voltage scan rate is 10mV/s from -0.4V to 0.4V versus Ag/AgCl. A reduction potential peak is present at 0.04V and an oxidation peak is at -0.08V. The CV midpoint potential E_m is -0.02V versus Ag/AgCl. This value is lower than the reported value of 0.06V for well-folded horse cyt *c* [108], which could be due to the protein being destabilized when it is in the vicinity of the NP or ITO-MPTMS surface.

Figure 4-20 shows the results of CV for NP-YCC conjugates immobilized on ITO. The voltage scan range is the same, but the rate is 100mV/s. A reduction peak is found at -0.12V and an oxidation peak at -0.22V. E_m is at -0.17V versus Ag/AgCl, which is significantly more negative than for horse cyt *c* on NPs. This is consistant with the CD results, showing structural deformation of YCC when site-specifically attached on BPS-NP.

From one ITO biofunctionalized slide to another, the height of the reduction and oxidation waves vary. In some CV experiments, the oxidation and reduction peaks were too small to accurately identify their position. Further characterization is needed in order to elucidate if this is due to a low density of conjugates adsorbed on the ITO-MPTMS surface, or to a significant proportion of proteins being electroinactive as observed before for YCC immobilized on self-assembled monolayers on Au [98]. AFM can be used to quantify conjugates density on the electrode surface [156]. In addition, running several CV experiments at various scan rates allow to calculate the density of eletroactive proteins, by using equation 4.1

$$I_p(r) = Nn^2F^2r/4RT \tag{4.1}$$

where I_p is the peak current, r is the voltage scan rate, N is the number of electroactive molecules, n is the number of electrons transferred per electroactive molecule (one for YCC), F is the Faraday constant, R is the gas constant and T the temperature.

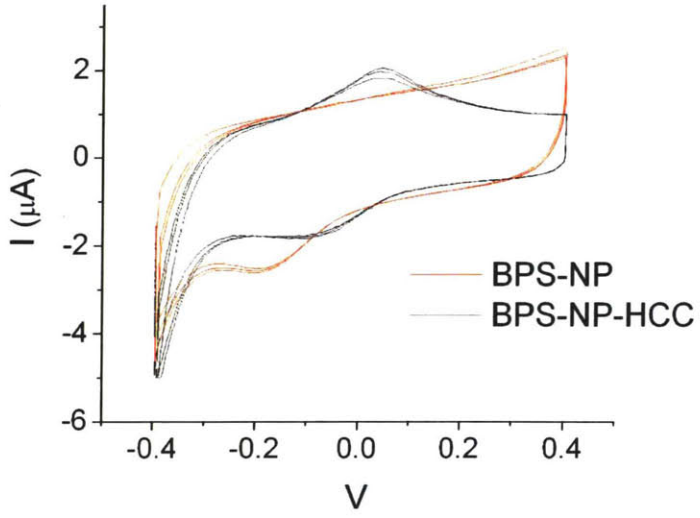

Figure 4-19: Cyclic voltammetry of NP-HCC conjugates and NPs immobilized on ITO.

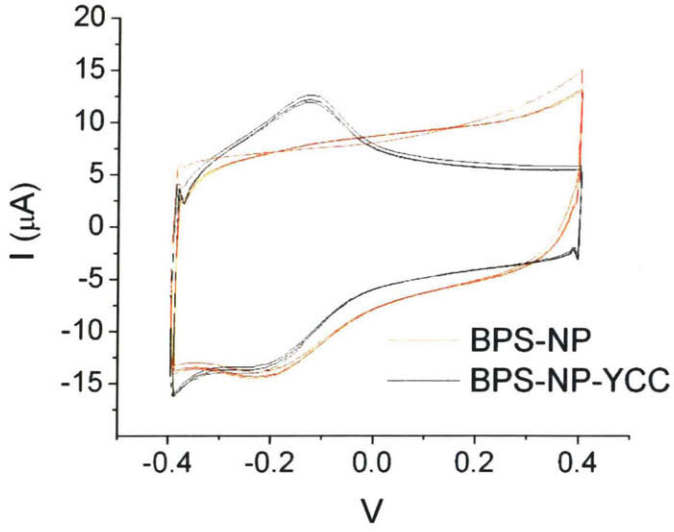

Figure 4-20: Cyclic voltammetry of NP-YCC conjugates and NPs immobilized on ITO.

4.6 Summary

In summary, it is observed that the charge of NP ligand endgroups significantly impacts the structure of a covalently attached, site specifically labeled protein. Au NPs with neutral PEG ligands linked to a specific cysteine of yeast cyt *c* are found to be ideal in maintaining a folded protein structure. Salt also helps in keeping the protein more folded. Therefore, electrostatic interactions of protein side-chains with the NP surface is a source of disturbance in the protein structure.

PEG ligands are also found to be able to block non-specific adsorption of horse cyt *c* on the surface of the NP. Only negatively charged NPs are linking to horse cyt *c*. The resulting BPS-NP-HCC conjugate keeps the protein well-folded as it is free to attach to the NP by any of its surface. Denaturation is more likely when the protein is forced to link *via* a specific amino acid which might be on a position that induces unfavorable NP-protein interactions.

The site of attachment can be controlled by inserting Cys mutations elsewhere on the surface of yeast cyt *c*. Attaching the NP in the vicinity of charged residues lead to more protein disturbance, which is consistant with the fact that denaturation is induced by electrostatic interactions with the structures nearest to the linking site.

It is also found that labeling structures that are crucial for proper folding is detrimental for the whole protein structure. However, if the NP is attached on flexible motifs, the disorder induced by the NP remains local.

Chapter 5

Cytochrome c - $CoFe_2O_4$ magnetic nanoparticle conjugates

Studies of magnetic NP-protein conjugates is of great importance, as bioconjugates of magnetic NPs are exceptionally promising for many applications in magnetic resonance imaging [3], biosensing [157], labeling, separation/capture/delivery of target molecules [158, 159], magnetic actuating of nano/microstructures [160], and hyperthermia [161, 162].

Interactions of protein side-chains with NPs is likely to depend on the NP material. In order to investigate this material dependance, cobalt iron oxide magnetic NPs are synthesized and conjugated with cyt c.

Au NPs have well-defined and controllable chemistry, and a wide variety of possible surface ligands. However, in comparison, surface modification of Fe-based magnetic NPs is not as versatile, so despite their utility in biology, analogous success with bioconjugation of magnetic NPs has not yet been achieved. Consequently, despite considerable advances made in the surface chemistry of magnetic oxide NPs [3, 163, 164, 165] conjugation to Fe-based NPs is not trivial, and much more challenging than for Au NPs [165, 166]. Also, Au NPs and Fe-based NPs have different affinity for protein side-chains, so we cannot assume that same rules are followed.

Therefore, in this thesis, the effect of labeling cyt c with $CoFe_2O_4$ NPs are explored. Yeast cyt c (YCC) is site-specifically labeled *via* covalent attachment of

cysteine (C102) with a free thiol of meso-2.3-dimercaptosuccinic acid (DMSA), the ligand at the surface of the NP (Figure 5-1). As a control for non-specific labeling, horse cyt *c* (HCC) is attached, similarly as in the work with Au NPs. HCC can only bind by non-specific adsorption of amino acid side chains on the surface of the NP core and/or electrostatic interactions with the negatively charged DMSA molecules. Protein attachment, protein secondary structure, and heme oxidation state are studied by gel electrophoresis, circular dichroism and optical absorption spectroscopies. Analogous surface modification strategies that have been successful for conjugation of proteins to Au NPs are used. Effects of NP surface functionalization with lysine (Lys) or hexapolyethylene glycol thiol (PEG-SH) are investigated. Structural behavior can be explained in terms of electrostatic effects and interaction of the carboxylic amino acids on the protein interacting with the Co and Fe atoms on the NP surface[1].

5.1 Synthesis and characterization of $CoFe_2O_4$ nanoparticles

$CoFe_2O_4$ NPs with oleic acid ligands are synthesized as described by Sun *et al* [167]. In summary, 1mmol of cobalt(II) acetylacetonate, 2mmol of iron(III) acetylacetonate, 10mmol of 1,2-hexadecanediol, 6mmol of oleic acid and 6mmol of oleylamine were mixed in 20mL benzyl ether under nitrogen and heated to 200°C for 2 hours. The mixture was then heated to reflux at approximately 300°C for 1 hour, and cooled down to room temperature. A black material was precipited with ethanol, and was resuspended in hexane in the presence of 50 μL oleic acid and 50 μL oleylamine. The resulting NPs were precipitated with ethanol and dissolved into toluene. This resulted in $CoFe_2O_4$ NPs of 6.4 $\pm$ 0.7 nm (Figure 5-3).

Then, the NPs were solubilized in water via ligand exchange with DMSA. The ligand exchange was done by vortex mixing 490 μL of NPs in toluene with a fresh

[1]Reproduced in part with permission of The Royal Society of Chemistry from: M.-E. Aubin-Tam, H. Zhou and K. Hamad-Schifferli, "Structure of cytochrome *c* at the interface with magnetic $CoFe_2O_4$ nanoparticles," *Soft Matter*, 2008, 4, 554-559. Copyright 2008 The Royal Society of Chemistry.

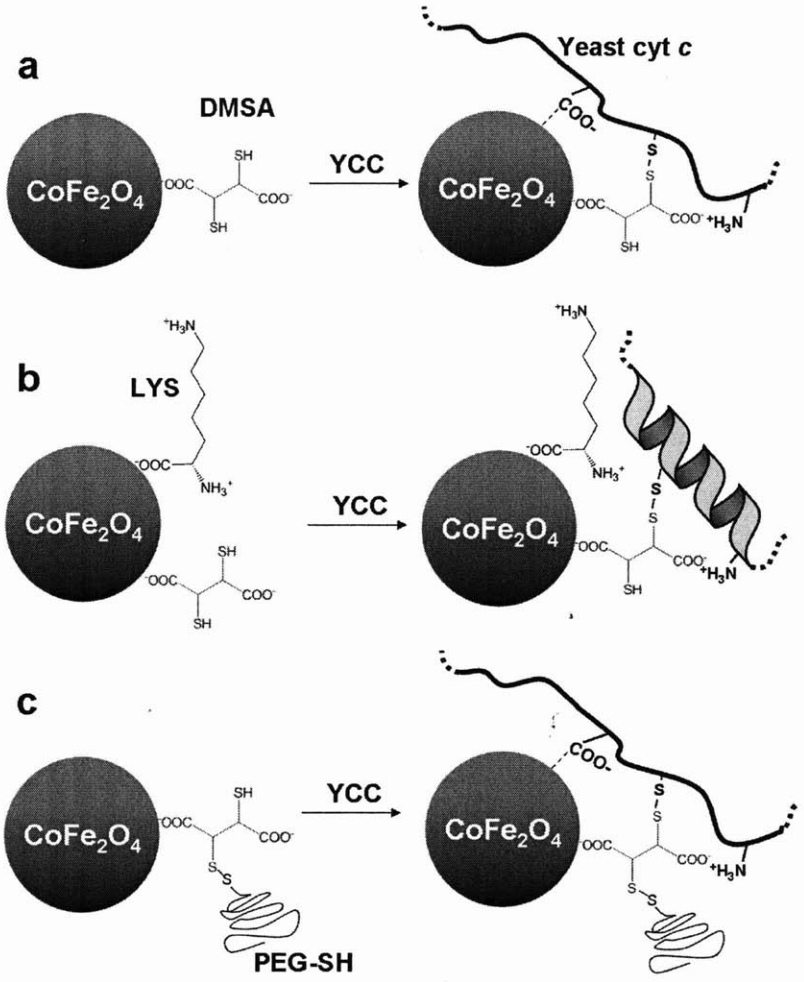

Figure 5-1: Scheme of site-specific covalent attachment of yeast cyt c to DMSA $CoFe_2O_4$ NPs. The NP is linked to cysteine C102 on the protein surface via a dithiol cross-linkage with free thiol of DMSA molecules (a). To further explore the NP-protein interface, NP is co-functionalized with Lys (b) or PEG-SH (c), and then incubated with the protein.

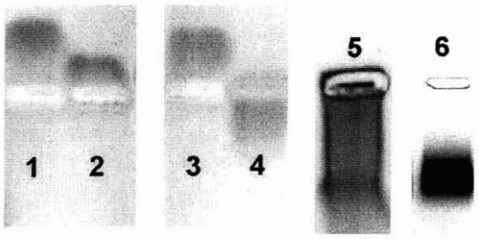

Figure 5-2: 1% agarose gel electrophoresis of HCC (lane 1), YCC (lane 2), HCC incubated with DMSA (lane 3) and YCC incubated with DMSA (lane 4). Lanes 5 and 6 contain respectively $CoFe_2O_4$ NPs before and after β-mercaptoethanol treatment.

solution of 200 gL^{-1} meso-2,3-dimercaptosuccinic acid (DMSA) in dimethyl sulfoxide during 24 hours. The NPs precipitated after ligand exchange.

Control of NP surface chemistry is key for increased NP stability and successful bioconjugation. As-prepared suspensions of $CoFe_2O_4$ NPs in water are found to result in broad gel bands (Figure 5-2, lane 5) and to aggregate and precipitate within hours. Also, excess DMSA can interact with YCC by dithiol formation between the DMSA and C102, causing the positively charged proteins to run towards the positive electrode, in the same direction as the NPs and the NP-YCC complexes (Figure 5-2, lane 4). Both of these effects would prevent the use of gel mobility shifts to characterize conjugation.

To prevent aggregation and improve stability, the NPs are treated with excess β-mercaptoethanol and magnetically purified. The NPs precipitate is resuspended in water in the presence of 0.3M β-mercaptoethanol and the NP solution is put in a sonicating bath for 30 minutes. After sonication, the NPs are purified from excess DMSA and β-mercaptoethanol with a magnet. For increased purity, an additional wash with Millipore water is done. This β-mercaptoethanol treatment reduces dithiol cross-linking between NPs by the DMSA. After purification with a magnetic field and agarose gel electrophoresis, dynamic light scattering (DLS) shows an average size of 10.6 nm (Figure 5-5), suggesting minor aggregation. TEM imaging (Figure 5-4) shows aggregates of 1-5 NPs on average. As-treated NPs run in a gel as a narrow band (Figure 5-2, lane 6). DLS measurements of these samples are identical after several weeks, confirming improved NP stability.

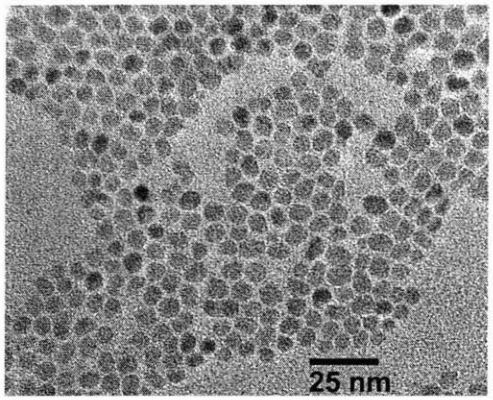

Figure 5-3: TEM image of $CoFe_2O_4$ NPs with oleic acids ligands.

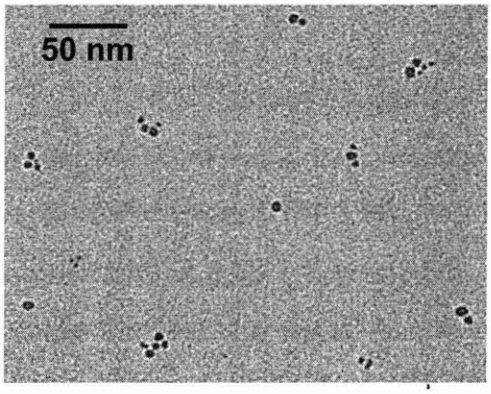

Figure 5-4: TEM of DMSA NPs, one month after purification.

ICP-OES (SPECTRO model Ciros-Vision) is used to measure the DMSA and NP molar ratios and to determine if the DMSA are forming a monolayer or multilayers on the NP surface. Sulfur molar concentration is found to be 3.9 times lower than the summation of cobalt and iron molar concentrations. Assuming 5434 atoms per NP of that size, that would correspond to 700 DMSA molecules on each NP. A surface area of $0.18nm^2$ is available per DMSA molecule, which is indicative of a single monolayer of DMSA. Thus, the Fe and Co atoms at the NP surface are not all interacting with DMSA molecules.

5.2 Conjugation of nanoparticles to cyt *c*

YCC and HCC are incubated with the synthesized DMSA NPs to form the conjugates. In order to investigate the effect of protein density on the NP surface, high and low

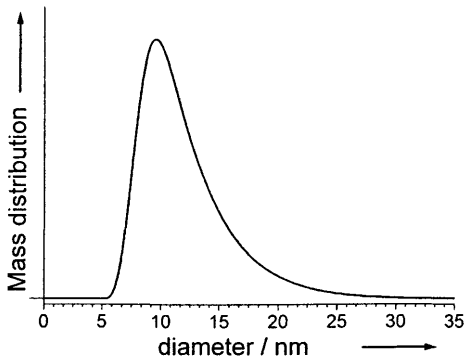

Figure 5-5: Dynamic light scattering measurements of DMSA $CoFe_2O_4$ NPs after incubation with β-mercaptoethanol, magnet purification and agarose gel electrophoresis purification.

coverage conjugates are made. After magnet purification, approximately 0.3nmol (for high coverage conjugates) or 0.6nmol (for low coverage) of NPs are purified and suspended in 60 μL of a solution of either 0.5× TBE, 2mM hexapolyethylene glycol thiol in 0.5× TBE, or in a solution of 0.25M L-lysine and 0.2M NaH_2PO_4 at pH 8. For control experiments, NPs are also suspended in 0.5× TBE with 0.25M NaCl, in 0.5× TBE with 3M glycine, or in 0.45M Tris buffer at pH 7. For conjugation, 7nmol of yeast or horse cyt *c* is added to the NP solution. Bioconjugation is rapidly done after magnet purification, preventing the use of ICP to measure the exact NP concentration before mixing with yeast or horse cyt *c*. For that reason, the cyt *c*:NP incubation ratios varied slightly from sample to sample and could be measured only after complex purification as explained below (Table 5.1). After 30 minutes of incubation, 1% agarose gel electrophoresis are run in 0.5× TBE with a field strength of 10 V/cm. Samples are extracted from the gel by cutting a selected gel area and centrifuging for 30 minutes in 0.2μm centrifugal filters at 10^4g at 4°C.

Gel electrophoresis is used to investigate conjugation of the proteins to the NPs (Figure 5-6). NPs run toward the positive electrode in the gel. When incubated with HCC and YCC, the NPs have lower electrophoretic mobility (lanes 1-3), indicating binding to both proteins. HCC has a net charge slightly higher than YCC at this pH, explaining the slower mobility of NP-HCC samples when compared to NP-YCC. No band indicative of free protein appears in these lanes, demonstrating that all of

	YCC conjugates	*# of YCC per NP*	*HCC conjugates*	*# of HCC per NP*
low	NP:YCC	12.6	NP:HCC	13.1
coverage	NP-PEG:YCC	13.0	NP-PEG:HCC	12.8
	NP-LYS:YCC	11.7	NP-PEG:HCC	10.0
high	NP:YCC	21.3	NP:HCC	24.9
coverage	NP-PEG:YCC	23.3	NP-PEG:HCC	26.6
	NP-LYS:YCC	29.7	NP-PEG:HCC	25.6

Table 5.1: Average number of proteins on the surface of $CoFe_2O_4$ NPs with low and high coverage. Protein coverage also corresponds to the cyt *c*:NP incubation ratio for labeling, except for NP-LYS:HCC.

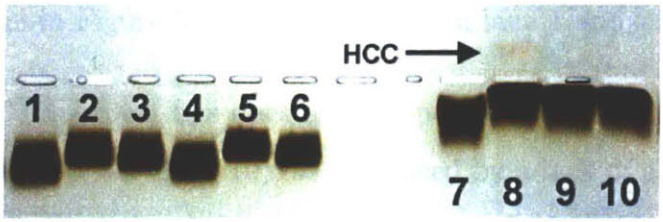

Figure 5-6: 1% agarose gel electrophoresis (a) of: NP (l), NP:HCC (2), NP:YCC (3), NP-PEG (4), NP-PEG:HCC (5), NP-PEG:YCC (6), NP-Lys (7), NP-Lys:HCC (8), NP-Lys:YCC (9) and NP-PEG-Lys:YCC (10). NP:cyt *c* incubation ratio is $\sim$ 1:25.

the proteins attach to the NPs under these incubation conditions. Free cyt *c* would run toward the negative electrode. The fact that all HCC are attaching shows that there is a strong tendency for non-specific adsorption to $CoFe_2O_4$ NPs. NP-HCC and NP-YCC conjugates are extracted from the bands cut out of the gel.

Optical absorption spectra of these samples (Figure 5-7) show a Soret band at 410nm indicative of cyt *c* on top of spectra from NPs (Figure 5-7 dash line), confirming conjugation between the NP and protein. Absorption spectra were obtained on a Varian Cary 50 Spectrophotometer at room temperature with a 1cm pathlength cuvette. The scan range was 800-200nm and the scan rate was 10nm per second.

Changing the NP surface ligand can diminish non-specific adsorption of proteins or DNA [23, 117, 58]. We find that addition of Lys in a 1:2500 (cyt *c*:Lys) ratio impedes non-specific adsorption and displaces HCC, resulting in a red band (lane 8, arrow) indicative of free HCC that runs in the opposite direction. Absorption spectra of the sample extracted from the gel area at the arrow shows that only HCC is present without NPs contribution (Figure 5-8), suggesting that Lys competes with non-specific

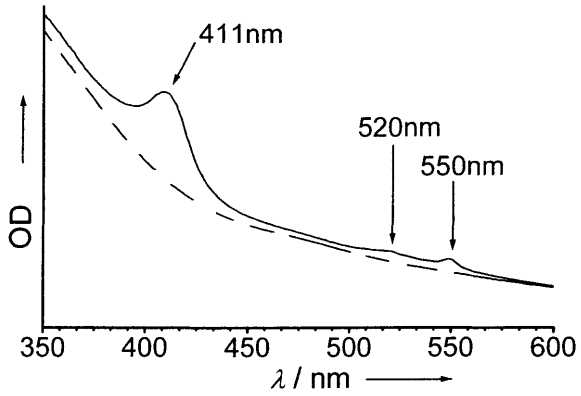

Figure 5-7: Absorption spectra of NP (dashed) and NP-HCC (plain) samples extracted from the gel in Figure 5-6 from the bands in lane 1 and 2.

adsorption of HCC. However, Lys does not compete with YCC attachment (lane 9) even in presence of PEG-SH (lane 10), as evidenced by a lack of a free YCC band in those lanes. This supports that YCC is covalently attached to the NP *via* C102. NP-Lys samples run slower because of reduced negative charge and higher ionic strength. Salt is not able to compete with HCC attachment (Figure 5-9a), showing that the effect of Lys is not simply due to charge screening. All HCC also remain attached to the NPs when Lys is replaced by a positively charged amine without carboxylic acid (Tris) or an uncharged carboxylic acid (Gly) molecule (Figure 5-9bc). Tris retarded the NPs in the gel similarly to Lys, suggesting electrostatic attachment to the NP surface. However, Gly did not affect the NPs gel mobility. Thus, it appears that both the carboxylic acid and the positive charge of Lys are necessary to displace HCC.

PEG-SH has been used previously to block non-specific adsorption to NP surfaces. PEG-SH has been successful in preventing protein attachment [23] and in obstructing interactions of protein side-chains with the NP as shown in Chapter 4. Here it could be used to bind to free thiols on the DMSA and possibly block interactions of the protein with the NP surface (Figure 5-1). However, incubation of the NPs with PEG-SH in a 1:20 (cyt *c*:PEG-SH) ratio does not noticeably affect mobility (lane 4-6), suggesting that it cannot prevent non-specific adsorption. In addition, bands indicative of free YCC (in the positive direction) do not appear, suggesting that the PEG-SH cannot displace the YCC from the DMSA.

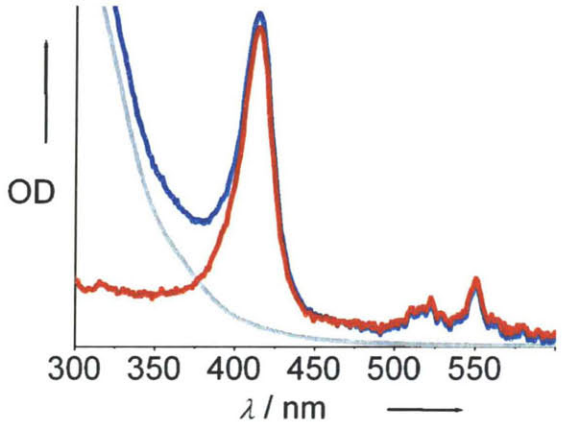

Figure 5-8: Absorption spectra of unbound HCC (red), corresponding to lysine absorption spectra (light gray) subtracted from the gel area (blue) pointed in Figure 5-6.

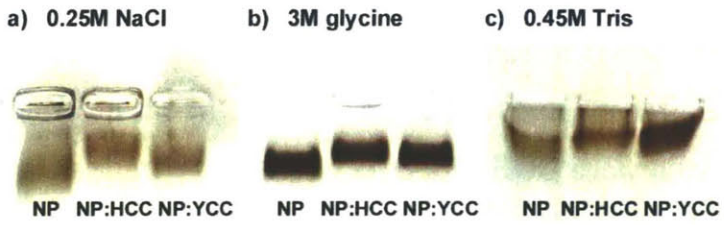

Figure 5-9: 1% agarose gel electrophoresis of NP incubated with HCC and YCC in presence of 0.25M NaCl (a), 3M glycine (b) and 0.45M Tris (c). The incubation ratio of NP:cyt c is $\sim$ 1:25.

Protein coverage is quantified from absorption spectra (Figure 5-7). The cyt *c* concentration is calculated after substraction of NP contribution, using the extinction coefficient at the Soret peak. NP concentrations are measured with ICP-OES from iron and cobalt content. Bioconjugates with low and high protein coverage are obtained (Table 5.1). The "low coverage" and "high coverage" NP-cyt *c* conjugates have respectively approximately 12 and 25 proteins per NP, which corresponds to a surface area of 10.7 nm^2 and 5.1 nm^2 available per protein on the NP surface. Cyt *c* has a radius of gyration of 1.3 nm and a mean cross-sectional area of 5.3 nm^2. Thus, the "low coverage" samples have a partial monolayer of proteins on the NP surface. The protein coverage is not a measure of the efficiency of attachment of cyt *c* to NP. Gel electrophoresis already shows that all YCC and HCC in solution are absorbing to the NPs (except for the NP-Lys:HCC solution). Thus, the protein coverage corresponds to the cyt *c*:NP incubation ratio for labeling, except for NP-Lys:HCC solutions which had a higher cyt *c*:NP incubation ratio.

5.3 Structure of nanoparticle-cyt *c* conjugates

Far UV circular dichroism (CD) determines the secondary structure of cyt *c* in the NP:YCC (Figure 5-10) and NP:HCC (Figure 5-11) bioconjugates. CD spectra were collected at 25^{o}C on a Aviv Model 202 in a 1mm pathlength cuvette. At least 4 scans taken at a scan rate of 0.1nm per second in the 250-195nm range were averaged. NPs absorbed in the far UV, which increased the noise in the spectra and limited the concentration of NP in the studied samples to less than 0.5 μM. The NP contribution to the CD signal is subtracted. Both YCC and HCC show a decrease in α-helicity when attached to NPs, as indicated by a higher mean residue molar ellipticity at 222nm (θ_{222}, Table 5.2). An isodichroic point is observed at approximately 205 nm, indicative of a helix-coil transition. Co-functionalization of the NPs with Lys helps to maintain the YCC structure, as demonstrated by an decrease in θ_{222}. Minimal effects of PEG-SH on the structure of the protein on $CoFe_2O_4$ NPs are observed. Higher protein coverage tends to improve folding for both YCC and HCC.

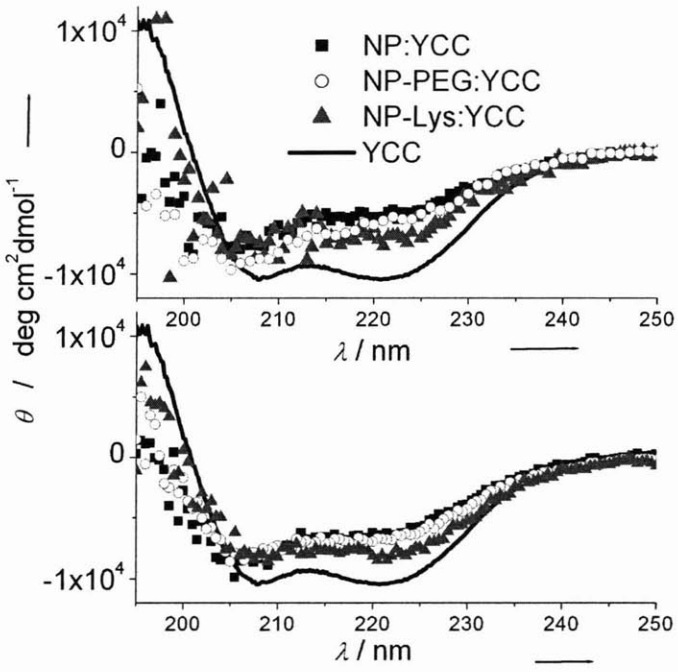

Figure 5-10: Circular dichroism of NP-YCC complexes with low (top) and high (bottom) protein coverage.

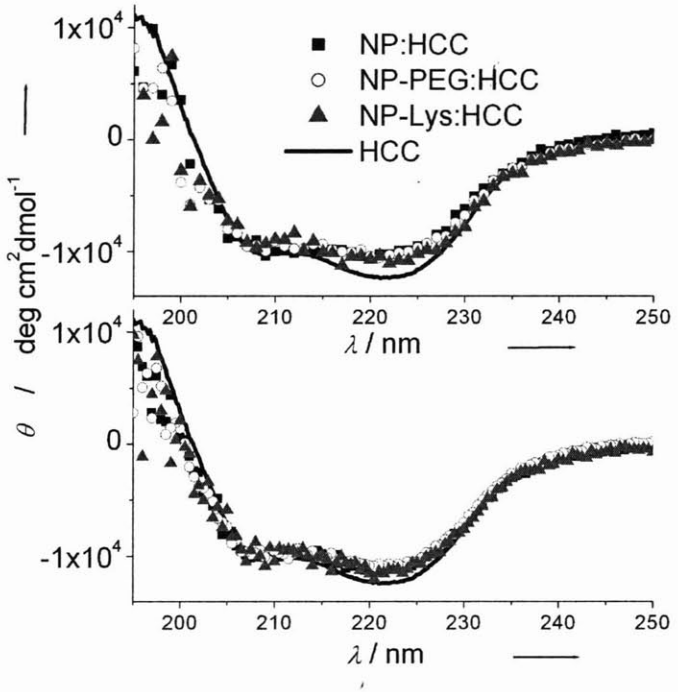

Figure 5-11: Circular dichroism of NP-HCC complexes with low (top) and high (bottom) protein coverage.

	YCC conjugates	θ_{222}	*HCC conjugates*	θ_{222}
cyt *c*	YCC	-10.3	HCC	-12.4
low	NP:YCC	-5.1	NP:HCC	-10.3
coverage	NP-PEG:YCC	-5.3	NP-PEG:HCC	-10.3
	NP-LYS:YCC	-6.8	NP-PEG:HCC	-11.1
high	NP:YCC	-6.4	NP:HCC	-11.0
coverage	NP-PEG:YCC	-6.7	NP-PEG:HCC	-10.8
	NP-LYS:YCC	-8.1	NP-PEG:HCC	-11.3

Table 5.2: Secondary structure analysis. θ_{222} units are 10^3 deg cm^2 dmol^{-1}.

Heme spectra also yield information on protein secondary structure. At normal pH, reduction of the heme red-shifts the Soret peak of cyt *c* from 408nm to 416nm, and splits the Q-band from a broad absorption at 530nm into two peaks at 520nm and 550nm. It is known that as cyt *c* unfolds, its redox potential decreases and the heme is thus more readily oxidized [154, 155]. The measured redox state can be affected by redox partners in solution and by the degree of unfolding (which changes the environment of the heme, hence its redox potential). Here, NP contribution is subtracted from the absorption spectra of NP-cyt *c* complexes, and we observe that the Soret (~410nm) and Q-band (520-550nm) absorption are changing with protein coverage (Figure 5-12). Higher protein coverage results in more reduced proteins, as it raises the Q-band intensity at 520nm and 550nm and red-shifts the Soret peak. This change in the redox state of the heme is most likely due to changes in protein structure, as the possible redox partners in solution would be the same for both coverages. This is consistent with CD, showing that electron transfer functions of cyt *c* are affected by the NP.

In the previous chapter, the use of the neutral PEG-SH as ligand for Au NPs was able to keep YCC fully folded. Similarly in the present study, the positively charged Lys molecules reduce the net charge of the $CoFe_2O_4$ NPs, maintaining YCC more folded. This suggests that electrostatic interactions are a source of YCC denaturation when covalently attached on $CoFe_2O_4$ NPs.

One novelty of this study was to find that HCC was also disturbed when non-specifically linked to the surface of $CoFe_2O_4$ NPs, as opposed to what was observed

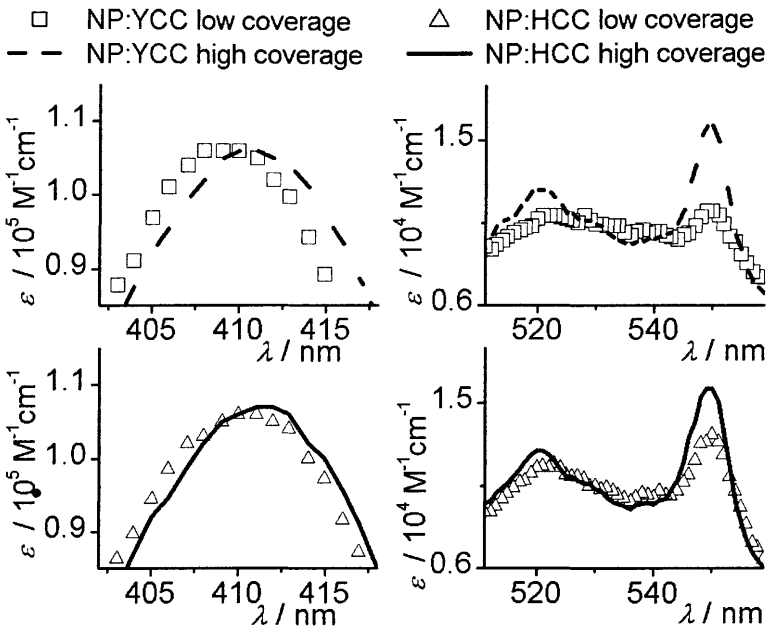

Figure 5-12: Electronic absorption spectra in the Soret and Q-band region for NP-cyt *c* conjugates with low and high protein coverage.

for HCC electrostatically attached to BPS Au NPs. Figure 5-13 shows that θ_{222} of HCC is increased only when attached on $CoFe_2O_4$. This observed disturbance is most likely due to interactions with the NP core material. Effectively, non-specific adsorption can result from the interaction of the carboxylic acids on the protein with surface Co/Fe. Studies of Fe_3O_4 NPs and Co NPs surfaces have shown that carboxylic acids coordinate strongly to Co or Fe surface atoms [168, 169], so residues that are most likely to adsorb are aspartic acids (Asp) and glutamic acids (Glu). The presence of Lys decreases non-specific adsorption to the NPs, as shown by improved protein structure and by the lower affinity of HCC for NPs. This might occur by Lys coordinating its carboxylic acids group to Co/Fe atoms on the surface, thus preventing adsorption of the carboxylic acids on the protein. The fact that higher protein coverage improves folding is consistent with this hypothesis, as fewer protein carboxylic acids can non-specifically interact with the NP surface due to crowding. A major decrease in activity has been observed for proteins attached to Fe-based NPs [90], possibly due to similar structural deformation.

Although PEG-SH has been used successfully to improve protein structure linked

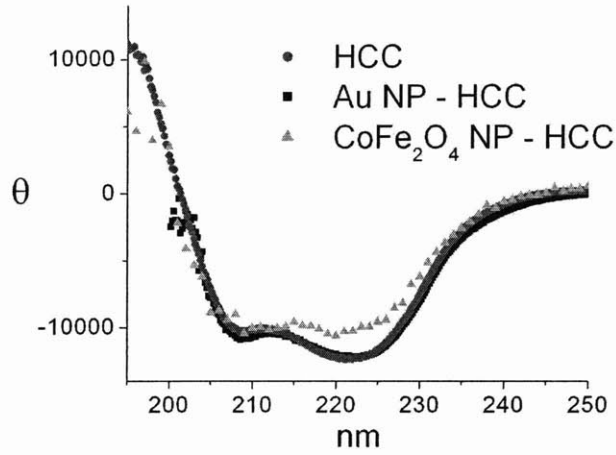

Figure 5-13: Circular dichroism of HCC conjugated to Au and $CoFe_2O_4$ NPs.

to or adsorbed on Au NPs, no significant effects of PEG-SH on the protein structure is observed for $CoFe_2O_4$ NPs.

Structural behavior of YCC can be explained in terms of residues in the local vicinity of the C102. Several charged residues within 1.0 nm of C102 (E21, R38, K99, E103) are likely to interact with DMSA and the NP surface (Figure 5-14, left, from PDB # 1YCC [170]). Because HCC is not constrained by the C102 linkage, any charged residue can interact with the NP. However, nine of the twelve carboxylic acids residues on HCC are grouped on the same surface (Figure 5-14, right, from PDB # 1HRC [171]) close to the positive end of the protein dipole moment (residue 82) [131]. Interaction of those residues with the NP surface is prone to lead to α-helices deformation as seven of them are part of helical motifs.

5.4 Summary

Yeast and horse cyt *c* are successfully attached to 6nm cobalt iron oxide magnetic oxide NPs. For yeast cyt *c*, the linkage is site-specific *via* a covalent bond between cysteine C102 and the thiol of the NP ligand. As a control for the site specificity of attachment and for a better characterization of non-specific interactions, horse cyt *c* is also linked to NPs non-specifically. The protein side-chains of horse cyt *c* can

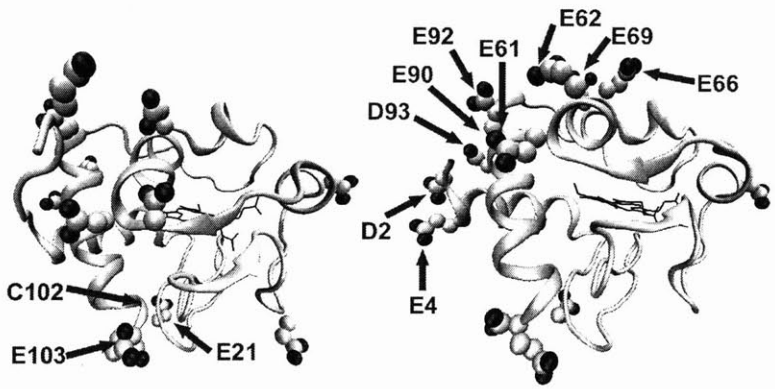

Figure 5-14: Ribbon structure of YCC (left) and HCC (right) with Van der Waals representation of carboxylic acid side-chains.

adsorb on the NP by electrostatic interactions and by linkage of carboxylic acids of glutamic acid and aspartic acid of the protein with cobalt and iron atoms.

It is found that co-functionalization of $CoFe_2O_4$ NPs with lysine can displace non-specific adsorption. Lys competes with horse cyt *c* attachment, but not with yeast cyt *c*, confirming covalent site-specific attachment of yeast cyt *c*. Salt, glycine or tris are not able to displace horse cyt *c*, indicating that both the carboxylic acid and the positive charge of lysine are contributing to displacing horse cyt *c*.

The NP has a strong tendency to disturb the protein structure but lysine aids in maintaining a folded structure as shown by CD, most probably by decreasing the net charge of the NP as well as by preventing direct adsorption of carboxylic acids side-chains on cobalt and iron atoms. PEG-SH does not significantly improve protein structure or non-specific adsorption. Further studies include studying the effect of longer polyethylene glycol thiols on the structure of site-specific NP-proteins conjugates. Heme optical absorption studies are consistent with CD, showing that higher protein coverage improves folding.

These results are significant for applications which utilize proteins adsorbed on surfaces or nanostructures that are charged or known to interact with carboxylic acids. For improved activity of proteins, particular caution should be taken to impede strong non-specific bonding between the protein side-chains and the NPs.

Chapter 6

Conclusions

6.1 Summary

This thesis investigates the NP-protein interface in order to build a set of rules to optimize protein structure and activity when immobilized on NP surface. Protein behavior is studied as a function of relevant parameters such as the NP surface chemistry, the NP material, the nature of the NP-protein attachment (covalent versus non-covalent), the density of proteins on the NP surface, and the position of the labeled site.

For this study, the proteins ribonuclease S and cytochrome *c* are covalently linked to Au and $CoFe_2O_4$ NPs by attachment of a specific surface cysteine. The cysteine forms a thiol-Au bond with Au NPs or a thiol-thiol bond with the thiolated ligand of $CoFe_2O_4$ NPs.

Ribonuclease S is labeled with a 3nm Au NPs by utilizing its two-piece structure. The smallest fragment, S-peptide, is mutated with a unique cysteine at its N-terminus which serves as the NP attachment site. Covalent attachment through thiol-Au interaction is confirmed by retained gel mobility after incubation with a competing thiolated molecule, mercaptopropionic acid. The NP-peptide conjugate is self-assembled with the other portion, S-protein, to form a complete and functioning enzyme. NP gel mobility decreases with peptide labeling and S-protein association. Gel electrophoresis also shows that there is an optimum S-peptide coverage for S-

protein attachment. Surface plasmon resonance is red-shifted upon incubation of the NP-peptide conjugates with S-protein. Moreover, incubation with an excess of S-peptide lacking the mutated cysteine was able to remove S-protein from the NP surface. These results support site-specific labeling. The enzymatic activity of Au labeled ribonuclease S is determined using RNA substrate with a FRET couple. The measured turnover rate is approximately two orders of magnitude lower, most likely because of negative charges and steric hindrance in close proximity of the S-peptide which could impede RNA in reaching the active site.

Yeast cyt *c* is linked on specific sites to NPs of various material and surface charge. For 1.5nm Au NPs, the neutral ligand and the presence of salt in the buffer improves folding. Molecular dynamics simulations of the conjugate reveal that electrostatic interactions with the NP ligand lead to local unfolding of α-helices of cyt *c*. All of this indicates that electrostatic interactions of charged amino acids with the charged ligands are prone to lead to protein denaturation. Furthermore, the attachment site can be controlled by mutations of surface residues to cysteines. Denaturation of yeast cyt *c* is worst for NP linked on motifs that are more crucial for folding. Horse cyt *c* attached to Au NPs by electrostatic interactions remains folded, which is not surprising as proteins are more likely to be disturbed when they are forced to link by a specific site. However, for 6nm $CoFe_2O_4$ NPs, yeast cyt *c* and horse cyt *c* are both disturbed by the NP attachment even if the linkage is non-covalent for the latter. Lysine and higher protein coverage are able to help folding by reducing the electrostatic unfavorable interactions and by decreasing the ratio of carboxylic acids that can interact with surface NP atoms.

These studies show that careful choice of ligand, material, attachment site and NP-protein stoichiometry can favor labeling at a specific unique site while retaining protein structure. These results have important implication for applications in which proteins are covalently linked to nanoscale systems as for sensors, energy harvesting complexes or protein assembly.

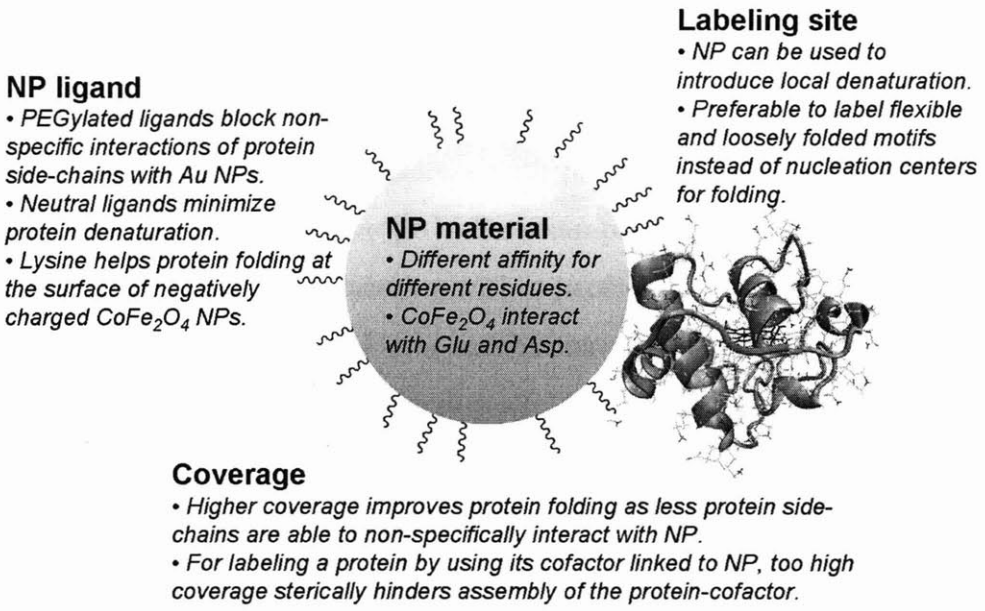

Figure 6-1: Effects of NP ligand, NP material, coverage and labeling site.

6.2 General labeling strategies

Overall, in synthesizing NP-protein conjugates, a general strategy for creating a biologically functional NP-protein conjugate is necessary. Because non-specific binding often leads to protein unfolding, the general goal of this strategy is to determine how to block non-specific adsorption on NP and maintain protein structure and function. This thesis shows that protein structure and function are influenced by the chemical nature of the NP ligand, the NP material, the coverage of protein on the NP, and the labeling site on the protein (Figure 6-1).

Choice of NP ligand

The NP ligand in a NP-protein conjugate can greatly influence protein structure. It is in close contact with the protein, and can interact with nearby residues, so choosing the right NP ligand is crucial.

In covalent NP-protein conjugates, ligands with charged species as endgroups are likely to denature the protein via electrostatic effects. Here, cytochrome *c* is covalently linked to 1.5nm Au NPs. The protein is denatured when the NP ligands are charged,

but remains folded when it is a neutral PEG ligand.

In the event of non-covalently bound proteins, the NP ligand can also influence protein structure. There are examples of how one can exploit the ability of the surface coating ligand of the NP to interact with proteins in a specific way, permitting control over the protein structure [31]. For example, NPs functionalized with positively charged NP ligands can interact with a peptide of a sequence with aspartates positioned at specific intervals. Upon incubation of the peptide with the NPs, the interaction between the two species induces folding of the peptide into an α-helix as measured by CD spectroscopy [32].

Charged ligands can also prevent or enhance linking chemistry *via* electrostatic repulsion or attraction and dramatically affect non-specific adsorption. PEG has been used to prevent non-specific adsorption for bulk 2D surfaces, NP and nanorod surfaces [55, 23, 50]. Here, PEG's floppy chains and charge neutrality prevented the non-specific adsorption of cyt *c* on NPs.

Choice of NP material

In addition, the NP material can affect protein structure and activity in the conjugate. For example, if amino acid side-chains have a strong affinity for a particular material, it could lead to strong non-specific interactions between the protein and NP and result in protein denaturation. NP materials for bioconjugates have been mostly of noble metals such as Au, magnetic oxide materials, and semiconductors for quantum dots. Quantum dots are typically coated with silica shell which largely resists protein adsorption. Au is relatively inert, though primary amines and carboxylic acid groups have been known to interact with Au. Magnetic nanoparticles utilized in biological applications are typically magnetic oxides, such as Fe_3O_4, Fe_2O_3, $CoFe_2O_4$, and $MnFe_2O_4$. Carboxylic acid groups have a strong affinity for the metal ions in the surface of the NP, and can coordinate to them. Interaction of carboxylic acids with iron [168], cobalt [169], and titanium [172] have been observed.

In the present study, a different protein behavior is observed for immobilization on $CoFe_2O_4$ NPs compared to Au NPs. Horse cyt *c* linked to $CoFe_2O_4$ is disturbed

by the NP attachment even if the linkage is non-covalent. Interactions between the protein carboxylic acid side-chains and surface cobalt and iron atoms are believed to be in cause. Higher protein coverage could improve folding as less carboxylic acids can interact with surface NP atoms.

Coverage on the NP surface

The NP-protein stoichiometry can also influence protein structure and activity. By immobilizing several proteins per NP, one can take advantage of multivalency [173] and exploit the cooperative effects. Polyvalency is especially useful for recognition and sensing applications, because of increased affinity for substrate. Considerable enhancement of the conjugate efficiency and selectivity is thus achieved [174].

High protein coverages on the NP surface could lead to crowding, and thus affect protein folding and also activity. Steric issues such as blocking of binding of the substrate may occur. Single molecule spectroscopy has been used to calculate the number of proteins per NP [175] , and it has been determined that the coverage is actually a distribution. In the case of Qdots functionalized with maltose binding protein, a Poisson distribution was obtained [176]. Here, higher coverage on the NP surface has been shown to improve protein folding for linked and adsorbed cyt *c* on $CoFe_2O_4$ NPs as less non-specific interaction with the NP surface are possible.

When linking NPs to proteins by using specific affinity for a cofactor, the density of cofactors on the NP surface will influence the labeling efficiency. For the labeling of ribonuclease S in two-step as described in this work, there is an optimum S-peptide coverage on the NP surface. A minimum coverage is necessary to reduce non-specific adsorption of S-proteins, but too high coverage sterically hinders the assembly of ribonuclease S.

Choice of NP labeling site

Finally, the choice of site on the protein can affect protein structure and activity. Interactions between the NP ligand or NP surface is typically with amino acids in the local vicinity of the labeling site. Therefore, these interactions would be strongly

influenced if the labeling site on the NP has a different local environment. Choosing a specific labeling site on the protein is crucial for creating a functional NP-protein conjugate.

Here, Au NPs introduce a different amount of disorder in cyt c depending on the position of the labeling site. Protein unfolding is more severe for NP attached in the vicinity of charged amino acids. When the NP is attached on the most essential motif for cyt c folding (N-C helices), it induces more structural disturbance. This motif is also the most stable of the protein. MD simulations indicate that the conjugates that disrupt the hydrophobic cluster at the interface between the N-terminal and C-terminal α-helices are also the ones that are the most unfolded as revealed by CD. Based on this, it is preferable to label flexible and loosely folded motifs instead of nucleation centers for folding, which typically include the most common labeling targets, the N- or C-termini. Furthermore, this result suggests that the NP can be used to introduce local denaturation.

A very large family of proteins have the N- and C-terminal motifs in contact, which has been suggested to control initial folding [151]. Incidentally, protein termini are the most common NP labeling sites: His tags that are typically put at N or C termini are convenient for cloning, labeling chemistry, and purification of the conjugate. However, if the protein is part of the very large family that possesses the N-C contact [151], it could potentially be the worst site for labeling, resulting in protein denaturation that cannot be rescued by salt screening, and ultimately loss of biological function. For these systems, labeling of low stability motifs would be optimal. In addition to choosing the least stable motifs for labeling, sites should also have minimal charged residues in the vicinity to reduce electrostatic interactions. It is found in the present study that the amount of denaturation for a given site correlates with the number of charged amino acids in the local vicinity of the NP labeling site.

6.3 Further studies

Effect of NP size

NP size can also affect protein structure and activity. For larger NPs, the effective protein surface area it can access is larger, so it may increase the likelihood of denaturing the protein as was obserbed for NP-lysozyme conjugates [69]. Also, smaller NPs due to their higher curvature will have a fewer number of NP ligands that can interact with the protein side-chains. In addition, the surface area on the NP accessible to the protein will be lower, and could potentially result in less denaturation. With regards to activity, larger NPs may sterically prevent substrates from reaching the binding site or active site more than for smaller NPs.

Several issues should be addressed in the study of the effect of NP size. First, one important requirement is to synthesize NPs with exactly the same ligand coverage, which might be difficult to obtain or to test for. This will insure that the effect observed is really due to the NP curvature and not to a different ligand density at the surface of the NP. Furthermore, increasing the NP size too much may result in NP solubility problems, as larger NPs are more difficult to keep soluble.

When the NP reaches a large enough size, the protein should behave as if it was immobilized on a flat surface, which is nothing else than an infinitely large NP. The critical size at which the NP can be considered as a flat surface depends on the size of the protein.

A study of the structure of cyt *c* covalently linked on NPs of various sizes could give insight on those effects. For larger NPs the disorder in the protein might not be as localized as what was observed for 1.5nm NPs. Therefore, the protein might be globally denatured to a same degree for all labeling positions.

The NP size would also probably affect the NP-RNase S conjugates. It was observed that the affinity of S-proteins for the NP-S18 complex depends on the S18 coverage. It is likely to also depends on the NP size. In addition, it would be interesting to investigate the effects of NP size on the ribonucleatic activity of the complex.

Labeling larger proteins

Most of the proteins that have been labeled with NPs so far are small and relatively simple. Labeling larger proteins that have much more complex functions is more challenging as engineering unique labeling sites may not be possible using all the strategies above. Hainfeld and coworkers [37] have demonstrated that site-specific labeling of a large protein complex can be achieved, enabling EM imaging that can reconstruct a three dimensional representation of the complex. This also shows that spectroscopic techniques are continually improving and becoming more sophisticated.

In vivo labeling

Another important challenge consists of labeling proteins in vivo. There are numerous exciting applications being developed for NP in biology, which become all the more powerful when employed in cells, tissue, and organisms. The strategies for labeling will become much more complex as protein folding is quite different inside the crowded environments in cells, and techniques for assaying structure and function will also face new challenges. Ting and coworkers have recently developed strategies for in vivo site-specific attachment of streptavidin-quantum dots conjugates to biotinylated proteins [177].

Molecular dynamics simulations as a tool for choosing the optimal site for labeling

In the present study, MD simulations show that a charge NP induces structural disorder on the protein on which it is attached. Even if MD simulations are usually significantly shorter than the unfolding timescale, results from MD simulations are found to be consistent with experimental data.

This opens up a whole new avenue for the selection of optimum labeling sites. Simulations of several NP-protein conjugates in parallel is signiticantly less time consuming than the production of many mutants with site-directed Cys mutations. A systematic study of several other labeling sites will allow to identify other "rules" to

follow in the choice of a labeling site.

Furthermore, it would allow the use of NPs to study structure-function relationship in proteins. MD simulations could locate the NP attachment sites that induce a structural disturbance that remains local. Testing experimentally the activity of those NP-protein conjugates would allow to determine the role of these specific parts of the protein in its function.

Appendix A

Derivation of kinetic parameters of ribonucleatic activity from fluorescence intensity

The enzyme E reacts with substrate S to produce product P in the following reaction.

$$\mathrm{E} + \mathrm{S} \underset{k_{-1}}{\overset{k_1}{\Longleftrightarrow}} \mathrm{ES} \xrightarrow{k_2} \mathrm{P} + \mathrm{E} \tag{1}$$

We assume that $[S] << K_M$

with $K_M = \frac{k_{-1}+k_2}{k_1}$ which represents the substrate concentration at which the reaction velocity is half-mamimum.

This leads to most of the enzyme having their active site empty, thus $[E] \approx [E]_{total}$ and $\frac{d[E]}{dt} \approx 0$.

From the expression for $\frac{d[E]}{dt}$ and $\frac{d[S]}{dt}$, we get

$$\frac{d[E]}{dt} = (k_{-1} + k_2)[ES] - k_1[E][S] = 0 \tag{A.1}$$

$$\Rightarrow [ES] = \frac{k_1[E][S]}{k_{-1} + k_2} \tag{A.2}$$

and

$$\frac{d[S]}{dt} = k_{-1}[ES] - k_1[E][S] \tag{A.3}$$

$$= (\frac{k_{-1}k_1}{k_{-1}+k_2} - k_1)[E][S] \tag{A.4}$$

$$= \frac{-k_2k_1}{k_{-1}+k_2}[E][S] \tag{A.5}$$

$$\Rightarrow \frac{d[S]}{[S]} = \frac{-k_2k_1}{k_{-1}+k_2}[E]dt \tag{A.6}$$

after integrating (A.6), we get

$$\Rightarrow [S] = [S]_0 exp\left[\frac{-k_2k_1}{k_{-1}+k_2}[E]t\right] \tag{A.7}$$

where $[S]_0$ is the initial concentration of substrate.

The substrate concentration $[S]$ at a certain time is proportional to the final fluorescence intensity I_f minus the fluorescence intensity at that time I.

$$[S] = A[I_f - I] \tag{A.8}$$

$$[S]_0 = A[I_f - I_0] \tag{A.9}$$

where A is a proportionality constant.

With $\frac{k_{cat}}{K_M} = \frac{k_2k_1}{k_{-1}+k_2}$ and $[E] \approx [E]_{total}$, we obtain

$$I = I_f - (I_f - I_0)exp\left[\frac{-k_{cat}}{K_M}[E]_{total}t\right] \tag{A.10}$$

Appendix B

Cytochrome *c* mutants expression, purification and labeling

Wild type cyt *c* from yeast *S. Cerevisiae* was purchased (Sigma). Plasmids for mutants were obtained from the groups of Harry Gray and Jay Winkler [138].

Received plasmids were sequenced at the MIT Biopolymers facility and compared to the sequences in the literature to verify the placement of the mutations. The plasmids were cloned into *E.coli* BL21DE3 Star cells (Invitrogen). To increase the yield of protein production, the cyt *c* maturation gene cassette pEC86 with Chloramphenicol (Chl) resistance [178] and the cyt *c* plasmid with Ampicillin (Amp) resistance were co-transformed. Colonies from LB agar plates with 100μg/ml Amp and 34μg/ml Chl were screened for best cyt *c* expression in 5mL of TB medium containing 100μg/ml Amp and 34μg/ml Chl grown for 24 hours shaking at 37^{o}C. When possible, colonies were selected by the pink color of the cell pellet (due to presence of cyt *c*) and saved for frozen stocks.

Cells from frozen stocks were used to inoculate 10 ml of TB medium containing 100μg/ml Amp and 34μg/ml of Chl. After overnight growth, large TB cultures (5-10L) containing 100μg/ml Amp and 34μg/ml of Chl were inoculated. The cells were grown for 36 hours at 37^{o}C. Cells were harvested by centrifugation and resuspended in 10 mM NaPi buffer (pH 7.0). To isolate the protein, the cells were lysed by French Press at 28 PSI (Constant Systems Basic Z Model). 20nM deoxyribonucle-

ase, 1mM phenylmethanesulphonylfluoride (PMSF) and 1mM dithiothreitol (DTT) were added and the suspension was centrifuged at 6,000 rpm for 30 min and the supernatant was collected. To purify the protein, the solution was loaded onto a Fast Flow CM Sepharose Econo-column equilibrated with 20 mM NaPi buffer with 1mM DTT and 1mM PMSF (pH 7.0). Cyt *c* was eluted with a stepwise salt gradient (0-0.5 M NaCl). Protein was further purified by ion-exchange chromatography with a Mono S Sepharose column using a FPLC system with same buffer. The last purification step was size exclusion chromatography with TSK-gel G4000PW column on a HPLC system (Varian ProStar). Purity of the protein was confirmed with SDS-Page gel electrophoresis. Concentrations of proteins were determined using an extinction coefficient of 106.1 mM^{-1} cm^{-1} at 410nm.

Immediately before conjugation, cyt *c* were washed from excess DTT with 5kDa centrifugal filters at 4^{o}C, and resuspended in 10mM NaPi buffer at pH 7.3 with or without 0.1M NaCl. NPs were attached to cyt *c* by incubation overnight in same buffer at 4^{o}C and then studied by CD and absorption spectroscopy.

Appendix C

Molecular dynamics simulations

MD simulations were performed using the CHARMM program version 32 [179], with a generalized Born with simple switching (GBSW) implicit solvent [180]. A 20Å cut-off was applied for nonbonded interactions with a switch function between 16Å and 20Å. The param22 atom force field [181] was used and modified to include NP parameters. The NP core was modeled as one dummy atom with Lennard-Jones parameters (epsilon=-0.02 and r_{min}=14Å) such that BPS ligands or protein side-chains cannot penetrate into the NP volume. Each BPS ligand was modeled explicitly with partial charges estimated from known parameters for the benzene ring and methyl sulfate. The BPS molecule was constructed from the coordinates of a triphenylphosphine molecule linked to an Au atom [182]. 21 BPS molecules were uniformly distributed on the NP surface. The proteins were constructed from PDB coordinates (PDB ID# 2BCN) [183] and mutated accordingly. The heme was covalently linked to Cys 14 and 17. Covalent bonds were also maintained between the heme iron and Met 80 and His 18, which are assumed to remain formed during the timescale of our simulations [129]. Cyt *c* was linked to the NP surface by replacing one BPS ligand by the labeled Cys. To prevent the formation of close contacts, the protein was approached to the NP sequentially by steps of 1Å, performing an energy minimization between each step, until the S atom of the thiol reached the target coordinate. During energy minimization and dynamics, the position of the S atom of the labeled Cys and the P atoms of BPS ligands were fixed at 10Å from the NP center, based on the reported

P-Au and S-Au bond lengths [182, 184].

Leap-frog dynamics trajectories were carried out with 2fs timesteps and the shake algorithm was used to constrain the bonds involving hydrogen atoms. The system was heated from 48K to 300K for 20 ps and then equilibrated at 300K during 8 ns. The system was also heated from 48K to 450K for 40 ps and then equilibrated at 450K during 8 ns.

Topology of BPS ligand

The following is added to top_all22_prot_cmap:

```
RESI BPS          -2.00 ! BPS molecule
GROUP
ATOM P    PT       0.345 !
GROUP                    !             CG1, CD1, CG2, etc... (with SO3-)
ATOM CG1  CA      -0.115 !            /
GROUP                    !           /
ATOM CD1  CA      -0.115 !          /    HD3  HE3
ATOM HD1  HP       0.115 !         /      |    |
GROUP                    !        /      CD3--CE3
ATOM CE1  CA      -0.115 !       /       //     \\
ATOM HE1  HP       0.115 !  AU-P--------CG3      CG4--HG4
GROUP                    !       \       \  __ /
ATOM CD2  CA      -0.115 !        \      CD4--CE4
ATOM HD2  HP       0.115 !         \      |   |
GROUP                    !          \    HD4  HE4
ATOM CE2  CA      -0.115 !           \
ATOM HE2  HP       0.115 !            \
GROUP                    !             CG5 etc... (with SO3-)
ATOM CG2  CA      -0.115 !
ATOM S1   SO3      1.065
ATOM O1   O       -0.650 ! partial charges on O from OSO3 in top_all27_prot_lipid
ATOM O2   O       -0.650
ATOM O3   O       -0.650
GROUP
ATOM CG3  CA      -0.115 !
GROUP
```

```
ATOM CD3  CA     -0.115 !
ATOM HD3  HP      0.115 !
GROUP
ATOM CE3  CA     -0.115
ATOM HE3  HP      0.115
GROUP
ATOM CG4  CA     -0.115
ATOM HG4  HP      0.115
GROUP
ATOM CD4  CA     -0.115
ATOM HD4  HP      0.115
GROUP
ATOM CE4  CA     -0.115
ATOM HE4  HP      0.115
GROUP                    !             CG1, CD1, CG2, etc... (with SO3-)
ATOM CG5  CA     -0.115 !            /
GROUP                    !           /
ATOM CD5  CA     -0.115 !          /    HD3  HE3
ATOM HD5  HP      0.115 !         /      |    |
GROUP                    !        /      CD3--CE3
ATOM CE5  CA     -0.115 !       /       //     \\
ATOM HE5  HP      0.115 !  AU-P--------CG3      CG4--HG4
GROUP                    !       \       \  __  /
ATOM CD6  CA     -0.115 !        \      CD4--CE4
ATOM HD6  HP      0.115 !         \      |    |
GROUP                    !          \    HD4  HE4
ATOM CE6  CA     -0.115 !           \
ATOM HE6  HP      0.115 !            \
GROUP                    !             CG5 etc... (with SO3-)
ATOM CG6  CA     -0.115 !
```

```
ATOM S2   SO3     1.065
ATOM O4   O      -0.650
ATOM O5   O      -0.650
ATOM O6   O      -0.650
BOND  P   CG1  CD1 CE1  CG2 CE2  CD2 CG1
BOND  CD1 HD1  CE1 HE1  CG2 S1   S1  O1
BOND  S1  O2   S1  O3   CE2 HE2  CD2 HD2
BOND  P   CG3  CD3 CE3  CG4 CE4  CD4 CG3
BOND  CD3 HD3  CE3 HE3  CG4 HG4
BOND  CE4 HE4  CD4 HD4
BOND  P   CG5  CD5 CE5  CG6 CE6  CD6 CG5
BOND  CD5 HD5  CE5 HE5  CG6 S2   S2  O4
BOND  S2  O5   S2  O6   CE6 HE6  CD6 HD6
DOUBLE   CG1 CD1  CE1 CG2  CE2 CD2
DOUBLE   CG3 CD3  CE3 CG4  CE4 CD4
DOUBLE   CG5 CD5  CE5 CG6  CE6 CD6
ACCEPTOR O1
ACCEPTOR O2
ACCEPTOR O3
ACCEPTOR O4
ACCEPTOR O5
ACCEPTOR O6
IC CD1  P    *CG1 CD2   1.4059 120.3200 -177.9600 120.7600  1.4062
IC P    CG1  CD1  CE1   1.5109 120.3200 -177.3700 120.6300  1.4006
IC CE1  CG1  *CD1 HD1   1.4006 120.6300  179.7000 119.6500  1.0814
IC P    CG1  CD2  CE2   1.5109 120.7600  177.2000 120.6200  1.4002
IC CE2  CG1  *CD2 HD2   1.4002 120.6200 -178.6900 119.9900  1.0811
IC CG1  CD1  CE1  CG2   1.4059 120.6300   -0.1200 119.9300  1.4004
IC CG2  CD1  *CE1 HE1   1.4004 119.9300 -179.6900 120.0100  1.0808
IC CG2  CD2  *CE2 HE2   1.4000 119.9600 -179.9300 119.8700  1.0811
```

```
IC CE1  CE2  *CG2 S1    1.4004 119.9800  179.5100 119.9700  1.0807
IC CG2  O2   *S1  O3    1.5109 112.7600  118.2700 109.1000  1.1119
IC CG2  O2   *S1  O1    1.5109 112.7600 -123.8300 111.1100  1.1113
IC O2   S1   CG2  CE2   1.5594 112.7600   90.0000 120.3200  1.4059
IC CD3  P    *CG3 CD4   1.4059 120.3200 -177.9600 120.7600  1.4062
IC P    CG3  CD3  CE3   1.5109 120.3200 -177.3700 120.6300  1.4006
IC CE3  CG3  *CD3 HD3   1.4006 120.6300  179.7000 119.6500  1.0814
IC P    CG3  CD4  CE4   1.5109 120.7600  177.2000 120.6200  1.4002
IC CE4  CG3  *CD4 HD4   1.4002 120.6200 -178.6900 119.9900  1.0811
IC CG3  CD3  CE3  CG4   1.4059 120.6300   -0.1200 119.9300  1.4004
IC CG4  CD3  *CE3 HE3   1.4004 119.9300 -179.6900 120.0100  1.0808
IC CG4  CD4  *CE4 HE4   1.4000 119.9600 -179.9300 119.8700  1.0811
IC CE3  CE4  *CG4 HG4   1.4004 119.9800  179.5100 119.9700  1.0807
IC CD5  P    *CG5 CD6   1.4059 120.3200 -177.9600 120.7600  1.4062
IC P    CG5  CD5  CE5   1.5109 120.3200 -177.3700 120.6300  1.4006
IC CE5  CG5  *CD5 HD5   1.4006 120.6300  179.7000 119.6500  1.0814
IC P    CG5  CD6  CE6   1.5109 120.7600  177.2000 120.6200  1.4002
IC CE6  CG5  *CD6 HD6   1.4002 120.6200 -178.6900 119.9900  1.0811
IC CG5  CD5  CE5  CG6   1.4059 120.6300   -0.1200 119.9300  1.4004
IC CG6  CD5  *CE5 HE5   1.4004 119.9300 -179.6900 120.0100  1.0808
IC CG6  CD6  *CE6 HE6   1.4000 119.9600 -179.9300 119.8700  1.0811
IC CE5  CE6  *CG6 S2    1.4004 119.9800  179.5100 119.9700  1.0807
IC CG6  O5   *S2  O6    1.5109 112.7600  118.2700 109.1000  1.1119
IC CG6  O5   *S2  O4    1.5109 112.7600 -123.8300 111.1100  1.1113
IC O5   S2   CG6  CE6   1.5594 112.7600   90.0000 120.3200  1.4059
```

Parameters for BPS ligand

The following parameters are added to par_all22_prot_cmap:

```
!BONDS
CA   SO3   350.0       1.725
SO3  O     540.0       1.448 !from methyl sulfate

!ANGLES
CA   CA   SO3     65.0     120.0
CA   SO3  O       85.0      98.0 ! from methylsulfate for O2L SL OSL
O    SO3  O       130.000  109.47   35.00   2.45 ! from methyl sulfate

!DIHEDRALS
X    CA   SO3  X        0.0000  3     0.00

!VAN DER WAALS
!Au NP
AU     0.0000    -0.0200      14.0000
```

CHARMM code for the construction of the BPS nanoparticle

```
!       LOAD RTF, PARAM
        stream ../project/setup.str

!============================
! Setup the NP molecule
!============================

set x1 6.086259647018915
set y1 -4.046259579269158
set z1 -6.825337129127159
set x2 9.738358289087264
set y2 1.752710471533869
set z2 -1.446507461557287
set x3 8.383512039931800
set y3 -5.372991351726756
set z3 0.920700717164942
set x4 -8.677616086752074
set y4 4.675761160885062
set z4 -1.684113006095614
set x5 -0.000000000000000
set y5 0.000000000000001
set z5 -10.000000000000000
set x6 -9.590468679102566
set y6 -2.809029203531201
set z6 0.363683170990274
set x7 3.837314437461909
set y7 9.120450117737915
set z7 -1.446515661132232
```

```
set x8 2.667646902709770
set y8 -9.489330053104846
set z8 -1.684124444838970
set x9 1.646946517105476
set y9 -7.729360024691036
set z9 6.127361649070694
set x10 -3.412267277266833
set y10 9.354611398620026
set z10 0.920694091054292
set x11 -7.203926746610883
set y11 -0.853098918758342
set z11 -6.882998014257861
set x12 -5.537498366024247
set y12 -4.435133725666581
set z12 7.047389636009469
set x13 -2.405903977954827
set y13 -6.843690509480070
set z13 -6.882988178059987
set x14 -4.835803769072720
set y14 -8.745439778685821
set z14 0.363710027909284
set x15 5.470694502945826
set y15 4.381634964644694
set z15 -7.132515453333515
set x16 0.000000000000000
set y16 0.000000000000000
set z16 10.000000000000000
set x17 6.926254198362567
set y17 5.547453498947547
set z17 4.610071849405336
```

```
set x18 6.809317437380654
set y18 -1.531724791696047
set z18 7.161495318680831
set x19 -2.619295915252131
set y19 6.823055760508149
set z19 -6.825335083154531
set x20 -0.007554523765784
set y20 6.979466043336965
set z20 7.161494025626002
set x21 -7.183059061995936
set y21 3.295327449378464
set z21 6.127355017725909

set a 1

!       READ COORDINATES FROM CRD for BPS (L1, L2, etc...)
        open unit 21 read card name ../project/pdb/bps2.crd
        read sequence coor unit 21
        generate L@a setup first none last none
        rewind unit 21
        read coordinate card append unit 21
        close unit 21
        coor trans select (segid L@a) END xdir @x1 ydir @y1 zdir @z1
        increase a by 1

        open unit 21 read card name ../project/pdb/bps2.crd
        read sequence coor unit 21
        generate L@a setup first none last none
        rewind unit 21
        read coordinate card append unit 21
```

```
close unit 21
coor trans select (segid L@a) END xdir @x2 ydir @y2 zdir @z2
increase a by 1

open unit 21 read card name ../project/pdb/bps2.crd
read sequence coor unit 21
generate L@a setup first none last none
rewind unit 21
read coordinate card append unit 21
close unit 21
coor trans select (segid L@a) END xdir @x3 ydir @y3 zdir @z3
increase a by 1

open unit 21 read card name ../project/pdb/bps2.crd
read sequence coor unit 21
generate L@a setup first none last none
rewind unit 21
read coordinate card append unit 21
close unit 21
coor trans select (segid L@a) END xdir @x4 ydir @y4 zdir @z4
increase a by 1

open unit 21 read card name ../project/pdb/bps2.crd
read sequence coor unit 21
generate L@a setup first none last none
rewind unit 21
read coordinate card append unit 21
close unit 21
coor trans select (segid L@a) END xdir @x5 ydir @y5 zdir @z5
increase a by 1
```

```
open unit 21 read card name ../project/pdb/bps2.crd
read sequence coor unit 21
generate L@a setup first none last none
rewind unit 21
read coordinate card append unit 21
close unit 21
coor trans select (segid L@a) END xdir @x6 ydir @y6 zdir @z6
increase a by 1

open unit 21 read card name ../project/pdb/bps2.crd
read sequence coor unit 21
generate L@a setup first none last none
rewind unit 21
read coordinate card append unit 21
close unit 21
coor trans select (segid L@a) END xdir @x7 ydir @y7 zdir @z7
increase a by 1

open unit 21 read card name ../project/pdb/bps2.crd
read sequence coor unit 21
generate L@a setup first none last none
rewind unit 21
read coordinate card append unit 21
close unit 21
coor trans select (segid L@a) END xdir @x8 ydir @y8 zdir @z8
increase a by 1

open unit 21 read card name ../project/pdb/bps2.crd
read sequence coor unit 21
```

```
generate L@a setup first none last none
rewind unit 21
read coordinate card append unit 21
close unit 21
coor trans select (segid L@a) END xdir @x9 ydir @y9 zdir @z9
increase a by 1

open unit 21 read card name ../project/pdb/bps2.crd
read sequence coor unit 21
generate L@a setup first none last none
rewind unit 21
read coordinate card append unit 21
close unit 21
coor trans select (segid L@a) END xdir @x10 ydir @y10 zdir @z10
increase a by 1

open unit 21 read card name ../project/pdb/bps2.crd
read sequence coor unit 21
generate L@a setup first none last none
rewind unit 21
read coordinate card append unit 21
close unit 21
coor trans select (segid L@a) END xdir @x11 ydir @y11 zdir @z11
increase a by 1

open unit 21 read card name ../project/pdb/bps2.crd
read sequence coor unit 21
generate L@a setup first none last none
rewind unit 21
read coordinate card append unit 21
```

```
close unit 21
coor trans select (segid L@a) END xdir @x12 ydir @y12 zdir @z12
increase a by 1

open unit 21 read card name ../project/pdb/bps2.crd
read sequence coor unit 21
generate L@a setup first none last none
rewind unit 21
read coordinate card append unit 21
close unit 21
coor trans select (segid L@a) END xdir @x13 ydir @y13 zdir @z13
increase a by 1

open unit 21 read card name ../project/pdb/bps2.crd
read sequence coor unit 21
generate L@a setup first none last none
rewind unit 21
read coordinate card append unit 21
close unit 21
coor trans select (segid L@a) END xdir @x14 ydir @y14 zdir @z14
increase a by 1

open unit 21 read card name ../project/pdb/bps2.crd
read sequence coor unit 21
generate L@a setup first none last none
rewind unit 21
read coordinate card append unit 21
close unit 21
coor trans select (segid L@a) END xdir @x15 ydir @y15 zdir @z15
increase a by 1
```

```
open unit 21 read card name ../project/pdb/bps2.crd
read sequence coor unit 21
generate L@a setup first none last none
rewind unit 21
read coordinate card append unit 21
close unit 21
coor trans select (segid L@a) END xdir @x16 ydir @y16 zdir @z16
increase a by 1

open unit 21 read card name ../project/pdb/bps2.crd
read sequence coor unit 21
generate L@a setup first none last none
rewind unit 21
read coordinate card append unit 21
close unit 21
coor trans select (segid L@a) END xdir @x17 ydir @y17 zdir @z17
increase a by 1

open unit 21 read card name ../project/pdb/bps2.crd
read sequence coor unit 21
generate L@a setup first none last none
rewind unit 21
read coordinate card append unit 21
close unit 21
coor trans select (segid L@a) END xdir @x18 ydir @y18 zdir @z18
increase a by 1

open unit 21 read card name ../project/pdb/bps2.crd
read sequence coor unit 21
```

```
generate L@a setup first none last none
rewind unit 21
read coordinate card append unit 21
close unit 21
coor trans select (segid L@a) END xdir @x19 ydir @y19 zdir @z19
increase a by 1

open unit 21 read card name ../project/pdb/bps2.crd
read sequence coor unit 21
generate L@a setup first none last none
rewind unit 21
read coordinate card append unit 21
close unit 21
coor trans select (segid L@a) END xdir @x20 ydir @y20 zdir @z20
increase a by 1

open unit 21 read card name ../project/pdb/bps2.crd
read sequence coor unit 21
generate L@a setup first none last none
rewind unit 21
read coordinate card append unit 21
close unit 21
coor trans select (segid L@a) END xdir @x21 ydir @y21 zdir @z21

!       READ COORDINATES FROM CRD for AU
open unit 22 read card name ../project/pdb/au.crd
read sequence coor unit 22
generate CTR setup first none last none
rewind unit 22
read coordinate card append unit 22
```

```
        close unit 22

! NON-BONDED INTERACTION MODEL
NBONd  CUTNb 17.0 CTOFnb 16.0 CTONnb 15.0 -
       VSWItch SWItch E14Fac 1.0 -
       CDIElectric -
       WMIN 1.0

!fix postion of Au and P
CONS FIX SELE (type AU .or. type P) END

! MINIMIZE THE SYSTEM USING A OF CONJUGATED GRADIENT ALGORITHM
  minimize conj nsteps 3000 nprint 100

!==============================
! write out coordinates
!==============================
! write crd
       OPEN WRITe CARD UNIT 15 NAME ../project/pdb/np.crd
       WRITe COORdinate CARD UNIT 15
       CLOSe UNIT 15
! write pdb
       OPEN UNIT 7 WRITe CARD NAME ../project/pdb/np.pdb
       WRITe COORD PDB UNIT 7
       CLOSe UNIT 7
! write PSF
       OPEN WRITe CARD UNIT 8 NAME ../project/pdb/np.psf
       WRITe PSF CARD UNIT 8
STOP
```

CHARMM code for the mutation of YCC and attachment of the BPS nanoparticle

```
*       PREPARATION OF MUTANT K72A C102S H39AU

!       LOAD RTF, PARAM
        stream ../project/setup.str

!============================
! Setup the YCC
!============================

!       READ SEQUENCE AND COORDINATES OF APOPROT FROM PDB
        open unit 21 read card name ../project/pdb/2BCN.pdb
        read sequence pdb unit 21
        generate YCC setup
        rewind unit 21
        read coordinate pdb unit 21
        close unit 21

!============================
! Make K72A and H39AUNP mutation
!============================

! Change name of residue to be mutated.
rename resname ALA select segid YCC .AND. resid 77 end
rename resname CAU select segid YCC .AND. resid 44 end

! Delete side chain atoms.
delete atom select segid YCC .and. resid 77 .and. -
```

```
.not. (type n .or. type ca .or. type c .or. type o -
.or. type ha .or. type hn) end

delete atom select segid YCC .and. resid 44 .and. -
.not. (type n .or. type ca .or. type c .or. type o -
.or. type ha .or. type hn) end

! Store the mutated protein that lacks the mutated side chains
open write card name temp.pdb unit 14
write coordinates pdb select all end unit 14
*Temporary
*
close unit 14

! Remove all memory from CHARMM of the protein
delete atom select all end

! Read in the protein (missing side chain atoms on the residue
! to be mutated and with this residue given the new name).
open read card name temp.pdb unit 14
read sequence pdb unit 14
generate YCC setup
rewind unit 14
read coordinate pdb unit 14
close unit 14

ic param
ic build
hbuild select hydrogen end
```

```
!       READ SEQUENCE AND COORD FOR HEME
         open unit 22 read card name ../project/pdb/heme.pdb
         read sequence pdb unit 22
         generate HEME setup first none last none
         rewind unit 22
         read coordinate pdb unit 22 append
         close unit 22

ic param
ic build
hbuild select hydrogen end
AUTOGENERATE ANGLES DIHEDRALs

!connect heme to prot
patch THI1 YCC 19 HEME 1 setup
patch THI2 YCC 22 HEME 1 setup
patch PSUL YCC 85 HEME 1 setup
patch PHEM YCC 23 HEME 1 setup
patch FHEM HEME 1 setup ! fix heme

! Delete the temporary coordinates with this system command
system "rm temp.pdb"

COOR ORIENT

! bring sulfur of mutated CYS at the position of P of ligand #5
!coor trans xdir -10.65 ydir -3.961 zdir -18.701
coor trans xdir -20.65 ydir -13.961 zdir -28.701

!       READ COORDINATES FROM CRD for NP-BPS
```

```
        open unit 21 read card name ../project/pdb/np.crd
        read sequence coor unit 21
        generate NPBPS setup first none last none
        rewind unit 21
        read coordinate card append unit 21
        close unit 21

! remove one ligand
delete atom select (resname BPS .and. resid 5 ) end


shake bonh param

! CALCULATE THE ENERGY
  energy

!fix postion of Au and P
CONS FIX SELE (type AU .or. (type P .and. resname BPS) -
.or. (type SG .and. resname CAU)) END

set n 0
label loop
cons fix sele none end
coor trans xdir 1 ydir 1 zdir 1 sele (.not. resname BPS -
.and. .not. resname CTR) END
CONS FIX SELE (type AU .or. (type P .and. resname BPS) -
.or. (type SG .and. resname CAU)) END

!       MINIMIZE
```

```
! Save coordinates also in comparsion coordinate set for later use
coor copy comp

! Harmonic constraints on all protein atoms
cons harm force 20.0 sele (segid YCC .or. resname BPS) end

! First used Steepest Descent (a gentle minimizer)
minimize sd nstep 50 cdie eps 1.0 fshift vshift cutnb 13.0 ctofnb 12.0

! Reduce harmonic constraints and minimize some more
cons harm force 10.0 sele (segid YCC .or. resname BPS) end
minimize abnr nstep 50
!coor orie rms sele (segid YCC .or. resname BPS) end
! turn off harmonic constraints
cons harm force 0.0 sele (segid YCC .or. resname BPS) end
! then small constraints on backbone only
cons harm force 5.0 sele (segid YCC .or. resname BPS)  .and. -
    (type C .or. type N .or. type CA .or. type O) end
minimize abnr nstep 50
cons harm force  0.0 sele (segid YCC .or. resname BPS) end
minimize abnr nstep 300

increment n by 1
if n lt 10 goto loop

coor orie rms sele (segid YCC .or. resname BPS) end

!==============================
! write out coordinates
!==============================
```

```
! write crd
        OPEN WRITe CARD UNIT 15 NAME ../project/pdb/H39AU.crd
        WRITe COORdinate CARD UNIT 15
        CLOSe UNIT 15
! write pdb
        OPEN UNIT 7 WRITe CARD NAME ../project/pdb/H39AU.pdb
        WRITe COORD PDB UNIT 7
        CLOSe UNIT 7
! write PSF
        OPEN WRITe CARD UNIT 8 NAME ../project/pdb/H39AU.psf
        WRITe PSF CARD UNIT 8
        close unit 8
STOP
```

CHARMM code for MD simulations

```
! PARAM PASSED
        set i h39au
        set j h39au

! SETUP SYSTEM
        stream ../project/setup.str

        open read unit 1 card name ../project/pdb/@i.psf
        read psf card unit 1
        close unit 1

        open unit 1 read card name ../project/pdb/@i.crd
        read coordinate card unit 1 append
        close unit 1

  prnlev 0
  stream ../project/radius.str
  prnlev 5
  scalar wmain statistics select .not. type H* end
  define check select (.not type H* ) .and. -
  ( property wmain .eq. 0.0 ) show end
  if ?nsel ne 0  stop       !some heavy atom have a zero radius

  GBSW sw 0.3 conc 0.0 sgamma 0.03 dgp 1.5 GBenergy

! fix position of Au nanoparticle
CONS FIX SELE (type AU .or. (type P .and. resname BPS) .or. -
(type SG .and. resname CAU)) END
```

```
NBOND atom switch cdie vdw vswitch -
        ctonnb 16 ctofnb 16 cutnb 20

open unit 12 write   form name ../project/pdb/@j/heatto300.res
open unit 21 write unform name ../project/pdb/@j/heatto300.dcd
open unit 22 write   form name ../project/pdb/@j/heatto300.mon

shake bonh param

! heat from 48 K to 300 K
dynamics start time 0.002 nstep 10000 -
   firstt 48.0 finalt 300.0 teminc 10.0 ihtfrq 350 -
   ieqfrq 2000 ichecw 1 twindl -5.0 twindh +5.0 iasors 0 -
   echeck 9999.0 nprint 100 iprfrq 500 -
   inbfrq -1 ihbfrq 0 -
   iunwrit 12 iuncrd 21 kunit 22 nsavc 1000

! reopen restart files
        OPEN READ FORMatted UNIT 12 NAME ../project/pdb/@j/heatto300.res
        OPEN WRITe FORMatted UNIT 31 NAME ../project/pdb/@j/2ns_gbsw.res
        OPEN WRITe UNFORMatted UNIT 50 NAME ../project/pdb/@j/2ns_gbsw.dcd

!dynamics for 2ns, timestep 2fs
DYNA LEAP VERLET RESTart NSTEP 1000000 TIMESTEP 0.002 -
IPRFRQ 1000 IHTFRQ 0 IEQFRQ 0 NTRFRQ 0 -
IUNREA 12 IUNWRI 31 IUNCRD 50 IUNVEL -1 KUNIT 70 -
NPRINT 100 NSAVC 1000 NSAVV 0 IHBFRQ 0 INBFRQ 5 -
PCONst PINTernal COMPress 4.63e-5 PCOUpling 5.0 PREFerence 1.0 -
```

```
TCONst TCOUpling 5.0 TREFerence 300.0 -
FIRSTT 300.0 FINALT 300.0 -
ISVFRQ 10000 IASORS 0 IASVEL 1 ISCVEL 0 ICHECW 0 TWINDH 0.0 TWINDL 0.0

! write crd
        OPEN WRITe CARD UNIT 15 NAME ../project/pdb/@j/2ns_gbsw.crd
        WRITe COORdinate CARD UNIT 15
        CLOSe UNIT 15
! write pdb
        OPEN UNIT 7 WRITe CARD NAME ../project/pdb/@j/2ns_gbsw.pdb
        WRITe COORD PDB UNIT 7
        close unit 17
! write PSF
        OPEN WRITe CARD UNIT 8 NAME ../project/pdb/@j/2ns_gbsw.psf
        WRITe PSF CARD UNIT 8
        close unit 8
stop
```

Bibliography

[1] M.-C. Daniel and D. Astruc. Gold nanoparticles: Assembly, supramolecular chemistry, quantum-size-related properties, and applications toward biology, catalysis, and nanotechnology. *Chemical Reviews*, 104:293–346, 2004.

[2] S. Chah, M. R. Hammond, and R. N. Zare. Gold nanoparticles as a colorimetric sensor for protein conformational changes. *Chemistry and Biology*, 12(3):323–328, 2005.

[3] J. Kim, S. Park, J. E. Lee, S. M. Jin, J. H. Lee, I. S. Lee, I. Yang, J. S. Kim, S. K. Kim, M. H. Cho, and T. Hyeon. Designed fabrication of multifunctional magnetic gold nanoshells and their application to magnetic resonance imaging and photothermal therapy. *Angewandte Chemie International Edition*, 45(46):7754–7758, 2006.

[4] J. F. Hainfield and R. D. Powell. New frontiers in gold labeling. *Journal of Histochemistry and Cytochemistry*, 48(4):471–480, 2000.

[5] M. Bruchez, M. Moronne, P. Gin, S. Weiss, and A. P. Alivisatos. Semiconductor nanocrystals as fluorescent biological labels. *Science*, 281(5385):2013–2016, 1998.

[6] P. Pengo, L. Baltzer, L. Pasquato, and P. Scrimin. Substrate modulation of the activity of an artificial nanoesterase made of peptide-functionalized gold nanoparticles. *Angewandte Chemie International Edition*, 46(3):400–404, 2007.

[7] T. Atanasijevic, M. Shusteff, P. Fam, and A. Jasanoff. Calcium-sensitive mri contrast agents based on superparamagnetic iron oxide nanoparticles and calmodulin. *Procedings of the National Academy of Science U.S.A.*, 103(40):14707–14712, 2006.

[8] I. Willner, R. Baron, and B. Willner. Integrated nanoparticle-biomolecule systems for biosensing and bioelectronics. *Biosensors & Bioelectronics*, 22:1841–1852, 2007.

[9] T. Neuberger, B. Schöpf, H. Hofmann, M. Hofmann, and B. v. Rechenberg. Superparamagnetic nanoparticles for biomedical applications: Possibilities and limitations of a new drug delivery system. *Journal of Magnetism and Magnetic Materials*, 293:483–496, 2005.

[10] S. Behrens, W. Habicht, K. Wagner, and E. Unger. Assembly of nanoparticle ring structures based on protein templates. *Advanced Materials*, 18(3):284–289, 2006.

[11] F. Patolsky, Y. Weizmann, and I. Willner. Actin-based metallic nanowires as bio-nanotransporters. *Nature Materials*, 3:692–695, 2004.

[12] X. Gao, R. Djalali, A. Haboosheh, J. Samson, N. Nuraje, and H. Matsui. Peptide nanotubes: Simple separation using size-exclusion columns and use as templates for fabricating one-dimensional single chains of an nanoparticles. *Advanced Materials*, 17(14):1753–1757, 2005.

[13] B. I. Ipe, A. Shukla, H. C. Lu, B. Zou, H. Rehage, and C. M. Niemeyer. Dynamic light-scattering analysis of the electrostatic interaction of hexahistidine-tagged cytochrome p450 enzyme with semiconductor quantum dots. *ChemPhysChem*, 7(5):1112–1118, 2006.

[14] C. M. Pitsillides, E. K. Joe, X. B. Wei, R. R. Anderson, and C. P. Lin. Selective cell targeting with light-absorbing microparticles and nanoparticles. *Biophysical Journal*, 84(6):4023–4032, 2003.

[15] R. Sarkar, S. S. Narayanan, L.-O. Palsson, F. Dias, A. Monkman, and S. K. Pal. Direct conjugation of semiconductor nanocrystals to a globular protein to study protein-folding intermediates. *Journal of Physical Chemistry B*, 111(42):12294–12298, 2007.

[16] B. N. G. Giepmans, S. R. Adams, M. H. Ellisman, and R. Y. Tsien. The fluorescent toolbox for assessing protein location and function. *Science*, 312(217-224), 2006.

[17] M. Hirshberg, K. Henrick, L. L. Haire, N. Vasisht, M. Brune, J. E. T. Corrie, and M. R. Webb. Crystal structure of phosphate binding protein labeled with a coumarin fluorophore, a probe for inorganic phosphate. *Biochemistry*, 37(29):10381 –10385, 1998.

[18] A. Honegger, S. Spinelli, C. Cambillau, and A. Pluckthun. A mutation designed to alter crystal packing permits structural analysis of a tight-binding fluorescein-scfv complex. *Protein Science*, 14(2537-2549), 2005.

[19] J. M. Thomas. Colloidal metals: past, present and future. *Pure and Applied Chemistry*, 60(10):1517–1528, 1988.

[20] D. L. Feldheim and C. A. Foss Jr. *Metal nanoparticles. Synthesis, characterization, and applications.* Marcel Dekker, 2002.

[21] S.-Y. Lin, Y.-T. Tsai, C.-C. Chen, C.-M. Lin, and C.-H. Chen. Two-step functionalization of neutral and positively charged thiols onto citrate-stabilized au nanoparticles. *Journal of Physical Chemistry B*, 108:2134–2139, 2004.

[22] C. Mangeney, F. Ferrage, I. Aujard, V. Marchi-Artzner, L. J. O. Ouari, E. D. Rekae, A. Laschewsky, I. Vikholm, and J. W. Sadowski. Synthesis and properties of water-soluble gold colloids covalently derivatized with neutral polymer monolayers. *Journal of the American Chemical Society*, 124(20):5811–5821, 2002.

[23] M. Zheng, Z. Li, and X. Huang. Ethylene glycol monolayer protected nanoparticles: Synthesis, characterization, and interactions with biological molecules. *Langmuir*, 20:4226–4235, 2004.

[24] M. Brust, M. Walker, D. Bethell, D. J. Schiffrin, and R. Whyman. Synthesis of thiol derivatised gold nanoparticles in a two phase liquid/liquid system. *Chemical Communications*, pages 801–804, 1994.

[25] W. W. Weare, S. M. Reed, M. G. Warner, and J. E. Hutchison. Improved synthesis of small (dcore 1.5 nm) phosphine-stabilized gold nanoparticles. *Journal of the American Chemical Society*, 122:12890–12891, 2000.

[26] G. Oberdoerster, E. Oberdoerster, and J. Oberdoerster. Nanotoxicology: An emerging discipline evolving from studies of ultrafine particles. *Environmental Health Perspectives*, 113:823–839, 2005.

[27] C. M. Goodman, C. D. McCusker, T. Yilmaz, and V. M. Rotello. Toxicity of gold nanoparticles functionalized with cationic and anionic side chains. *Bioconjugate Chemistry*, 15:897–900, 2004.

[28] H. S. Choi, W. Liu, P. Misra, E. Tanaka, J. P. Zimmer, B. I. Ipe, M. G. Bawendi, and J. V. Frangioni. Renal clearance of quantum dots. *Nature Biotechnology*, 25(10):1165–1170, 2007.

[29] E. E. Connor, J. Mwamuka, A. Gole, C. J. Murphy, and M. D. Wyatt. Gold nanoparticles are taken up by human cells but do not cause acute cytotoxicity. *Small*, 1(3):325–327, 2005.

[30] M. J. Hostetler, A. C. Templeton, and R. W. Murray. Dynamics of place-exchange reactions on monolayer-protected gold cluster molecules. *Langmuir*, 15(11):3782–3789, 1999.

[31] A. Verma and V. M. Rotello. Surface recognition of biomacromolecules using nanoparticle receptors. *Chemical Communications*, 3:303–312, 2005.

[32] A. Verma, H. Nakad, J. M. Simard, and V. M. Rotello. Recognition and stabilization of peptide a-helices using templatable nanoparticle receptors. *Journal of the American Chemical Society*, 126:10806–10807, 2004.

[33] W. D. Geoghegan and G. A. Ackerman. Adsorption of horseradish peroxidase, ovomucoid and anti-immunoglobulin to colloidal gold for the indirect detection of concanavalin a, wheat germ agglutinin and goat anti-human immunoglobulin

g on cell surfaces at the electron microscopic level: a new method, theory and application. *Journal of Histochemistry and Cytochemistry*, 25(11):1187–1200, 1977.

[34] H. Bayraktar, C.-C. You, V. M. Rotello, and M. J. Knapp. Facial control of nanoparticle binding to cytochrome *c*. *Journal of the American Chemical Society*, 129(10):2732–2733, 2007.

[35] J. M. Abad, S. F. L. Mertens, M. Pita, V. M. Fernndez, and D. J. Schiffrin. Functionalization of thioctic acid-capped gold nanoparticles for specific immobilization of histidine-tagged proteins. *Journal of the American Chemical Society*, 127(15):5689 –5694, 2005.

[36] J. F. Hainfeld, W. Liu, C. M. R. Halsey, P. Freimuth, and R. D. Powell. Ni-nta-gold clusters target his-tagged proteins. *Journal of Structural Biology*, 127:185–198, 1999.

[37] M. Hu, L. Qian, R. P. Brinas, E. S. Lymar, and J. F. Hainfeld. Assembly of nanoparticle-protein binding complexes: From monomers to ordered arrays. *Angewandte Chemie International Edition*, 46(27):5111–5114, 2007.

[38] J. Schmitt, H. Hess, and H. G. Stunnenberg. Affinity purification of histidine-tagged proteins. *Molecular Biology Reports*, 18(3):223–230, 1993.

[39] S. Wang, N. Mamedova, N. A. Kotov, W. Chen, and J. Studer. Antigen/antibody immunocomplex from cdte nanoparticle bioconjugates. *Nano Letters*, 2(8):817–822, 2002.

[40] Y. M. Huh, Y. W. Jun, H. T. Song, S. Kim, J. S. Choi, J. H. Lee, S. Yoon, K. S. Kim, J. S. Shin, J. S. Suh, and J. Cheon. In vivo magnetic resonance detection of cancer by using multifunctional magnetic nanocrystals. *Journal of the American Chemical Society*, 127(35):12387–12391, 2005.

[41] M.-E. Aubin-Tam, H. Zhou, and K. Hamad-Schifferli. Structure of cytochrome *c* at the interface with magnetic $cofe_2o_4$ nanoparticles. *Soft Matter*, 4:554–559, 2008.

[42] Y. Xiao, F. Patolsky, E. Katz, J. F. Hainfeld, and I. Willner. Plugging into enzymes: Nanowiring of redox enzymes by a gold nanoparticle. *Science*, 299:1877–1881, 2004.

[43] N. M. Green. Avidin and streptavidin. *Methods in enzymology*, 184:51–67, 1990.

[44] I. Chen and A. Y. Ting. Site-specific labeling of proteins with small molecules in live cells. *Current Opinion in Biotechnology*, 16(1):35–40, 2005.

[45] V. Bagalkot, L. Zhang, E. Levy-Nissenbaum, S. Jon, P. W. Kantoff, R. Langer, and O. C. Farokhzad. Quantum dot-aptamer conjugates for synchronous cancer imaging, therapy, and sensing of drug delivery based on bi-fluorescence resonance energy transfer. *Nano Letters*, 7(10):3065–3070, 2007.

[46] T. C. Chu, F. Shieh, L. A. Lavery, M. Levy, R. Richards-Kortum, B. A. Korgel, and A. D. Ellington. Labeling tumor cells with fluorescent nanocrystal-aptamer bioconjugates. *Biosensors & Bioelectronics*, 21(10):1859–1866, 2006.

[47] S. J. Rosenthal, I. Tomlinson, E. M. Adkins, S. Schroeter, S. Adams, L. Swafford, J. McBride, Y. Wang, L. J. DeFelice, and R. D. Blakely. Targeting cell surface receptors with ligand-conjugated nanocrystals. *Journal of the American Chemical Society*, 124(17):4586–4594, 2002.

[48] C.-C. Lin, Y.-C. Yeh, C.-Y. Yang, C.-L. Chen, G.-F. Chen, C.-C. Chen, and Y.-C. Wu. Selective binding of mannose-encapsulated gold nanoparticles to type 1 pili in escherichia coli. *Journal of the American Chemical Society*, 124(14):3508–3509, 2002.

[49] C. J. Ackerson, P. D. Jadzinsky, G. J. Jensen, and R. D. Kornberg. Rigid, specific, and discrete gold nanoparticle/antibody conjugates. *Journal of the American Chemical Society*, 128:2635, 2006.

[50] M.-E. Aubin-Tam and K. Hamad-Schifferli. Gold nanoparticle cytochrome *c* complexes: The effect of nanoparticle ligand charge on protein structure. *Langmuir*, 21(26):12080–12084, 2005.

[51] L. Montesano-Roditis, D. G. Glitz, R. R. Traut, and P. L. Stewart. Cryo-electron microscopic localization of protein l7/l12 within the escherichia coli 70 s ribosome by difference mapping and nanogold labeling. *Journal of Biological Chemistry*, 276(17):14117–14123, 2001.

[52] R. A. McMillan, C. D. Paavola, J. Howard, S. L. Chan, N. J. Zaluzec, and J. D. Trent. Ordered nanoparticle arrays formed on engineered chaperonin protein templates. *Nature Materials*, 1(4):247–252, 2002.

[53] J. D. Patel, R. O'Carra, J. Jones, J. G. Woodward, and R. J. Mumper. Preparation and characterization of nickel nanoparticles for binding to his-tag proteins and antigens. *Pharmaceutical Research*, 24(2):343–352, 2007.

[54] I. L. Medintz, J. H. Konnert, A. R. Clapp, I. Stanish, M. E. Twigg, H. Mattoussi, J. M. Mauro, and J. R. Deschamps. A fluorescence resonance energy transfer-derived structure of a quantum dot-protein bioconjugate nanoassembly. *Proceedings of the National Academy of Science*, 101(26):9612–9617, 2004.

[55] M. Veiseh, H. M. Zareie, and M. Zhang. Highly selective protein patterning on gold-silicon substrates for biosensor application. *Langmuir*, 18(17):6671–6678, 2002.

[56] C. Buechel, E. Morris, E. Orlova, and J. Barber. Localisation of the psbh subunit in photosystem ii: a new approach using labelling of his-tags with a ni2+-nta gold cluster and single particle analysis. *Journal of Molecular Biology*, 312(2):371–379, 2001.

[57] L. Bumba, M. Tichy, M. Dobakova, J. Komenda, and F. Vacha. Localization of the psbh subunit in photosystem ii from the synechocystis using the his-tagged ni-nta nanogold labeling. *Journal of Structural Biology*, 152:28–35, 2005.

[58] M.-E. Aubin, D. G. Morales, and K. Hamad-Schifferli. Labeling ribonuclease s with a 3nm au nanoparticle by two-step assembly. *Nano Letters*, 5(3):519–522, 2005.

[59] S. S. Narayanan, R. Sarkar, and S. K. Pal. Structural and functional characterization of enzyme-quantum dot conjugates: Covalent attachment of cds nanocrystal to a-chymotrypsin. *Journal of Physical Chemistry C*, 111(31):11539–11543, 2007.

[60] H. Mattoussi, J. M. Mauro, E. R. Goldman, G. P. Anderson, V. C. Sundar, F. V. Mikulec, and M. G. Bawendi. Self-assembly of cdse-zns quantum dot bioconjugates using an engineered recombinant protein. *Journal of the American Chemical Society*, 122(49):12142–12150, 2000.

[61] D.-B. Shieh, C.-H. Su, F.-Y. Chang, Y.-N. Wu, W.-C. Su, J. R. Hwu, J.-H. Chen, and C.-S. Yeh. Aqueous nickel-nitrilotriacetate modified fe_3o_4-nh_3^+ nanoparticles for protein purification and cell targeting. *Nanotechnology*, 17:4174–4182, 2006.

[62] C. J. Xu, K. M. Xu, H. W. Gu, X. F. Zhong, Z. H. Guo, R. K. Zheng, X. X. Zhang, and B. Xu. Nitrilotriacetic acid-modified magnetic nanoparticles as a general agent to bind histidine-tagged proteins. *Journal of the American Chemical Society*, 126(11):3392–3393, 2004.

[63] J. L. Brennan, N. S. Hatzakis, T. R. Tshikhudo, N. Dirvianskyte, V. Razumas, S. Patkar, J. Vind, A. Svendsen, R. J. M. Nolte, A. E. Rowan, and M. Brust. Bionanoconjugation via click chemistry: The creation of functional hybrids of lipases and gold nanoparticles. *Bioconjugate Chemistry*, 17(6):1373–1375, 2006.

[64] C. F. W. Becker, Y. Marsac, P. H. J. Moser, R. S. Goody, and C. M. Niemeyer. Functional immobilization of the small gtpase rab6a on dna-gold nanoparticles by using a site-specifically attached poly(ethylene glycol)linker and thiol place-exchange reaction. *ChemBioChem*, 8:32–36, 2007.

[65] H. Xie, A. G. Tkachenko, W. R. Glomm, J. A. Ryan, M. K. Brennaman, J. M. Papanikolas, S. Franzen, and D. L. Feldheim. Critical flocculation concentrations, binding isotherms, and ligand exchange properties of peptide-modified gold nanoparticles studied by uv-visible, fluorescence, and time-correlated single photon counting spectroscopies. *Analytical Chemistry*, 75(21):5797–5805, 2003.

[66] D. Zanchet, C. M. Micheel, W. J. Parak, D. Gerion, and A. P. Alivisatos. Electrophoretic isolation of discrete au nanocrystal/dna conjugates. *Nano Letters*, 1(1):32–35, 2001.

[67] N. N. Mamedova, N. A. Kotov, A. L. Rogach, and J. Studer. Albumin-cdte nanoparticle bioconjugates: Preparation, structure, and interunit energy transfer with antenna effect. *Nano Letters*, 1(6):281–286, 2001.

[68] C. M. Soto, A. S. Blum, C. D. Wilson, J. Lazorcik, M. Kim, B. Gnade, and B. R. Ratna. Separation and recovery of intact gold-virus complex by agarose electrophoresis and electroelution: Application to the purification of cowpea mosaic virus and colloidal gold complex. *Electrophoresis*, 25(17):2901–2906, 2004.

[69] A. Vertegel, R. W. Siegel, and J. S. Dordick. Silica nanoparticle size influences the structure and enzymatic activity of adsorbed lysozyme. *Langmuir*, 20:6800–6807, 2004.

[70] X. Jiang, J. Jiang, Y. Jin, E. Wang, and S. Dong. Effect of colloidal gold size on the conformational changes of adsorbed cytochrome *c*: Probing by circular dichroism, uv-visible, and infrared spectroscopy. *Biomacromolecules*, 6(1):46–53, 2005.

[71] I. D. G. Macdonald and W. E. Smith. Orientation of cytochrome *c* adsorbed on a citrate-reduced silver colloid surface. *Langmuir*, 12(3):706–713, 1996.

[72] C. D. Keating, K. M. Kovaleski, and M. J. Natan. Protein:colloid conjugates for surface-enhanced raman scattering: Stability and control of protein orientation. *Journal of Physical Chemistry B*, 102:9404–9413, 1998.

[73] M. Lundqvist, P. Nygren, B.-H. Jonsson, and K. Broo. Induction of structure and function in a designed peptide upon adsorption on a silica nanoparticle. *Angewandte Chemie International Edition*, 45(48):8169–8173, 2006.

[74] S. Srivastava, A. Verma, B. L. Frankamp, and V. M. Rotello. Controlled assembly of protein-nanoparticle composites through protein surface recognition. *Advanced Materials*, 17(5):617–621, 2005.

[75] K. Yokoyama and D.R. Welchons. The conjugation of amyloid beta protein on the gold colloidal nanoparticles surfaces. *Nanotechnology*, 18:105101–105107, 2007.

[76] J. Al-Bassam, R. S. Ozer, D. Safer, S. Halpain, and R. A. Milligan. Map2 and tau bind longitudinally along the outer ridges of microtubule protofilaments. *Journal of Cell Biology*, 157:1187–1196, 2002.

[77] R. A. Milligan, M. Whittaker, and D. Safer. Molecular structure of f-actin and location of surface binding sites. *Nature*, 348:217–221, 1990.

[78] C. Barat, P. P. Datta, V. S. Raj, A. Kaji, and R. K. Agrawal. Progression of the ribosome recycling factor through the ribosome dissociates the two ribosomal subunits. *Molecular Cell*, 27:250–261, 2007.

[79] P. P. Datta, M. R. Sharma, L. Qi, J. Frank, and R. K. Agrawal. Interaction of the g0 domain of elongation factor g and the c-terminal domain of ribosomal protein l7/l12 during translocation as revealed by cryo-em. *Molecular Cell*, 104:293–346, 2004.

[80] H. Wille, M. D. Michelitsch, V. Gu/acuteenebaut, S. Supattapone, A. Serban, F. E. Cohen, D. A. Agard, and S. B. Prusiner. Structural studies of the scrapie prion protein by electron crystallography. *Proceedings of the National Academy of Science U.S.A.*, 99:3563–3568, 2002.

[81] S. Rice, A. W. Lin, D. Safer, C. L. Hart, N. Naber, B. O. Carragher, S. M. Cain, E. Pechatnikova, E. M. Wilson-Kubalek, M. Whittaker, E. Pate, R. Cooke, E. W. Taylor, R. A. Milligan, and R. A. Vale. A structural change in the kinesin motor protein that drives motility. *Nature*, 402:778–784, 1999.

[82] A. L. Wells, A. W. Lin, L.-Q. Chen, D. Safer, S. M. Cain, T. Hasson, B. O. Carragher, R. A. Milligan, and H. L. Sweeney. Myosin vi is an actin-based motor that moves backwards. *Nature*, 401:505–508, 1999.

[83] A. M. Jackson, J. W. Myerson, and F. Stellacci. Spontaneous assembly of subnanometre-ordered domains in the ligand shell of monolayer-protected nanoparticles. *Nature Materials*, 3(5):330–336, 2004.

[84] R. Ionov, A. El-Abed, M. Goldman, and P. Perett. Structural organization of alpha-helical peptide antibiotic alamethicin at the air/water interface. *Journal of Physical Chemistry B*, 108:8485–8488, 2004.

[85] Y. Sugiyama, Y. Inoue, E. Muneyuki, H. Haneda, and M. Fujimoto. Afm and tem observations of α-helix to β-sheet conformation change occuring on carbon nanotubes. *Journal of Eletronic Microscopy*, 55:143–149, 2006.

[86] X.-H. Chen, L. Zhang, Y.-X. Weng, L.-C. Du, M.-P. Ye, G.-Z. Yang, R. Fujii, Y. Yasushi Koyama, and J. P. Zhang. Protein structural deformation induced lifetime shortening of photosynthetic bacteria light-harvesting complex lh2 excited state. *Biophysical Journal*, 88:4262–4273, 2005.

[87] A. Gole, C. Dash, C. Soman, S. R. Sainkar, M. Rao, and M. Sastry. On the preparation, characterization, and enzymatic activity of fungal protease-gold colloid bioconjugates. *Bioconjugate Chemistry*, 12:684–690, 2001.

[88] A. Gole, C. Dash, V. Ramakrishnan, S. R. Sainkar, A. B. Mandale, M. Rao, and M. Sastry. Pepsin-gold colloid conjugates: Preparation, characterization, and enzymatic activity. *Langmuir*, 17(5):1674–1679, 2001.

[89] Y.-F. Huang, C.-C. Huang, and H.-T. Chang. Exploring the activity and specificity of gold nanoparticle-bound trypsin by capillary electrophoresis with laser-induced fluorescence detection. *Langmuir*, 19(18):7498–7502, 2003.

[90] A. Dyal, K. Loos, M. Noto, S. W. Chang, C. Spagnoli, Kvpm Shafi, A. Ulman, M. Cowman, and R. A. Gross. Activity of candida rugosa lipase immobilized on gamma-fe_2o_3 magnetic nanoparticles. *Journal of the American Chemical Society*, 125(7):1684–1685, 2003.

[91] C.-C. You, M. De, G. Han, and V. M. Rotello. Tunable inhibition and denaturation of α-chymotrypsin with amino acid-functionalized gold nanoparticles. *Journal of the American Chemical Society*, 127(37):12873–12881, 2005.

[92] E. J. Bjerneld, Z. Földes-Papp, M. Käll, and R. Rigler. Single-molecule surface-enhanced raman and fluorescence correlation spectroscopy of horseradish peroxidase. *Journal of Physical Chemistry B*, 106(6):1213 –1218, 2002.

[93] G. K. Kouassi, J. Irudayaraj, and G. McCarty. Examination of cholesterol oxidase attachment to magnetic nanoparticles. *Journal of Nanobiotechnology*, 3(1):1–9, 2005.

[94] P. Asuri, S. S. Karajanagi, A. A. Vertegel, J. S. Dordick, and R. S. Kane. Enhanced stability of enzymes adsorbed onto nanoparticles. *Journal of Nanoscience and Nanotechnology*, 7(4-5):1675–1678, 2007.

[95] S. Phadtare, V. P. Vinod, K. Mukhopadhyay, A. Kumar, M. Rao, R. V. Chaudhari, and M. Sastry. Immobilization and biocatalytic activity of fungal protease on gold nanoparticle-loaded zeolite microspheres. *Biotechnology and Bioengineering*, 85(6):629–637, 2004.

[96] S. Shleev, J. Tkac, A. Christenson, T. Ruzgas, A. I. Yaropolov, J. W. Whittaker, and L. Gorton. Direct electron transfer between copper-containing proteins and electrodes. *Biosensors & Bioelectronics*, 20:2517–2554, 2005.

[97] Y. Wu and S. Hu. Biosensors based on direct electron transfer in redox proteins,. *Microchimica Acta*, 159:1–17, 2007.

[98] X. X. Chen, R. Ferrigno, J. Yang, and G. A. Whitesides. Redox properties of cytochrome *c* adsorbed on self-assembled monolayers: A probe for protein conformation and orientation. *Langmuir*, 18(18):7009–7015, 2002.

[99] A. E. Kasmi, J. M. Wallace, E. F. Bowden, S. M. Binet, and R. J. Linderman. Controlling interfacial electron-transfer kinetics of cytochrome *c* with mixed self-assembled monolayers. *Journal of the American Chemical Society*, 120:225–226, 1998.

[100] L. Wang and E. Wang. Direct electron transfer between cytochrome *c* and a gold nanoparticles modified electrode. *Electrochemical Communications*, 6:49–54, 1993.

[101] K. R. Brown, A. P. Fox, and M. J. Natan. Morphology-dependent electrochemistry of cytochrome *c* at au colloid-modified sno_2 electrodes. *JACS*, 118:1154–1157, 1996.

[102] Y. Huang, W. Zhang, H.n Xiao, and G. Li. An electrochemical investigation of glucose oxidase at a cds nanoparticles modified electrode. *Biosensors and Bioelectronics*, 21(817-821), 2005.

[103] J. Zhao, J. P. O'Daly, R. W. Henkens, J. Stonehuerner, and A. L. Crumbliss. A xanthine oxidase/colloidal gold enzyme electrode for amperometric biosensor applications. *Biosensors and Bioelectronics*, 11(5):493–502, 1996.

[104] E. Katz and I. Willner. Integrated nanoparticle-biomolecule hybrid systems: Synthesis, properties, and applications. *Angewandte Chemie International Edition*, 43(45):6042–6108, 2004.

[105] X. Gan, T. Liu, J. Zhong, X. Liu, and G. Li. Effect of silver nanoparticles on the electron transfer reactivity and the catalytic activity of myoglobin. *ChemBioChem*, 5(12):1686–1691, 2004.

[106] E. Laviron. General expression of the linear potential sweep voltammogram in the case of diffusionless electrochemical systems. *Journal of Electroanalytical Chemistry and Interfacial Electrochemistry*, 101:19–28, 1979.

[107] H. Liu, Y. Tian, and Z. Deng. Morphology-dependent electrochemistry and electrocatalytical activity of cytochrome *c*. *Langmuir*, 23:9487–9494, 2007.

[108] T. Pascher, J. P. Chesick, J. R. Winkler, and H. B. Gray. Protein folding triggered by electron transfer. *Science*, 271:1558–1560, 1996.

[109] I. Sondi, O. Siiman, S. Koester, and E. Matijević. Preparation of aminodextran-cds nanoparticle complexes and biologically active antibody-aminodextran-cds nanoparticle conjugates. *Langmuir*, 7:3107–3118, 2000.

[110] G. S. von Banchet and H.-G. Schaible. Localization of the neurokinin 1 receptor on a subset of substance p-positive and isolectin b4-negative dorsal root ganglion neurons of the rat. *Neuroscience Letters*, 274:175–178, 1999.

[111] G. S. Ratnaparkhi and R. Varadarajan. X-ray crystallographic studies of the denaturation of ribonuclease s. *Proteins*, 36:282–294, 1999.

[112] R. T. Raines. Ribonuclease a. *Chemical Reviews*, 98:1045–1066, 1998.

[113] J.-S. Kim and R. T. Raines. Peptide tags for a dual affinity fusion system. *Analytical biochemistry*, 219(1):165–166, 1994.

[114] J. Beesley. *Colloidal gold: a new perspective for cytochemical marking.* Oxford University Press, 1989.

[115] J. J. Dwyer, M. A. Dwyer, and A. A. Kossiakoff. High affinity rnase s-peptide variants obtained by phage display have a novel "hot-spot" of binding energy. *Biochemistry*, 40(45):13491–13500, 2001.

[116] S. Park. *Control of oligonucleotide conformation on nanoparticle surfaces for nanoscale heat transfer study.* Master's thesis, MIT, 2004.

[117] S. Park, K. A. Brown, and K. Hamad-Schifferli. Changes in oligonucleotide conformation on nanoparticle surfaces by modification with mercaptohexanol. *Nano Letters*, 4(10):1925–1929, 2004.

[118] A. Ulman. Formation and structure of self-assembled monolayers. *Chemical Reviews*, 96(4):1533–1554, 1996.

[119] M. De, C.-C. You, S. Srivastava, and V. M. Rotello. Biomimetic interactions of proteins with functionalized nanoparticles: a thermodynamic study. *Journal of the american chemical society*, 129:10747–10753, 2007.

[120] A. Velazquez-Campoy, S. A. Leavitt, and E. Freire. Characterization of protein-protein interactions by isothermal titration calorimetry. *Methods in Molecular Biology*, 261:35–54, 2004.

[121] M. F. M. Engel, C. P. M. van Mierlo, and A. J. W. G. Visser. Kinetic and structural characterization of adsorption-induced unfolding of bovine-lactalbumin. *Journal of Biological Chemistry*, 277(13):10922–10930, 2002.

[122] E. Ostuni, B. A. Grzybowski, M. Mrksich, C. S. Roberts, and G. M. Whitesides. Adsorption of proteins to hydrophobic sites on mixed self-assembled monolayers. *Langmuir*, 19(5):1861–1872, 2003.

[123] B. Holtz, Y. Wang, X.-Y. Zhu, and A. Guo. Denaturing and refolding of protein molecules on surfaces. *Proteomics*, 7(11):1771–1774, 2007.

[124] E. D. Kaufman, J. Belyea, M. C. Johnson, Z. M. Nicholson, J. L. Ricks, P. K. Shah, M. Bayless, T. Pettersson, Z. Feldotö, E. Blomberg, P. Claesson, and S. Franzen. Probing protein adsorption onto mercaptoundecanoic acid stabilized gold nanoparticles and surfaces by quartz crystal microbalance and potential measurements. *Langmuir*, 23:6053–6062, 2007.

[125] P. S. Jensen, Q. Chi, F. B. Grumsen, J. M. Abad, A. Horsewell, D. J. Schiffrin, and J. Ulstrup. Gold nanoparticle assisted assembly of a heme protein for enhancement of long-range interfacial electron transfer. *Journal of Physical Chemistry C*, 111:6124 - 6132, 2007.

[126] G. V. Louie, W. L. B. Hutcheon, and G. D. Brayer. Yeast iso-1-cytochrome *c* - a 2.8a resolution three-dimensional structure determination. *Journal of Molecular Biology*, 199:205–314, 1988.

[127] H. Maity, M. Maity, and S. W. Englander. How cytochrome *c* folds, and why: Submolecular foldon units and their stepwise sequential stabilization. *Journal of Molecular Biology*, 343(1):223–233, 2004.

[128] D. R. Hostetter, G. T. Weatherly, J. R. Beasley, K. Bortone, D. S. Cohen, S. A. Finger, P. Hardwidge, D. S. Kakouras, A. J. Saunders, S. K. Trojak, J. C. Waldner, and G. J. Pielak. Partially formed native tertiary interactions in the a-state of cytochrome *c*. *Journal of Molecular Biology*, 289(3):639–644, 1999.

[129] D. Roccatano, I. Daidone, M.-A. Ceruso, C. Bossa, and A. D. Nola. Selective excitation of native fluctuations during thermal unfolding simulations: Horse heart cytochrome *c* as a case study. *Biophysical Journal*, 84:1876–1883, 2003.

[130] A. E. García and G. Hummer. Conformational dynamics of cytochrome *c*: Correlation to hydrogen exchange. *Proteins: Structure, Function, and Genetics*, 36:175–191, 1999.

[131] W. H. Koppenol and E. Margoliash. The asymmetric distribution of charges on the surface of horse cytochrome *c* - functional implications. *Journal of Biological Chemistry*, 257(8):4426–4437, 1982.

[132] J. M. Pachence and J. K. Blasie. The location of cytochrome *c* on the surface of ultrathin lipid multilayer films using x-ray diffraction. *Biophysical Journal*, 52:735–747, 1987.

[133] D. Hobara, S. Imabayashi, and T. Kakiuchi. Preferential adsorption of horse heart cytochrome *c* on nanometer-scale domains of a phase-separated binary self-assembled monolayer of 3-mercaptopropionic acid and 1-hexadecanethiol on au(111). *Nano Letters*, 2:1021–1025, 2002.

[134] N. Sreerama and R. W. Woody. Computation and analysis of protein circular dichroism spectra. *Methods in Enzymology*, 383:318–351, 2004.

[135] S. J. Moench and J. D. Satterlee. Proton nmr comparison of the saccharomyces cerevisiae ferricytochrome *c* isozyme-1 monomer and covalent disulfide dimer. *Journal of Biological Chemistry*, 264(17):9923–9931, 1989.

[136] M. W. Kennedy, C. Britton, N. C. Price, S. M. Kelly, and A. Cooper. The dva-1 polyprotein of the parasitic nematode dictyocaulus viviparus. *Journal of Biological Chemistry*, 270(33):19277–19281, 1995.

[137] M. White, L. A. Fothergill-Gilmore, S. M. Kelly, and N. C. Price. Dissociation of the tetrameric phosphoglycerate mutase from yeast by a mutation in the subunit contact region. *Biochemical Journal*, 295:743–748, 1993.

[138] E. V. Pletneva, H. B. Gray, and J. R. Winkler. Many faces of the unfolded state: Conformational heterogeneity in denatured yeast cytochrome c. *Journal of Molecular Biology*, 345:855–867, 2005.

[139] E. V. Pletneva, H. B. Gray, and J. R. Winkler. Snapshots of cytochrome c folding. *Proceedings of the National Academy of Science U.S.A.*, 102(51):1839718402, 2005.

[140] W. B. R. Pollock, F. I. Rosell, M. B. Twitchett, M. E. Dumont, and A. G. Mauk. Bacterial expression of a mitochondrial cytochrome *c*. trimethylation of lys72 in yeast iso-1-cytochrome *c* and the alkaline conformational transition. *Biochemistry*, 37(17):6124–6131, 1998.

[141] C. Bongiovanni, F. Sinibaldi, T. Ferri, and R. Santucci. Glycerol-induced formation of the molten globule from acid-denatured cytochrome *c*: Implication for hierarchical folding. *Journal of Protein Chemistry*, 21:35–41, 2002.

[142] M. Friedel, A. Baumketner, and J.-E. Shea. Stability of a protein tethered to a surface. *The Journal of Chemical Physics*, 126:095101, 2007.

[143] C. E. Nordgren, D. J. Tobias, M. L. Klein, and J. K. Blasie. Molecular dynamics simulations of a hydrated protein vectorially oriented on polar and nonpolar soft surfaces. *Biophysical Journal*, 83:2906–2917, 2002.

[144] W. D. Luedtke and U. Landman. Structure and thermodynamics of self-assembled monolayers on gold nanocrystallites. *Journal of Physical Chemistry B*, 102:6566–6572, 1998.

[145] P. K. Ghorai and S. C. Glotzer. Molecular dynamics simulation study of self-assembled monolayers of alkanethiol surfactants on spherical gold nanoparticles. *Journal of Physical Chemistry C*, 111(43):15857–15862, 2007.

[146] S. Rapino and F. Zerbetto. Dynamics of thiolate chains on a gold nanoparticle. *Small*, 3:386–388, 2007.

[147] M.-E. Aubin-Tam, W. Hwang, and K. Hamad-Schifferli. Site-directed nanoparticle labeling of cytochrome *c*. *in preparation*, 2008.

[148] R. Day, B. J. Bennion, S. Ham, and V. Daggett. Increasing temperature accelerates protein unfolding without changing the pathway of unfolding. *Journal of Molecular Biology*, 322(1):189–203, 2002.

[149] W. Humphrey, A. Dalke, and K. Schulten. Vmd - visual molecular dynamics. *Journal of the Molecular Graphics*, 14:33–38, 1996.

[150] D. Frishman and P. Argos. Knowledge-based protein secondary structure assignment. *Proteins*, 23:566–579, 1995.

[151] M. M. G. Krishna and S. W. Englander. The n-terminal to c-terminal motif in protein folding and function. *Proceedings of the National Academy of Science U.S.A.*, 102:1053–1058, 2005.

[152] O. B. Ptitsyn. Protein folding and protein evolution: Common folding nucleus in different subfamilies of *c*-type cytochromes? *Journal of Molecular Biology*, 278:655–666, 1998.

[153] W. Colón, G. A. Eloeve, L. P. Wakem, F. Sherman, and H. Roder. Side chain packing of the n- and c-terminal helices plays a critical role in the kinetics of cytochrome *c* folding. *Biochemistry*, 35(17):5538–5549, 1996.

[154] J. Bixler, G. Bakker, and G. McLendon. Electrochemical probes of protein folding. *Journal of the American Chemical Society*, 114:6938–6939, 1992.

[155] F. A. Tezcan, J. R. Winkler, and H. B. Gray. Effects of ligation and folding on reduction potentials of heme proteins. *Journal of the American Chemical Society*, 120(51):13383 –13388, 1998.

[156] B. Bonanni, D. Alliata, A. R. Bizzarri, and S. Cannistraro. Topological and electron-transfer properties of yeast cytochrome *c* adsorbed on bare gold electrodes. *ChemPhysChem*, 4:1183–1188, 2003.

[157] R. Weissleder, K. Kelly, E. Y. Sun, T. Shtatland, and L. Josephson. Cell-specific targeting of nanoparticles by multivalent attachment of small molecules. *Nature Biotechnology*, 23:1418–1423, 2005.

[158] C. T. Yavuz, J. T. Mayo, W. W. Yu, A. Prakash, J. C. Falkner, S. Yean, L. L. Cong, H. J. Shipley, A. Kan, M. Tomson, D. Natelson, and V. L. Colvin. Low-field magnetic separation of monodisperse fe_3o_4 nanocrystals. *Science*, 314(5801):964–967, 2006.

[159] H. Gu, P.-L. Ho, K. W. T. Tsang, L. Wang, and B. Xu. Using biofunctional magnetic nanoparticles to capture vancomycin-resistant enterococci and other gram-positive bacteria at ultralow concentration. *Journal of the American Chemical Society*, 125(51):15702–15703, 2003.

[160] B. M. Hutchins, M. Platt, W. O. Hancock, and M. E. Williams. Motility of $cofe_2o_4$ nanoparticle-labelled microtubules in magnetic fields. *Micro & Nano Letters*, 1(1):47–52, 2006.

[161] R. Hergt and S. Dutz. Magnetic particle hyperthermia-biophysical limitations of a visionary tumour therapy. *Journal of Magnetism and Magnetic Materials*, 311(1):187–192, 2007.

[162] S. Mornet, S. Vasseur, F. Grasset, and E. Duguet. Magnetic nanoparticle design for medical diagnosis and therapy. *Journal of Materials Chemistry*, 14:2161–2175, 2004.

[163] M. Kim, Y. F. Chen, Y. C. Liu, and X. G. Peng. Super-stable, high-quality fe3o4 dendron-nanocrystals dispersible in both organic and aqueous solutions. *Advanced Materials*, 17(11):1429, 2005.

[164] E. A. Schellenberger, F. Reynolds, R. Weissleder, and L. Josephson. Surface-functionalized nanoparticle library yields probes for apoptotic cells. *Chembiochem*, 5(3):275–279, 2004.

[165] D. B. Robinson, H. H. J. Persson, H. Zeng, G. Li, N. Pourmand, S. Sun, and S. X. Wang. Dna-functionalized mfe$_2$o$_4$ (m = fe, co, or mn) nanoparticles and their hybridization to dna-functionalized surfaces. *Langmuir*, 21:3096–3103, 2005.

[166] A.-H. Lu, E. L. Salabas, and F. Schüth. Magnetic nanoparticles: Synthesis, protection, functionalization, and application. *Angewandte Chemie International Edition*, 46(8):1222–1244, 2007.

[167] S. H. Sun, H. Zeng, D. B. Robinson, S. Raoux, P. M. Rice, S. X. Wang, and G. X. Li. Monodisperse mfe$_2$o$_4$ (m = fe, co, mn) nanoparticles. *Journal of the American Chemical Society*, 126(1):273–279, 2004.

[168] C. Rocchiccioli-Deltcheff, R. Franck, V. Cabuil, and R. Massart. Surfacted ferrofluid. *Journal of Chemical Research (Synopses)*, 5:126–127, 1987.

[169] N. Wu, L. Fu, M. Su, M. Aslam, K. C. Wong, and V. P. Dravid. Interaction of fatty acid monolayers with cobalt nanoparticles. *Nano Letters*, 4(2):383–386, 2004.

[170] G. V. Louie and G. D. Brayer. High-resolution refinement of yeast iso-1-cytochrome *c* and comparisons with other eukaryotic cytochromes *c*. *Journal of Molecular Biology*, 214:527–555, 1990.

[171] G. W. Bushnell, G. V. Louie, and G. D. Brayer. High-resolution three-dimensional structure of horse heart cytochrome *c*. *Journal of Molecular Biology*, pages 585–595, 1990.

[172] A. D. Roddick-Lanzilotta and A. J. McQuillan. An *insitu* infrared spectroscopic study of glutamic acid and of aspartic acid adsorbed on tio$_2$: implications for the biocompatibility of titanium. *Journal of Colloid Interface Sciences*, 227:48–54, 2002.

[173] M. Mammen, S.-K. Choi, and G. M. Whitesides. Polyvalent interactions in biological systems: Implications for design and use of multivalent ligands and inhibitors. *Angewandte Chemie International Edition*, 37(20):2754–2794, 1998.

[174] L. Pasquato, P. Pengo, and P. Scrimin. Functional gold nanoparticles for recognition and catalysis. *Journal of Materials Chemistry*, 14(24):3481–3487, 2004.

[175] D. Casanova, D. Giaume, M. Moreau, J.-L. Martin, T. Gacoin, J.-P. Boilot, and A. Alexandrou. Counting the number of proteins coupled to single nanoparticles. *Journal of the American Chemical Society*, 129:12592–12593, 2007.

[176] T. Pons, I. L. Medintz, X. Wang, D. S. English, and H. Mattoussi. Solution-phase single quantum dot fluorescence resonance energy transfer. *Journal of the American Chemical Society*, 128(47):15324 –15331, 2006.

[177] W. Liu, M. Howarth, A. B. Greytak, Y. Zheng, D. G. Nocera, A. Y. Ting, and M. G. Bawendi. Compact biocompatible quantum dots functionalized for cellular imaging. *Journal of the American Chemical Society*, 130:1274–1284, 2008.

[178] L. Thöny-Meyer, P. Künzler, and H. Hennecke. Requirements for maturation of bradyrhizobium japonicum cytochrome c550 in escherichia coli. *European Journal of Biochemistry*, 235:754–761, 1996.

[179] B. R. Brooks, R. E. Bruccoleri, B. D. Olafson, D. J. States, S. Swaminathan, and M. Karplus. Charmm: A program for macromolecular energy, minimization, and dynamics calculations. *Journal of Computational Chemistry*, 4(2):187–217, 1983.

[180] W. Im, M. S. Lee, and C. L. Brooks III. Generalized born model with a simple smoothing function. *Journal of Computational Chemistry*, 24(14):1691–1702, 2003.

[181] A. D. Jr MacKerell, M. Feig, and C. L. Brooks III. Extending the treatment of backbone energetics in protein force fields: limitations of gas-phase quantum mechanics in reproducing protein conformational distributions in molecular dynamics simulations. *Journal of Computational Chemistry*, 25:1400–1415, 2004.

[182] J.-C. Wang and Y. Wang. Structure of [au(pph3)2][c(cn)3]. *Acta Cryst.*, C49:131–132, 1993.

[183] S. A. Kang, K. R. Hoke, and B. R. Crane. Solvent isotope effects on interfacial protein electron transfer in crystals and electrode films. *Journal of the American Chemical Society*, 128:2346–2355, 2006.

[184] C. Majumder and S. K. Kulshreshtha. Structural and electronic properties of au_n (n=2-10) clusters and their interactions with single s atoms: Ab initio molecular dynamics simulations. *Physical Reviews B*, 73:155427–155437, 2006.